University of Stavanger
FACULTY OF SCIENCE AND TECHNOLOGY

# Master Thesis

| | |
|---|---|
| Study program/specialization:<br><br>**Petroleum Engineering/ Drilling Technology** | Fall semester, 2021<br><br>Open |
| Author: **Rahmat Mohammadi** | ……. Rahmat Mohammadi ……<br>(Signature of author) |
| Supervisor(s): **Mesfin Belayneh** | |
| Title of Master's thesis:<br>***Experimental Study of Loss Circulation Materials Bridging Performance in K/Na-formate based Drilling Fluids*** | |
| Credits: 30 | |
| **Keywords:**<br><br>LCM materials<br>Quartz<br>$CaCO_3$<br>Pistachio<br>Nutshell<br>Na-Formate<br>K-Formate | Number of pages: 89……<br>+ Supplemental material/other:-<br><br>Date/year 15/12/2021<br><br>Stavanger |

# ACKNOWLEDGEMENTS

I would like to acknowledge and express my sincere gratitude to my supervisor, Mesfin Belayneh who made this work possible. His exceptional guidance, motivational support and advice carried me through all the stages of writing my thesis.

# ABSTRACT

The loss of drilling fluid is one of the main concerns of the petroleum industry, causing excessive expenditure both for operational and increasing the non-productive drilling time (NPT). The NPT associated with loss circulation issues cost the oil industry a lot. The preventive and corrective methods are the main techniques to manage the loss circulation in a wellbore. Lost circulation materials (LCM) have been widely used to prevent fluid loss into the formation, but the use of these materials depends on the types of formation, the loss zones, and the degree of severity of the losses.

In this thesis, a total of four experimental tests are designed to systematically investigate the bridging performance of LCM in laboratory synthesized K- and Na-formate based drill-in fluids. The static high pressure LCM bridge test apparatus with different artificial fracture slot widths were used for the investigations.

The test results showed that the bridging performance of LCM materials in the K- and Na-formate drilling fluids are almost the same, and a strong fracture bridge is obtained by mixing very small with medium and coarse that creates an improved packing of pistachio particles. Another observation from this work is that the LCM used in drill-in drilling fluid, $CaCO_3$, is mechanically weak. However, the blending of $CaCO_3$ with Quartz increased the bridge strength and showed positive synergy as compared with their separate performances.

# Table of Contents

# List of Figure

# List of Table

# List of Symbols

| | |
|---|---|
| $A_s$ | Surface area exposed to shear [$m^2$] |
| F | Applied Force [N] |
| $G^{'}$ | Storage modulus [Pa] |
| $G^{''}$ | Loss modulus [Pa] |
| k | Consistency index [lbf $s^n$/100sqft] |
| n | Flow index [dimensionless] |
| $N_{Re}$ | Reynolds number [dimensionless] |
| r | Radius [m] |
| t | Time [s] |
| v | Velocity [m/s] |
| $\dot{\gamma}$ | Shear rate [$s^{-1}$] |
| $\delta$ | Phase angle [degrees] |
| $\mu$ | Viscosity [cP] |
| $\mu_a$ | Apparent viscosity [cP] |
| $\mu_P$ | Plastic viscosity [cP] |
| µm | Micrometer |
| $\gamma_o$ | Shear strain amplitude |
| $\tau_o$ | Shear stress amplitude [Pa] |
| $\tau_y$ | Yield stress [lbf/100sqft] |
| $\omega$ | Angular frequency [rad/s] |

# List of Abbreviations

| | |
|---|---|
| AV | Apparent viscosity |
| BHP | Bottom hole pressure |
| bbl | barrel |
| $CaCO_3$ | Calcium carbonate |
| DIF | Drill-in fluid |
| DF | Drilling fluid |
| ECD | Equivalent circulating density |
| FCS | Fracture closure stress |
| HPHT | High pressure high temperature |
| IPT | Ideal packing theory |
| K | Potassium |
| LCM | Lost circulation material |
| MW | Mud weight |
| MPa | Mega pascal |
| Na | Sodium |
| NP | Nanoparticle |
| NPT | Non-productive time |
| NADF | Nonaqueous-Based Drilling Fluid |
| OBM | Oil-based drilling fluids |
| PSD | Particle size distribution |
| PV | Plastic viscosity |
| PDC | Polycrystalline diamond compacts |
| RPM or rpm | Revolutions per minute |
| ROP | Rate of penetration |
| TVD | True vertical depth |
| UIS | University of Stavanger |
| WBM | Water-based drilling fluids |
| WSM | Wellbore strength material |
| wt | Weight |
| YP | Yield point |

# 1 Introduction

This thesis presents the experimental study of loss circulation materials (i.e Nutshell, Pistachio-nutshell, $CaCO_3$ and Quartz) in the Potassium -and Sodium-fomate drilling fluids. The birding performance of the LCM materials were tested at 100, 150, 175, 200, 250 micrometer (μm) artificial fracture, slots. During the test, the effect of single, and hybrid particles were evaluated.

## 1.1 Background

Figure 1.1 shows a typical rotational drilling system. Drilling through the geological formation is conducted by the action of the drill bit that is connected at the bottom of the drill string. In the rotary system, drilling fluid is circulated. The function of the drilling fluid among others is to maintain well pressure, lubricate and cool the wellbore and the bit as well as to bring cuttings to the surface [1].

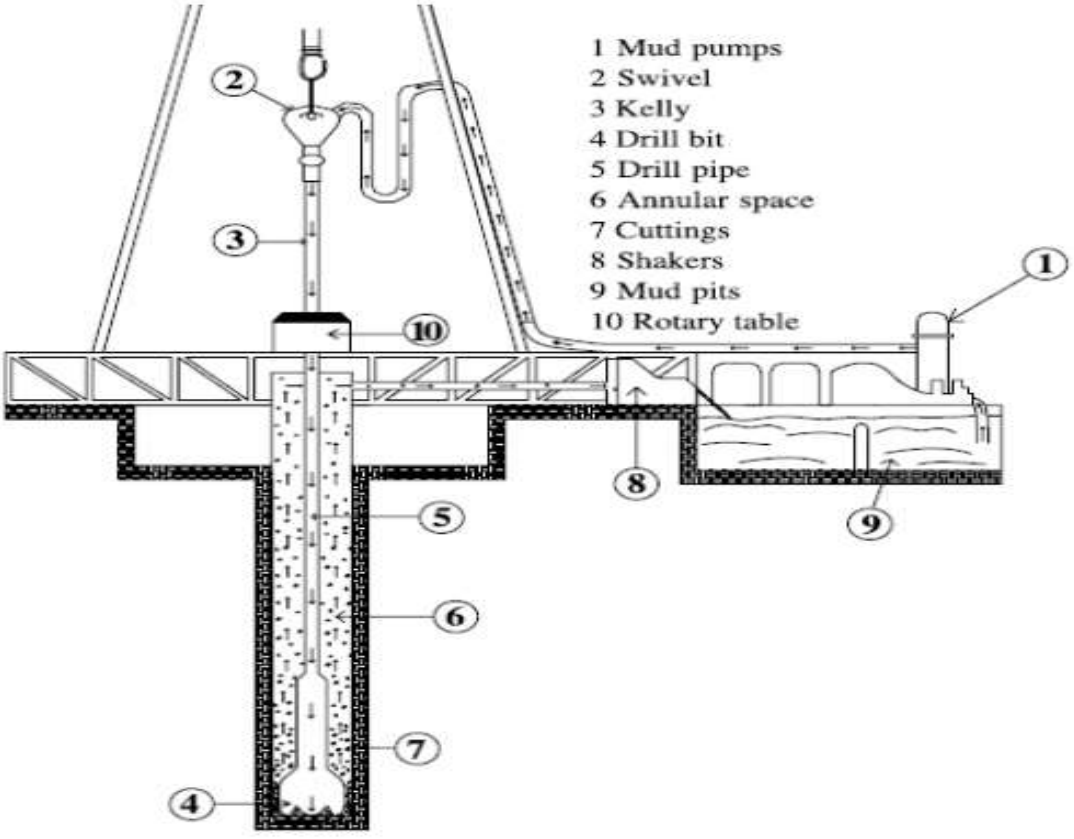


Figure 1.1: Drilling system [2]

During drilling, the well pressure is determined from the circulation pressure and the static drilling fluid weight, from which the Equivalent Circulating Density (ECD) is calculated as [3]:

$$ECD\ (sg) = \rho_{static} + \frac{\Delta P_{annulus}(bar)}{0.0981.TVD(m)} \quad (1.1)$$

Where,

- $\rho_{static}$ the density of drilling fluid at static condition
- $\Delta P_{annulus}$ is the annular pressure loss, which is a function of flow rate, density of fluid, the rheological parameters of the drilling fluid and annular flow path
- TVD is the true vertical depth of the well

The ECD is a key parameter to consider in regard to lost circulation, specifically in depleted zones and deep-water formations. Drilling through depleted zone can lead to lost circulation due to reduction of mud weight windows. As is shown in figure 1.2 (a), the reduction in pore pressure results in a corresponding reduction in fracture gradient, making it very demanding to maintain ECD [4].

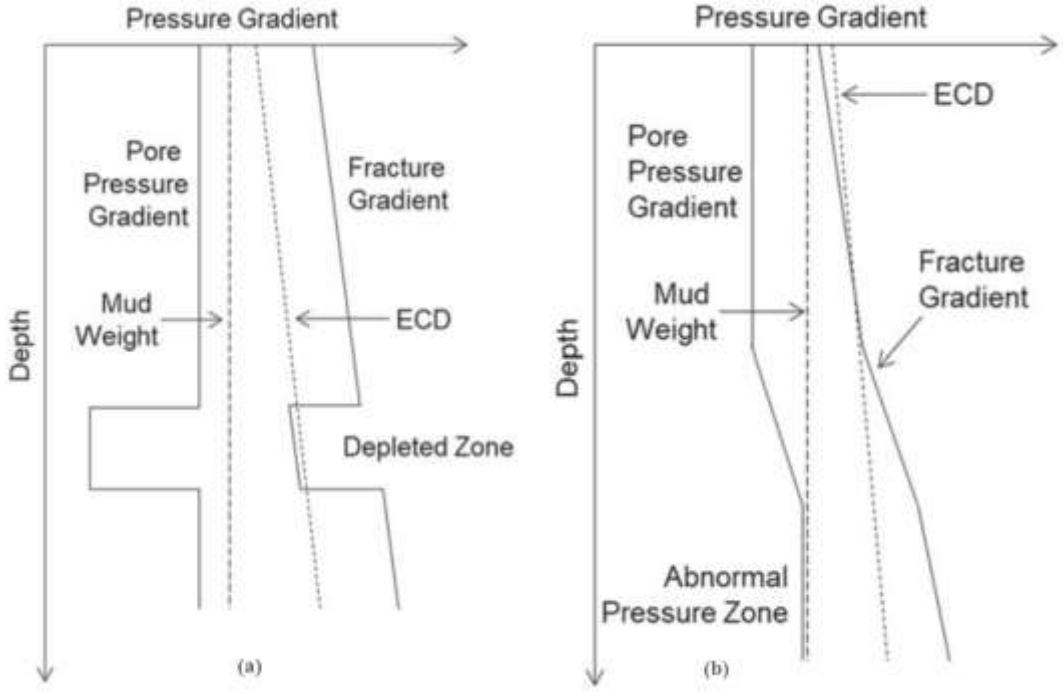


Figure 1.2: (a) Pore pressure and fracture gradient plot in depleted zone. (b) Pore pressure and fracture gradient plot in deep-water formation with abnormal pressure zone [4].

In addition, as sea water does not provide as much overburden loading as sediment and rock, the total vertical stress may be very low in deep-water formations. If abnormal pressures are also present, the drilling fluid weight window may become further narrow. This scenario is shown in figure 1.2 (b), and under these circumstances, it may be challenging to avoid hydraulic fracturing and maintain the proper wellbore pressure. Moreover, having pre-existing fractures in the formation can have a substantial effect on the pressure capacity of the wellbore. The tensile strength of the formation may decrease when small pre-existing fractures are present in the wellbore rock, leading to a small mud weight window. If mud pressure in the wellbore exceeds the specific fracture gradient, the fracture may propagate, and cause severe lost circulation unexpectedly [5]. The uncontrolled leakage of drilling fluid into the formation during drilling is known as lost circulation or lost returns [6]. Lost returns are partial or entire loss of drilling fluid into the formation, and it has been a major cause of non-productive time (NPT) in the drilling industry. The drilling operation must be stopped when fluid losses are too large, or no drilling fluid returns are experienced. However, the drilling operation may continue when the loss rate is small and partial fluid returns can be maintained [4,7]

The fluid level in the well annulus may drop if large fluid losses occur. Consequently, the bottom hole pressure (BHP) may become insufficient to balance formation pressure, resulting in a fluid flow from the formation into the borehole. In addition, the lower BHP may cause wellbore collapse, where the consequence may be stuck pipe and buried drilling tools. These incidents further increase drilling operation costs and NPT [4].

Studies from European wells have shown that due to the technological PDC development, the drilling rate per day increases. However, as shown in the figure 1.3 and 1.4, the NPT kept maintaining flat up to 25%. [8]. In deep-water environments, in the Gulf of Mexico, NPT associated wellbore integrity that includes stuck pipe, wellbore collapse, sloughing shales and lost circulation account for about 44% of nonproductive time (NPT) [9]. Figures 1.5 and 1.6 show the NPT in offshore and onshore. According to Pilisi et al, about one third of the overall NPT incidents is due to loss circulation (>10%), kick (>10%) and stuck pipe (>10%) [10]. In terms of cost, the wellbore integrity related NPT increased the overall drilling budget by about 10% to 20% [11].

From the reviewed information, we can observe that NPT alone costs a lot for the industry. Among others, loss circulation is an issue in the industry. This thesis will therefore experimentally study the bridging performance of LCM materials to be used for reservoir sections. For this, the LCM materials used to evaluate are the one suitable drill-in formate based

drilling fluids. Hydraulic fracturing experiments using drill-in Cesium/potassium-formate and $CaCO_3$ with and without Quartz showed that the LCM increased the wellbore strength [12]. In this present thesis, other alternative LCM material for the reservoir section to be used are evaluated with artificial fracture slots. These are Nutshell, Pistachio nutshell, $CaCO_3$ (micro and nanosized) as well as their blending with Quartz are evaluated. The main reason for the selection of Pistachio shell is that it is mechanically strong, acid soluble as well as reduces filtrate loss [13]. These properties are believed to be suitable like $CaCO_3$ currently used for the reservoir section as LCM when drilling with formate based drill-in fluids.

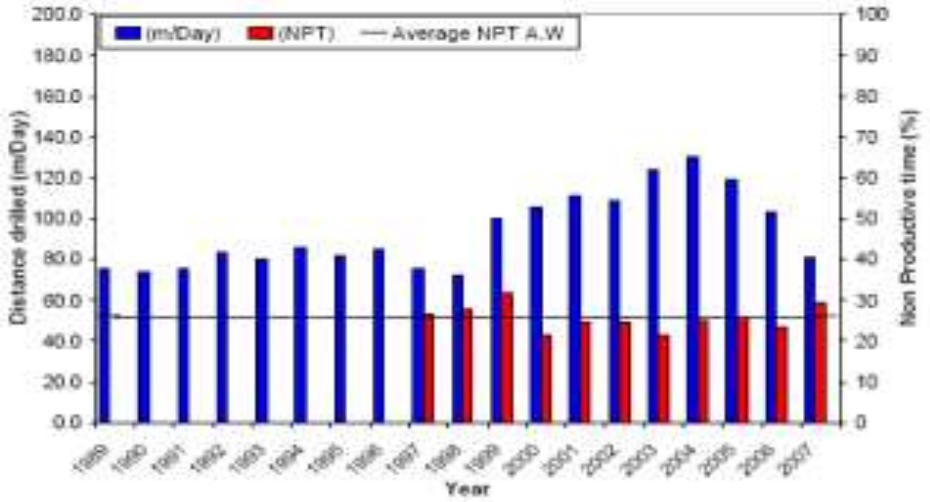


Figure 1.3: NPT and drilling distance per day of 5900 wells all types [8].

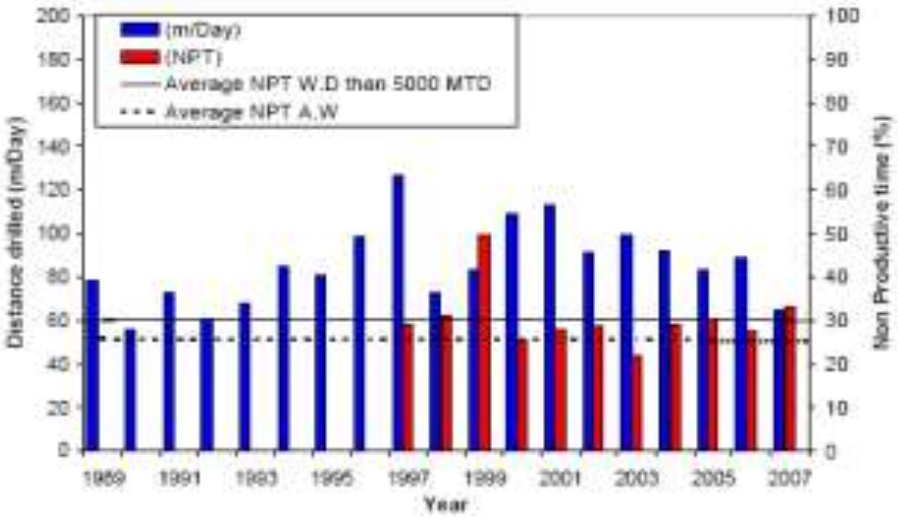


Figure 1.4: NPT and drilling distance per day of 5900 wells where MD >5000m [8].

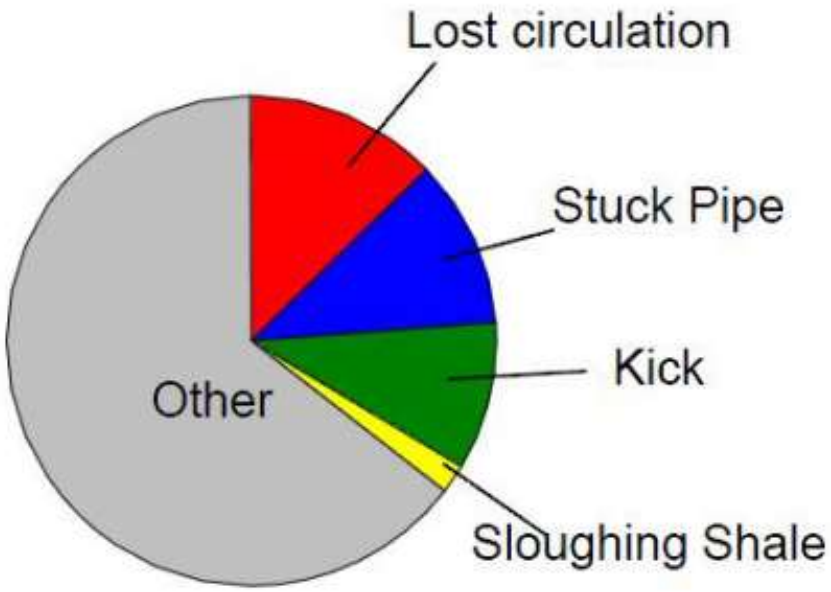


Figure 1.5: Main sources of non-productive times [10].

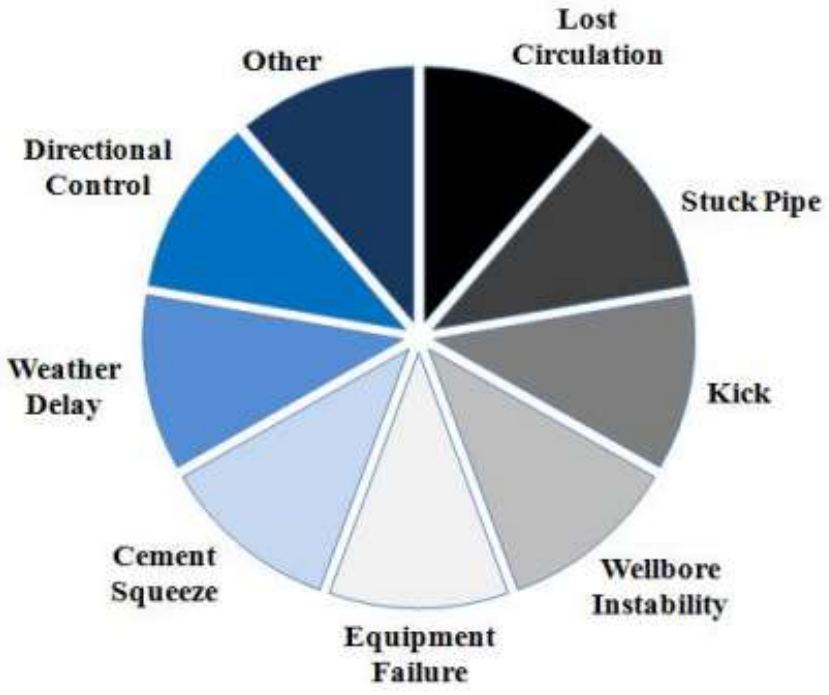


Figure 1.6: Source of non-productive time for onshore wells [10].

## 1.2 Scope and Objective

Drill-in fluids are commonly used to drill reservoir sections. The drill-in fluids do not contain barite in order to avoid the possible formation damage due to the barite particle deposition in the pore spaces around the wellbore. In the absence of barite, the drill-in fluids use heavy brine such as cesium formate, potassium formate to control the weight, and $CaCO_3$ as LCM material. Reference [14] gives a good overview of several fields that are drilled with barite free, drill-in fluids. In the North Sea, Martin Linge, Total drilled reservoir section with cesium/potassium-formate based drilling fluid [15].

As mentioned earlier in reference [12], the $CaCO_3$ and Quartz LCM has shown a self-healing mechanism of fractured wellbore and increases wellbore strength. To learn more the bridging performance of the commonly used $CaCO_3$ LCM material and the alternative material to be used in the reservoir, this thesis activities deal with investigating:

- The performance of Quartz, $CaCO_3$ and their blending to evaluate if there is positive or negative synergy
- The performance and comparisons of alternative LCMs (Nutshell and Pistachio shell) in drill-in fluids
- The impact of particle size spectrum designed based on small, medium, and coarse on bridging performance
- The performance of the LCM materials in K-formate and Na-formate based drill-in fluids to evaluate if the atomic weight /ions have impact on the bridging performance
- Data analysis of the bridging test dataset for better evaluation of the LCM bridging performances.

# 2 Literature study

This chapter presents a brief introduction about the drilling fluid, loss circulation, loss circulation management as well as drilling fluid characterization theory for rheology and viscoelasticity. The theory will be used to quantify the fluids properties in chapter 4.

## 2.1 Drilling fluid

Drilling operation success depends heavily on properties of the drilling fluid. The cost of the drilling fluid alone is not very high in comparison to the overall cost of drilling fluid, but the correct selection of drilling fluid and maintenance of its properties during drilling extremely influence the overall well costs. For instance, the time required to drill to total depth depends on the rate of penetration (ROP) of the bit, and the avoidance of drilling problems such as loss of circulation and stuck pipe, all of which are influenced by properties of the drilling fluid. The selection of a suitable drilling fluid and its properties are the concern not only of the mud specialist, but also other engineers who are involved in the completion of the well. A detailed knowledge of drilling fluid is not necessary for all personnel, but it is important to understand the basic principle governing their behavior and the relation of these principles to drilling and production performance [16].

### 2.1.1 Functions of drilling fluid system

The main purpose of a drilling fluid includes [16, 17], providing appropriate well pressure that prevents inflow of formation fluids into the wellbore and minimize causing fractures in the wellbore. The ECD that controls these functions can be achieved by monitoring the density -and the rheological parameters of the drilling fluids. Transporting rock cuttings to the surface. The cutting lifting efficiency of the drilling fluids are controlled by the flow velocity, the rheological and density of the drilling fluid. Hold cuttings and weighting additives in suspension during static -and dynamic circulation process. Here, as well the rheological, gel strength and density of the drilling fluids are the main controlling parameters. Form a filter cake that is impermeable and thin on the borehole walls. The filter cake seals pores and small fractures, thus, reducing mud loss into a permeable formation. This function is achieved by monitoring and optimizing the particle size distribution (PSD) of the solids and maintaining the proper wellbore strengthening materials.

Other functions of the drilling fluids are:

- Cooling and lubricating the rotating bit and drill string
- Support drill string and casing weight
- Allows logging data transmission through and transmit hydraulic horsepower to the bit

### 2.1.2 Classification of drilling fluid systems

Drilling fluid systems are classified according to their base fluid. A classification of drilling fluids regarding their base fluid is shown in figure 2.1 [16].

- Water-Based Muds (WBM). Water is the continuous phase. Viscosity and density control solid particles are suspended in water or brine.
- Nonaqueous-Based Drilling Fluids (NADF). Oil is the continuous phase. Brine water or another low-activity liquid is emulsified, and solid particles are suspended in oil.
- Pneumatic Systems. In this system drill cuttings are removed by a high- velocity stream of air, natural gas, methane, nitrogen, or carbon dioxide.

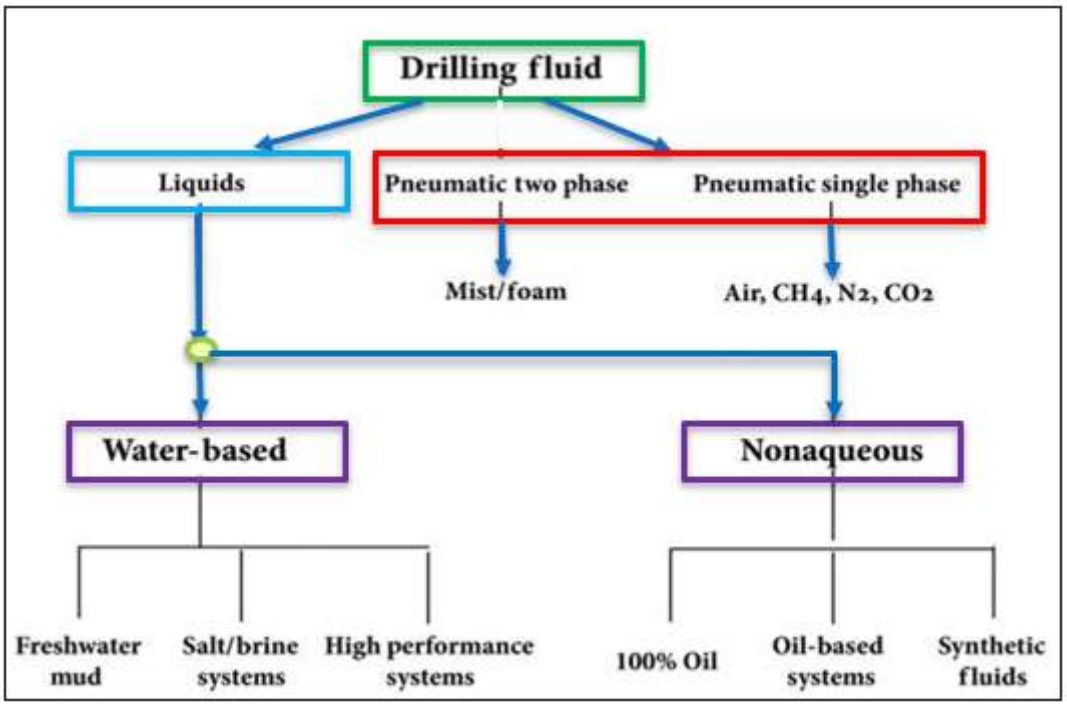


Figure 2.1: Drilling fluid systems by base fluid [16].

## 2.2 Potential types of mud loss zones

Drilling fluid loss can occur during any drilling operation where a drilling fluid is pumped down the hole. The following two conditions must be taken in place for lost circulation to occur [3].

- There must be a formation with flow channels that allows drilling fluid to flow from the well and into the formation.
- The fluid present in the well must be in overbalance or positive pressure differential between the borehole and formation.

Figure 2.2 illustrates the four most common lost circulation zones that are encountered during drilling of hydrocarbon wells. This drilling fluid can be lost into fractures induced by excessive mud pressures, into natural fractures, cavernous- and highly permeable formations. Each of these conditions are discussed further below. Induced fractures

The mechanism of induced fracturing is like hydraulic fracturing, but hydraulic fracturing is deliberate and desirable, while the induced fracturing is unintentional and most unwelcome. These fractures can be induced in any type of rock but are most common in weak formation such as shale. A fracture is induced when the borehole pressure exceeds the tensile strength of the formation. In general, in a drilling well, drilling fluid density must be kept great enough to control formation fluid, but not so great as to induce a fracture. Fractures induced by too high mud pressures are known to cause loss of circulation in wells [3, 16].

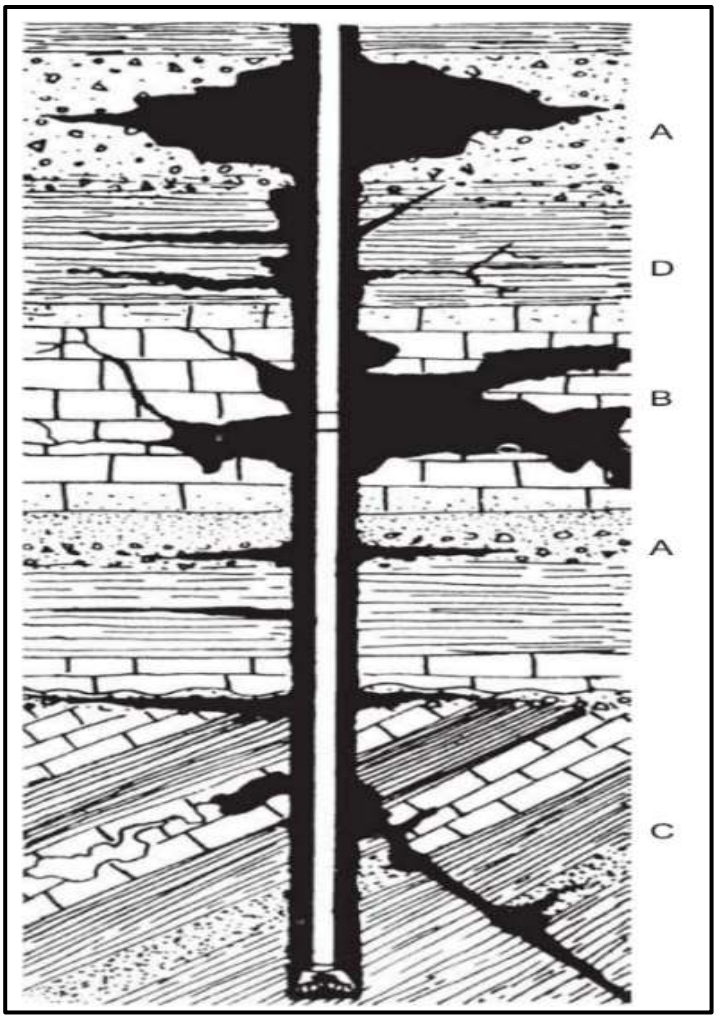


Figure 2.2: Lost circulation zones: A) Permeable, B) Caverns, C) Natural fractures D) Induced fractures [3]

### 2.2.1 Natural fractures

Natural fractures may occur in any type of rock. A complete loss of drilling fluid may be encountered if drilling is continued, and more natural fractures are exposed. These fractures may be either horizontal or vertical depending on formations depth, mechanical properties, and stress environment. The presence of natural fractures in a reservoir is desirable from the aspect of well productivity but is a problem during drilling. The drilling fluid level decreases gradually in the mud pit with a horizontal fracture network but will take progressively increasing amounts of mud as drilling progresses and more of the vertical fractures are exposed [3].

### 2.2.2 Highly permeable zones

Lost circulation into highly permeable formations most often manifest itself as a gradual drop in pit level. If drilling is continued and more formations with high permeability are exposed, such as unconsolidated formation, gravel beds, loose conglomerates and shallow or highly depleted sandstone, there can be a complete loss of drilling fluid [3].

### 2.2.3 Cavernous formations

Cavernous or extremely vugular formations are most limited to limestones that have been leached by water. The most severe lost circulation problems occur when large voids spaces in these formations are encountered [3].

There are several situations that can result in lost circulation with various severity. The severity of lost circulation depends on the types of loss zones and it is mainly classified based on loss rate in terms of cubic meter per hour or barrels per hour; seepage is approximately 10 bbl/h (1.5$m^3$/h), partial is between 10bbl/h to 50bbl/h (1.5$m^3$ /h to 7.5$m^3$ /h), severe loss is more than 50bbl/h (7.5 $m^3$ /h) and total loss, there is not any return back to mud pit [18].

Seepage losses can occur with any type of loss zone but are most common in unconsolidated formation and gravel beds with high permeability and porosity. Partial loss of drilling fluids might occur in unconsolidated sand, gravel, and natural or induced fractures and are defined as those drilling fluid losses that still give returns to surface. Severe loss is a scenario where drilling fluid continues to flow into formation with higher degree because of large natural or induced fractures or highly permeable unconsolidated sand or gravel. A sudden and total loss occurs normally in vugular or cavernous formations, heavily fractured rocks with large fracture width [3].

## 2.3 Lost circulation material

Many lost circulation materials (LCMs) are available for combating lost circulation. However, there is not a universal LCM appropriate to all kinds of drilling fluid losses due to the complexity of formation properties and different loss zones, so that a proper LCM choice is greatly dependent on the formation types, loss zones and the severity of loss rate. In the following subsection a brief overview of LCMs is given that can be utilized to mitigate drilling fluid losses in various loss zones [4, 7].

LCMs are products utilized to bridge and seal the pores, fractures, and vugs through which the drilling fluids are lost into the formation. However, if the wrong material is used when drilling through these formations, wellbore instability issues may occur. To improve the safety and save drilling cost, it is crucial to have a good understanding of how the LCM seals off the fracture. As the drilling fluid loss ranges from seepage to severe or total loss, most LCMs are found in grades as ultra-fine, fine, medium, and coarse to accommodate a distinct scenario.

The conventional LCMs are classified based on their appearance, as granular, fibrous, and flaky. Frequently, a mixture of granular, fibrous, and flaky are used to enhance the bridging capacity of LCM. The combinations of all these materials might mitigate drilling fluid losses due to the diverse properties and particle size distributions. A fully optimized LCM should be able to seal a wide range of fracture widths [19].

### 2.3.1 Granular materials

Granular materials are a wide range of products that can form a seal at the formation face or within the fracture to prevent the losses into formation. Most frequently used granular materials to treat fluid losses include calcium carbonate, nutshells, graphite, and coarse bentonite. These materials are available in a wide particle size distribution and often used for wellbore strengthening applications due to their rigidity [19].

### 2.3.2 Fibrous materials

According to oilfield glossary, fibrous material is a type of LCM that is long, slender, and flexible material with various sizes and lengths. Fibrous materials are found in a wide range of sizes. These materials can be used both in water-based mud and oil-based mud but have some limitations when used in oil-based mud. Fibrous LCMs include saw dust, bark, cellulose fibers, and shredded paper [19, 20].

### 2.3.3 Flaky materials

Flaky LCMs is a type of lost circulation material that is thin and flat in shape, with a large surface area. This type of lost circulation material may or may not have any degree of stiffness and they can form mat over the permeable formation face. Examples of Flaky materials are mica, cellophane, and cottonseed hulls [19].

## 2.4 Description of the fracturing process

Well fracture in general when the hoop stress exceeds the tensile strength of the wellbore. The hoop stress is a function of the well pressures. in the presence of mud cake the fracture imitation growth, and particle birding phenomenon at the gate of the fracture, Aadnøy et al have presented the qualitative description of the fracturing process [21]

**Event 1: Filter cake formation**

Initially, a small filtrate loss occurs which ensures formation of a filter cake. A soft filter cake is formed due to drilling fluid flow across permeable formations. The filter cake thickness depends on the equilibrium between the filtrate attraction and the erosion due to flow.

**Event 2: Fracture initiation**

Increase in borehole pressure reversing the hoop stress in the rock from compression towards tension. The increase of filtrate loss ensures that the filter cake is in place, helping to resist the pressure in the wellbore. As the pressure reaches a critical limit the borehole wall may start to fracture.

**Event 3: Fracture growth**

A further increase in wellbore pressure results in an increase in fracture width. Fracture growth is being opposed by in-situ stress and the filter cake will remain in place because a stress bridge is formed across the fracture. The mechanical strength of particles of the filter cake is the factor that is preventing the bridge from collapsing. In this phase, both the rock stress and the strength of the filter cake resist failure.

**Event 4: Further fracture growth**

A further fracture growth is caused by a further pressure increase in the borehole. Thus, the stress bridge expands and becomes thinner. As the geometry increases the stress bridge becomes weaker.

**Event 5: Filter cake collapse**

The rock bridge collapses once a critical pressure is reached because the filter cake is no longer strong enough. The collapse occurs when the yield strength of the particles is exceeded which establishes drilling fluid flow into the formation. In other words, a loss of circulation event is initiated.

| Event | Fig | Main controlling parameters |
|---|---|---|
| Filter cake formation | 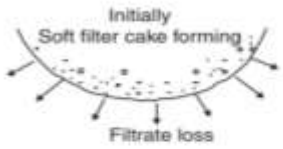 | Filtrate loss |
| Fracture initiation | 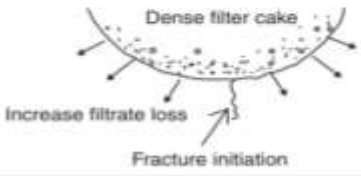 | Filtrate loss,<br>Stress |
| Fracture growth | 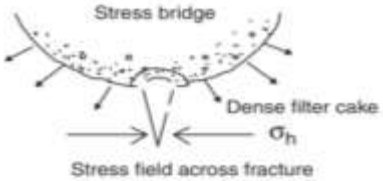 | Bridge stress<br>Rock stress |
| Further fracture growth | 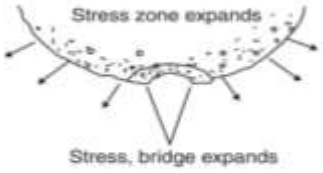 | Bridge/rock stress<br>Particle strength |
| Filter cake collapse | 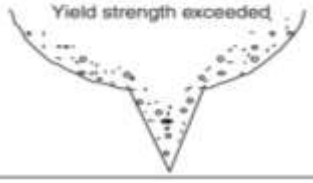 | Particle strength |

Figure 2.3: Qualitative description of the fracturing process [21].

## 2.5 Particle size distribution

Proper size gradation of the lost circulation material is important to attaining an effective bridge. That is, the LCM should contain a variety of particle sizes before it can plug a pore channel larger than the diameter of the plugging material. It is well known that using a mixture such as a combination of fine-, medium-, and coarse- sized LCMs is more effective than using only on size. Proper size gradations should be selected based on the $D_{90}$, $D_{50}$ and $D_{10}$. Several approaches have been developed in the drilling fluid industry to optimize bridging blends to seal the formation surface. The most common approaches are as follows [22- 25]:

- Abram's rule
- Ideal packing theory
- Vickers method
- Halliburton method

### 2.5.1 Abram's rule

In 1977, A. Abrams designed drilling fluid to minimize rock impairment due to particle invasion. His experiments were conducted on two different types of rock systems, and he concluded that drilling fluids containing bridging material that meets the one- third rule for bridging impair rock to depths less than 1 in. The rule requires that the average particle size of a bridging agent should be equal to or slightly greater than 1/3 the median pore size of the formation. In addition, the concentration of these bridging materials must be at least 5 percent by volume of the total solids in the final fluid mix. However, Abram's rules only address the size of the particles required to initiate a bridge. Thus, it does not give an optimum size or addresses the best packing sequence for minimizing fluid invasion and optimizing formation sealing [22].

### 2.5.2 Ideal packing theory

In 2000 Ideal packing theory (IPT) was developed by M. Dick stating IPT:

> *"which provides the full range of particle size distribution required to effectively seal all voids, including those created by bridging agents. This subsequent layering of bridging agents results in a tighter and less invading filter cake".*

This theory represents an approach to improving bridging efficiency for drilling fluids, which describes that perfect packing appears when the percent of cumulative volume versus the square root of the particle diameters creates a straight line. This concept is based on an estimation of the pore size estimated from permeability by taking the square root of the permeability [23].

### 2.5.3 Vickers method

Vickers method of particle size distribution (PSD) offers an improvement approach over the often-used Abram's rule by selecting a more effective PSD of graded LCMs for the entire range of expected pore sizes. In this rule $D_{90}$ is set equal to the largest pore throat. In addition, $D_{75}$ and $D_{25}$ are included for the bridging blend which may provide a broader range of bridging agents that might result in better bridging performance, hence minimizing fluid loss into formation. Moreover, the Vickers criteria suggest that the concentration of bridging agent need to be greater than 30 ppb for water-based fluid but may be reduced for oil-based fluid. All five Vickers criteria are listed as below [24]:

- $D_{90}$ = largest pore throat
- $D_{75}$ < 2/3 of largest pore throat
- $D_{50}$ +/- 1/3 of the mean pore throat
- $D_{25}$ 1/7 of the mean pore throat
- $D_{10}$ > smallest pore throat

### 2.5.4 Halliburton method

This method was developed to select the best suitable particle size distribution to form a bridge just at or just inside the point of fracture initiation. The main goal of this was to isolate pressure communication between mouth- and tip of the fracture. Pressure isolation between these two points may stop further fracture development. To ensure that both smaller and larger particles are present to seal both smaller and larger fracture widths, the $D_{50}$ of the PSD is set equal to the estimated fracture width to offset uncertainty in the estimation [25].

## 2.6 Wellbore strengthening treatments

The risk of borehole tensile failure, with subsequent drilling fluid loss is huge during drilling depleted zones with a high overbalance, or fracture which has been induced during drilling operations, or was pre-existing natural fracture. To minimize these risks, the wellbore strengthening theory has been developed. Two of the theories are the stress cage, and fracture closure stress theory.

### 2.6.1 Stress cage model

According to the stress cage model, wellbore strengthening can be achieved by changing the stress state around the borehole. The hoop stress around the borehole is increased by deliberately allowing fractures to form in the wellbore wall and sealing them with bringing agents of sufficient size and concentration, so that they act as a proppant and consequently isolate fluid pressure in the wellbore from most of the fracture. The fluid trapped beyond the bridge can eventually dissipate to the formations pore pressure and the fracture will attempt to close. The attempted closure of the fracture onto the blockage creates compression at the blockage which increases the hoop stress. However, the ability to form a blockage in the fracture will depend on the fracture aperture and particle sizes within the mud [26, 27]. Figure 2.4 shows an illustration of particle plugging at the mouth of the fracture and the hoop stress increment to form stress a cage [28].

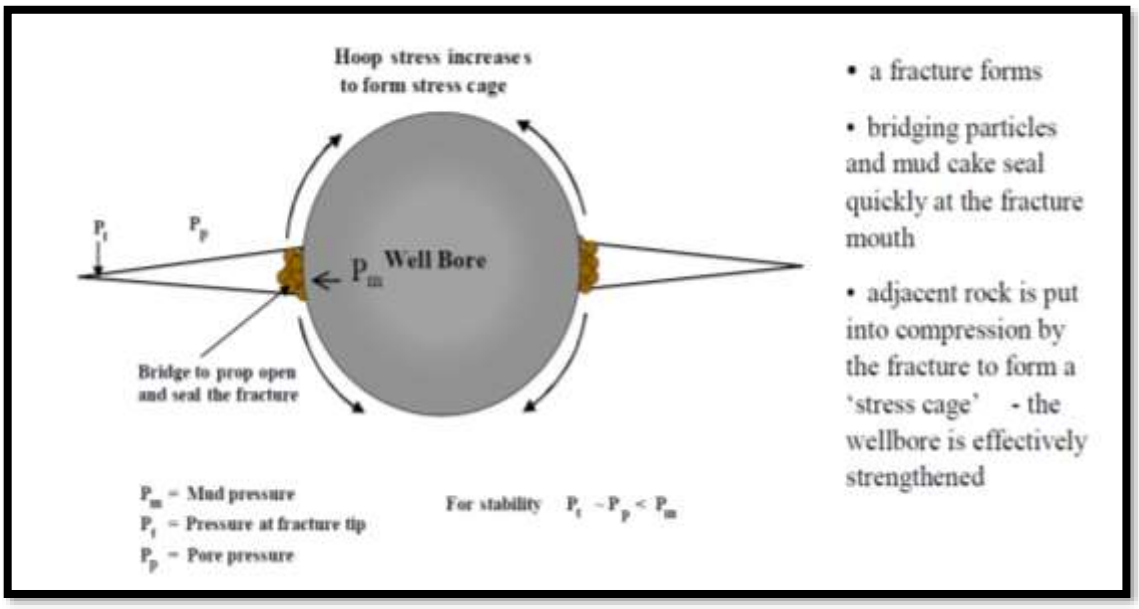


Figure 2.4: Stress cage theory for wellbore strengthening effect [28]

Figure 2.5 (a) and 2.5 (b) also illustrate the fracture sealing in permeable rocks that experience leakage through the wall of the fracture and the fracture sealing in the impermeable rock without leak off [28].

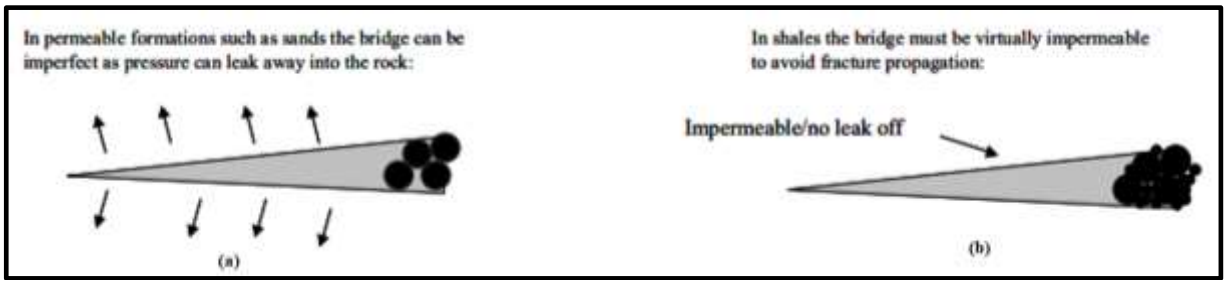


Figure 2.5: (a) Fracture sealing in permeable rock and fracture sealing in impermeable rock (b)[28]

Aston et al [28] have conducted field extended leak-off tests with designer fluid, which contained 80 ppb bridging solids ranging from 10 to 800 microns. The LCMs are the blending of graphitic/calcium carbonate. The leak-off test using the pill is shown in figure 2.6 compared with the conventional drilling fluids. Results showed that the particles sealed the fracture and increased the pressure over 2000psi before the bridging collapse. This example shows that LCM materials are used as a preventative treatment and increase the wellbore strength as well. The mechanism for fracture pressure increment is due to the presence of particles illustrated in figure 2.4 and then forming a stress cage.

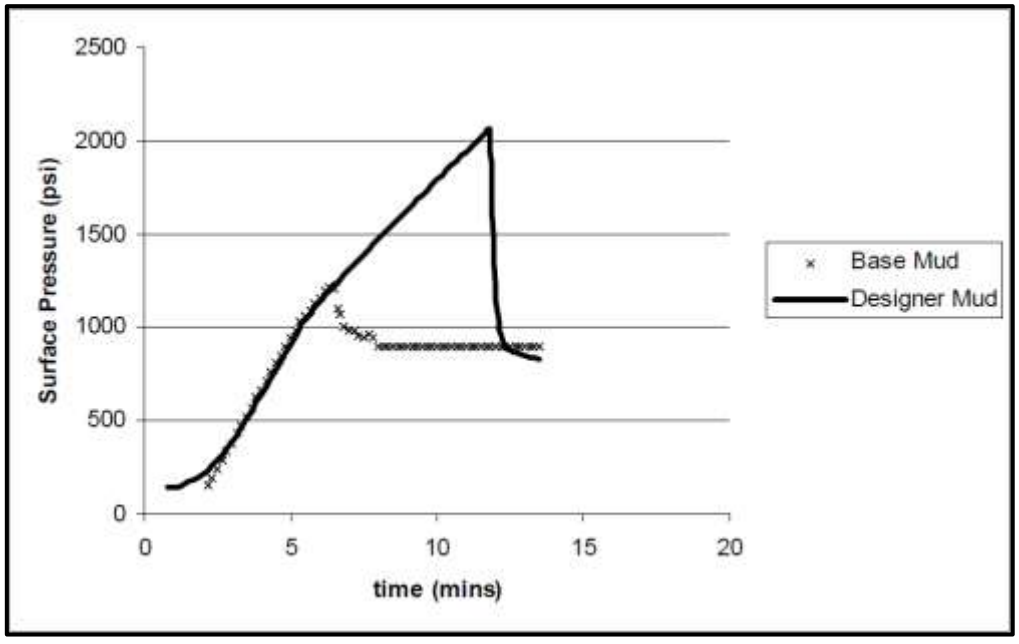


Figure 2.6: Effect of LCM on the extended leak-off test basin [28]

In reference [11], hydraulic fracturing tests were conducted on a hollow cylinder. The test results showed that the blending of 2wt% micron sized Quartz LCM with the cesium/potassium-based drilling fluid increased the fracturing and re-fracturing pressure by 6.5% and 5.4% respectively.

### 2.6.2 Fracture closure model

Dupriest (2005) proposed the fracture closure stress (FCS) model, which is quite similar to the stress cage model [29]. Both result in an increment of hoop stresses around the well. Figure 2.7 shows schematic of the fracture closure stress model. The fundamental of the FCS technique is to increase the fracture closure stress by increasing fracture width, and particles are forced deep within the fracture. Thus, the fracture closure stress in the formation is increased [29].

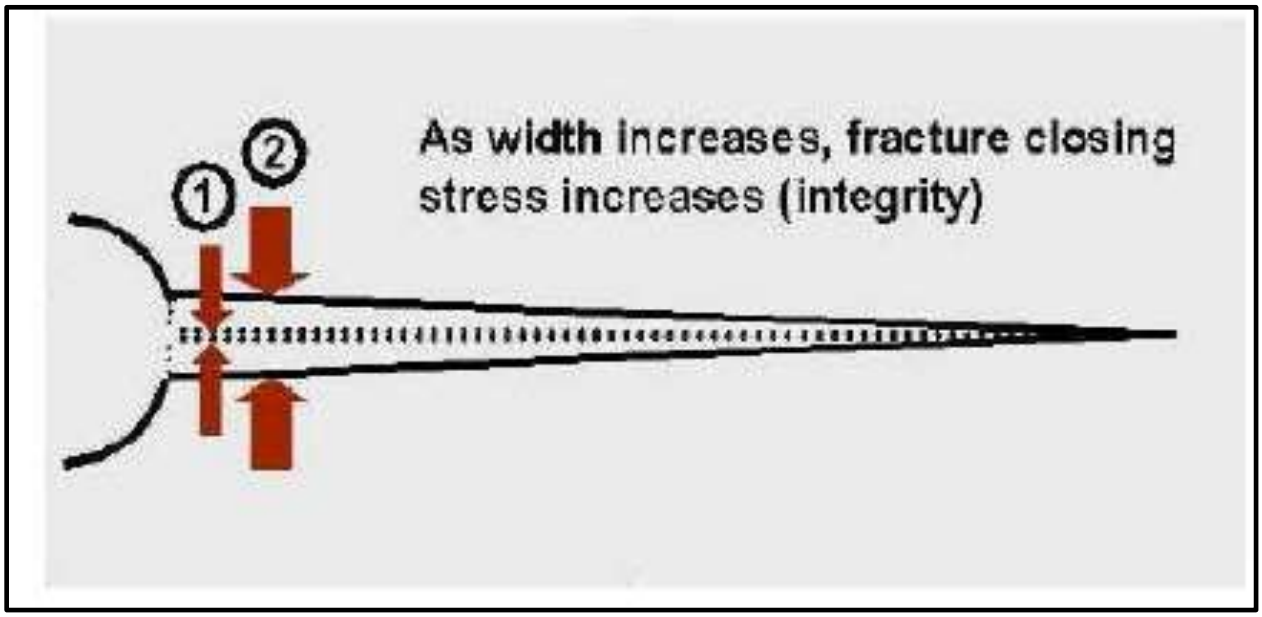


Figure 2.7: Schematic of the fracture closure stress model [29].

Figure 2.8 A-D: shows the processes of the fracture width build up by isolating the tip with an immobile mass. As a result, it allows to apply more pressure as more materials are deposited in layers [29].

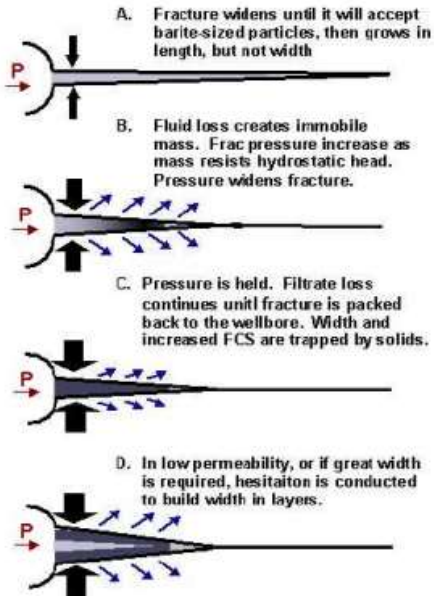


Figure 2.8 A-D: Processes of wellbore strengthening [29]

## 2.7 lost circulation management

Although materials and techniques used to combat circulation loss problems vary, techniques and approaches to mitigate the drilling fluid loss issues may be classified as preventive and remedial treatments as shown in figure 2.9.

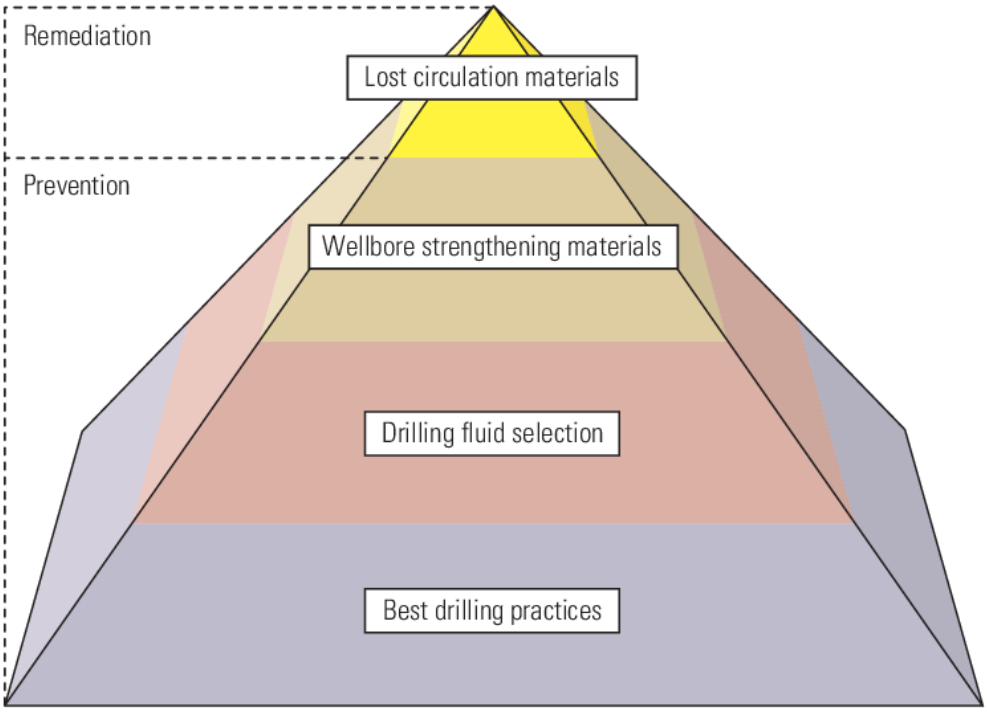


Figure 2.9: Loss circulation management program to select proper method to mitigate lost circulation [9].

### 2.7.1 Preventive treatments

As shown figure 2.9. the preventive actions include wellbore strengthened materials, drilling fluid selections as well as best drilling practices. The best drilling practices deal with designing of the appropriate well collapse and well fracturing profiles as shown in figure 1.2. Based on the allowable operational window bounded by the fracture and collapse gradient, the right ECD can be determined that avoids well instability issues. When it comes to drilling fluid selection, it deals with designing of drilling fluid that control the proper hydraulics performance and has good mud cake properties to minimize fluid loss. These are related with the rheological and filtrate properties of the drilling fluids. Studies have shown that loss circulation materials increase the wellbore strength [28,30]. Moreover, loss circulation material prevents huge mud loss by birding at the mouth of the fracture. For this, designing the right size and particle types are the key elements for efficient wellbore strengthening and preventing losses.

### 2.7.2 Remedial treatments

The second part of loss circulation management as shown in the top of the pyramid is the remedial action of mud losses by using loss circulation materials. Depending on the severity of the losses, the commonly used method is to conduct remedial action in order to minimum further losses. This can be conducted as a cure by conditioning the drilling fluid by loss circulation materials or by using stop loss pills. This thesis will evaluate preventive performance of nutshells, $CaCO_3$ and Quartz. Here, the effect of particle size spectrum and synergy of particles will be investigated.

***Loss Circulation Treatment Decision Tree for Field Application Example***

Different companies do have different decision trees for loss circulation management. Depending on the severity of the loss, the practical application is to design loss circulation treatment decision trees. Figure 2.10 shows an illustration of the decision tree workflow to manage a lost circulation problem, which is designed for preventive and corrective actions [31]. As shown in the figure, the corrective action is conducted based on the seepage or partial loss, severe loss, and total loss per hour. The detail is beyond the scope of the thesis except for indicating the practical application of loss circulation management in the industry.

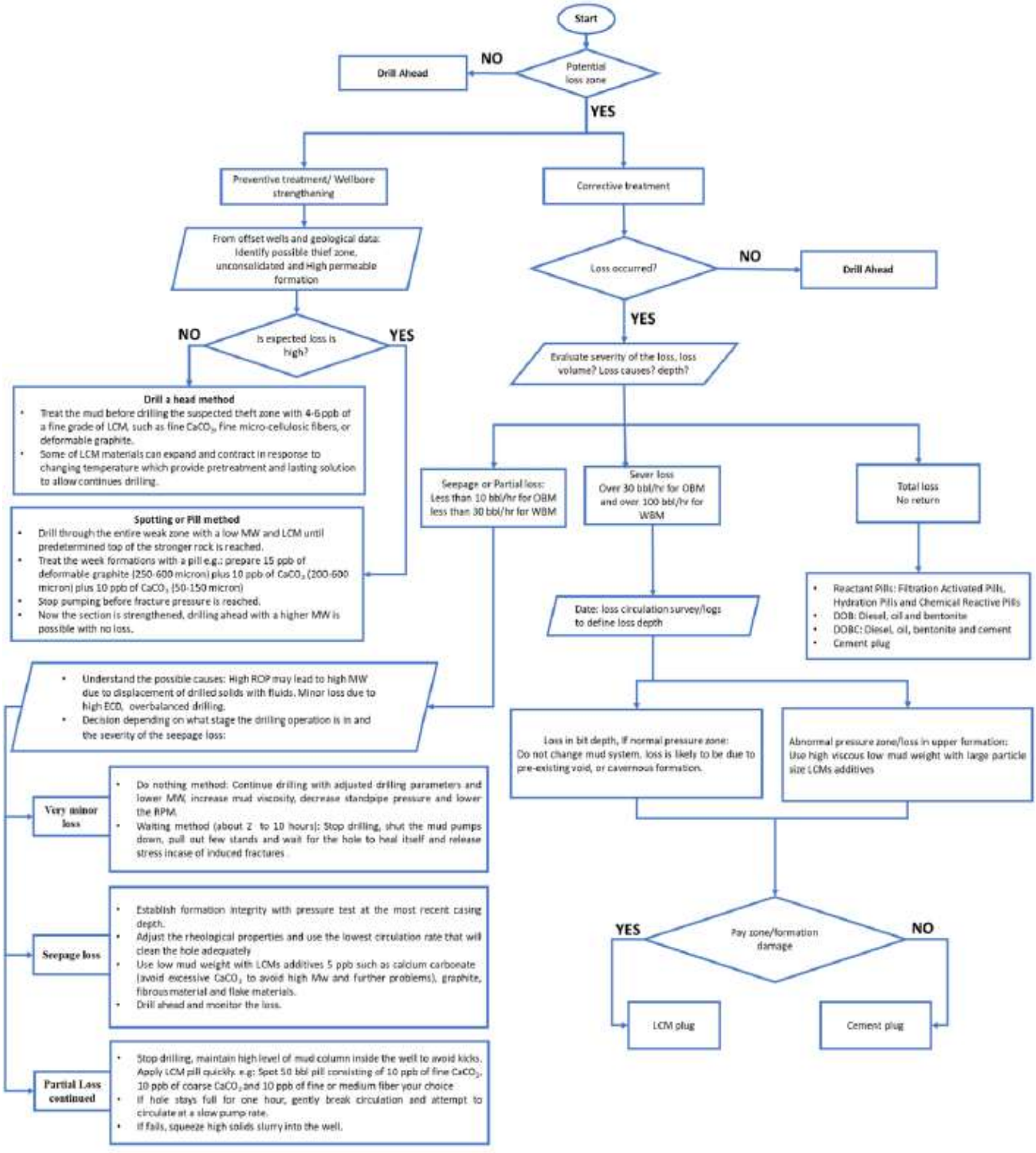


Figure 2.10: Workflow for Loss circulation prevention and corrective action treatment [31]

## 2.8 Rheology

Rheology is the theory of deformation and flow of matter and is especially important in the characterization of drilling fluids [32]. Rheology can help us understand and explain the behavior of the fluids under a variety of conditions including pressure, temperature, and external forces. Drilling fluid flow properties are characterized based on specific parameters. Examples of rheology parameters that explain the flow behavior of the drilling fluid are as following:

- Flow regime (laminar/ turbulent)
- Viscosity (plastic viscosity & apparent viscosity)
- Yield point
- Gel strength
- Shear stress & shear rate

### 2.8.1 Viscosity, Gel strength and Yield stress

Fluid viscosity is a measure of the internal friction of a fluid (μ). Fluid flows in layers with one layer sliding over the other through a pipe. The fluid layer in the centre of the pipe moves faster than close to the boundary layers. The internal friction arises between these layers as they slide over one another is called shear stress [33].

**Shear stress**

Shear stress is defined as the force required to sustain the movement of a particular type of fluid flowing through an area [34].

$$\tau = \frac{F}{A_s} \tag{2.1}$$

Where:

- $\tau$= Shear stress [Pa]
- F= The force applied [N]
- $A_s$= Surface area exposed to shear [$m^2$]

**Shear rate**

Shear rate is the rate at which fluid layers move past each other [34]. Mathematically,

$$\dot{\gamma} = \frac{v}{r} \qquad (2.2)$$

Where:

- $\dot{\gamma}$ = Shear rate [$s^{-1}$]
- v = Velocity [m/s]
- r = Distance from tubing wall [m]

**Plastic viscosity**

As mentioned earlier, viscosity is the resistance of a fluid to flow, and plastic viscosity is the mechanical friction resistance that occurs in the drilling fluid. For a Newtonian fluid, the relationship between viscosity is defined in terms of the shear stress and shear rate [35].

$$\mu = \frac{\tau}{\dot{\gamma}} \qquad (2.3)$$

Where:

- $\mu$ = viscosity [cP]
- $\dot{\gamma}$ = Shear rate [$s^{-1}$]
- $\tau$= Shear stress [Pa]

**Gel strength**

Gel strengths describe the stiffness of the drilling fluid during static conditions. This property is one of the most important because it demonstrates the ability of the fluid to suspend drill solid and weighting material when circulation is stopped. The gel strength of drilling fluid is measured with the viscometer [35].

**Yield point**

Yield point in drilling fluid is defined as the necessary force per area to be applied for a fluid to flow. Yield point and gel strengths are somewhat related in that yield point will decrease as the gel strengths decrease [35].

## 2.8.2 Rheological models

### 2.8.2.1 Newtonian fluids

Newtonian fluids are those fluids that obey Newton's law of viscosity, and particles in these fluids are no larger than fluid molecules. Thus, the viscosity of these fluids remains

constant, no matter the amount of shear applied for a constant temperature and pressure. Newtonian fluids have a linear relationship when shear stress plotted versus shear rate. Fluids such as water, mineral oil, solutions of low-molecular weight inorganic salts, and alcohol can be characterized as a Newtonian fluid. Mathematically, a Newtonian fluid is defined by equation 2.4. From the equation 2.4, we can see that shear stress is proportional to the rate of shear. The constant of proportionality is dynamic viscosity [36,37].

$$\tau = \mu\dot{\gamma} \tag{2.4}$$

Where:

- $\tau$ = Shear stress [Pa]
- $\mu$ = Viscosity [cP]
- $\dot{\gamma}$ = Shear rate [$s^{-1}$]

The linear relationship of a Newtonian fluid is shown in figure 2.11. Shear stress ($\tau$) plotted versus shear rate ($\dot{\gamma}$).

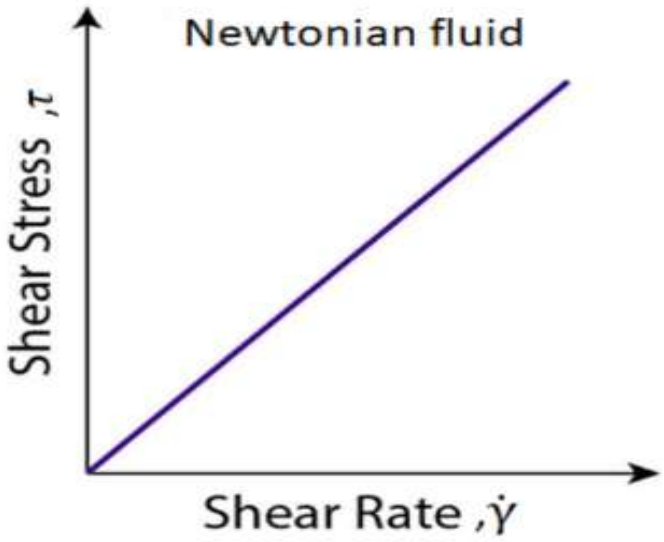


Figure 2.11: Linear relationship of shear stress vs. shear rate of a Newtonian fluid [36].

### 2.8.2.2 Non- Newtonian fluid

Non – Newtonian fluids are not described by Newton's law of viscosity. Drilling fluid is one example of non-Newtonian fluid. As shown in the figure, unlike the Newtonian fluid, the viscosity drilling fluid decreases as shear rate varies and the fluid requires an external pressure

to set the fluid in motion. It means that the applied pressure should exceed the yield stress of the drilling fluid. As displayed in figure 2.12, at zero shear rate, the non-Newtonian fluid does not pass through the origin and/ or does not result in a linear relationship between shear stress and shear rate [36,37].

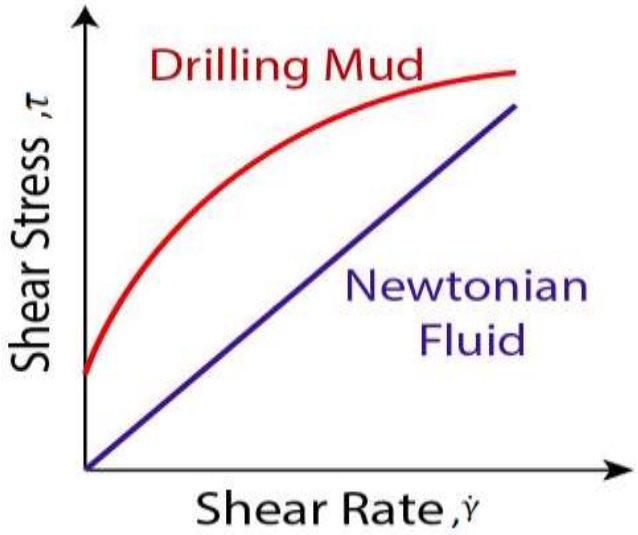


Figure 2.12: Shear stress-shear rate relationship of a drilling fluid and Newtonian fluid [36].

Different rheological models have been developed to characterize non- Newtonian fluids. The most commonly used models are Bingham plastic model, Power-law model, Herschel-Bulkley model, Unified model, and Robertson-Stiff model. All these models are briefly described in the subsections below. The models will be used to quantify the rheological parameters of the drilling fluids synthesized in Chapter 4.

#### 2.8.2.3 Bingham plastic model

The Bingham plastic model is the most used rheological model in the drilling industry to describe flow properties of drilling fluids. This model is a two-parameter model that includes the yield point where the shear rate is zero and the plastic viscosity. The plastic viscosity is the slope of the shear stress and the shear rate. This relationship is clearly displayed in figure 2.13. Bingham plastic model can be described mathematically as follows [35, 36]:

$$\tau = \tau_y + \mu_p \dot{\gamma} \tag{2.5}$$

Where:

- $\tau$ = Shear stress for Bingham plastic model $[\frac{\text{lbf}}{100\text{ft}^2}]$

- $\tau_y$ = Yield stress $[\frac{lbf}{100ft^2}]$
- $\mu_p$ = Plastic viscosity [cP]
- $\dot{\gamma}$ = Shear rate $[s^{-1}]$

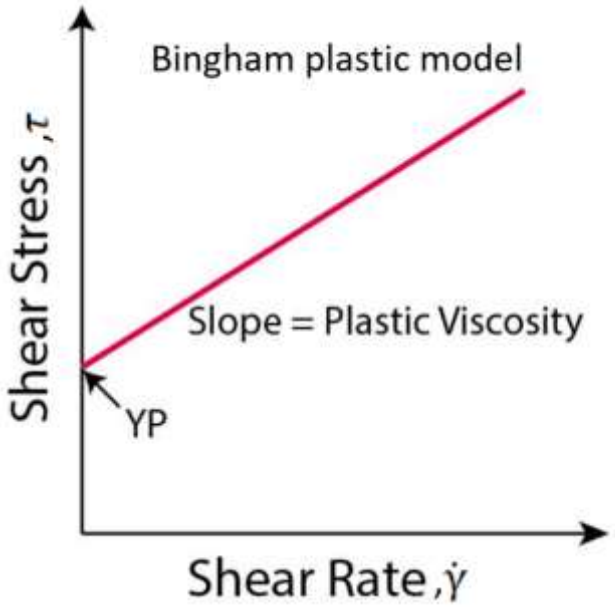


Figure 2.13: Shear stress-shear rate relationship of the Bingham plastic model [36].

As it is shown in figure 2.13, there is a requirement external pressure that exceeds the yield stress to start fluid flow, and after the fluid starts to flow there is a linear relationship between shear stress and shear rate. The Bingham plastic rheological parameters plastic viscosity($\mu_p$), the yield point ($\tau_y$), and apparent viscosity ($\mu_a$) can be determined from the measured high rotational speed viscometer data as [34, 35]:

$$\mu_p = R_{600} - R_{300} \tag{2.6}$$

$$\tau_y = R_{300} - \mu_p = 2 \cdot R_{300} - R_{600} \tag{2.7}$$

$$\mu_a = \frac{R_{600}}{2} \tag{2.8}$$

Where:

- $R_{600}$ = Viscometer dial reading at 600 RPM
- $R_{300}$ = Viscometer dial reading at 300 RPM
- $\mu_a$ = Apparent viscosity

#### 2.8.2.4 Power-law model

Power law is another API rheological model that describes the behavior of a pseudo-plastic fluid (shear-thinning fluid). Mathematically, the power law model is expressed in equation 2.9 [35, 36]:

$$\tau = k\,\dot{\gamma}^{n} \tag{2.9}$$

Where:

- $\tau$ = Shear stress for Power-law model $[\frac{lbf}{100ft^2}]$
- $\dot{\gamma}$ = Shear rate $[s^{-1}]$
- n = Flow index [dimensionless]
- k = Consistency index $[\frac{lbf^n}{100ft^2}]$

A graphical representation of the power law model is illustrated in figure 2.14. This model requires two parameters, consistency index (k) and flow behavior index (n) for fluid characterization. Flow behavior index less than one represent a shear thinning pseudoplastic fluid (n<1), flow behavior index equal one represents a Newtonian fluid (n=1), and flow behavior index greater than one represent a shear thickening fluid or a dilatant fluid (n>1). These two rheological parameters are calculated by the equation (2.10) and (2.11).

$$n = 3.32 \log\left(\frac{R_{600}}{R_{300}}\right) \tag{2.10}$$

$$k = \frac{R_{300}}{511^{n}} = \frac{R_{600}}{1022^{n}} \tag{2.11}$$

Where:

- $R_{600}$ = Viscometer dial reading at 600 RPM
- $R_{300}$ = Viscometer dial reading at 300 RPM

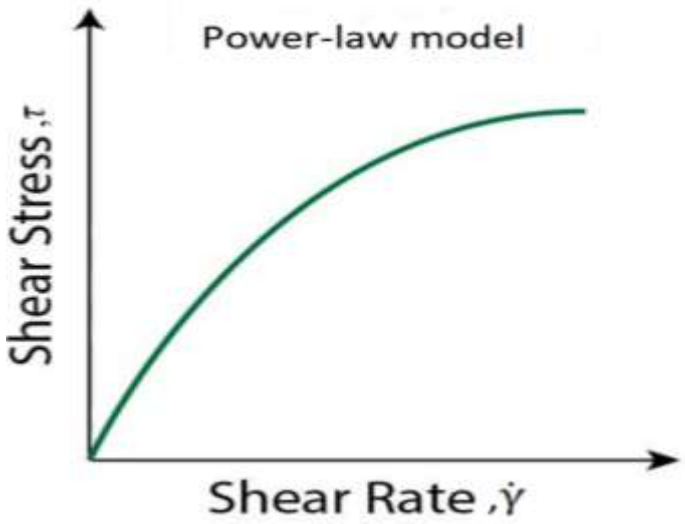


Figure 2.14: Shear stress-shear rate relationship of the power-law model [36].

#### 2.8.2.5 Herschel-Bulkley model

The Herschel-Bulkley model is basically a modified model of the Power law which includes a yield stress parameter. For most drilling fluids, the model describes more accurately than the simpler Power law and Bingham models. Mathematically, the Herschel-Bulkley model is expressed by the following equation [38].

$$\tau = \tau_y + k\,\dot{\gamma}^n \tag{2.12}$$

Where:

- $\tau$ = Shear stress for Herschel-Bulkley model
- $\tau_y$ = Yield stress
- $\dot{\gamma}$ = Shear rate
- n = Flow behavior index
- k = Consistency index

A graphical representation of the Herschel-Bulkley model is displayed in figure 2.15. The parameters n and k can be determined graphically. $\tau_0$ is determined by using equation (2.13) [38]:

$$\tau_0 = \frac{\tau^{*2} - \tau_{min} \cdot \tau_{max}}{2\tau^* - \tau_{min} - \tau_{max}} \tag{2.13}$$

The parameter $\tau^*$is determined from the corresponding geometric average value of shear rate, $\gamma^*$, which is determined by equation 2.14 [38].

$$\gamma^* = \sqrt{\gamma_{min}\gamma_{max}} \tag{2.14}$$

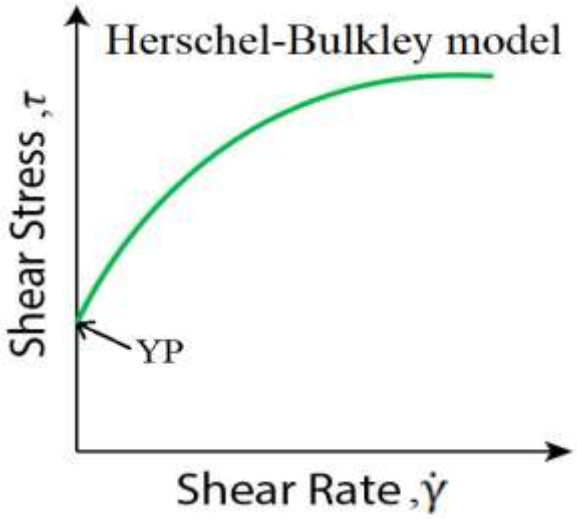


Figure 2.15: Shear stress-shear rate relationship of the Herschel-Bulkley model [36].

### 2.8.2.6 Unified model

The unified model is a modified power law model, and the expression is similar to the Herschel-Bulkely model except for the estimation of the yield stress. The model reads [38].

$$\tau = \tau_{yl} + k\,\dot{\gamma}^n \tag{2.15}$$

Where:

- $\tau$ = Shear stress for Herschel-Bulkley model
- $\tau_{yl}$ = Yield stress
- $\dot{\gamma}$ = Shear rate
- n = Flow behavior index
- k = Consistency index

Here, the yield stress ($\tau_{yl}$ ) is determined from the fann lower RPM readings as

$$\tau_{yl} = 2\theta_3 - \theta_6$$

Once the yield stress is estimated, the n and k values will be determined graphically by curve fitting.

#### 2.8.2.7 Robertson-Stiff model

Robertson-Stiff model is three model parameters, and it describes rheological shear rate and shear stress for most drilling fluids and cement slurries [39].

$$\tau = \mathrm{A}(\dot{\gamma} + \mathrm{C})^{\mathrm{B}} \tag{2.16}$$

Where:

- $\tau$ = Shear stress
- $\dot{\gamma}$= shear rate intercept
- A, B and C are Robertson-Stiff correlation parameters

The parameters, A and B are determined by curve fitting after the shear rate correction parameters (C) is estimated. The parameter C is estimated by

$$\mathrm{C} = \frac{\gamma_{\min} \cdot \gamma_{\max} - \gamma^{*2}}{2\gamma^{*} - \gamma_{\min} - \gamma_{\max}} \tag{2.17}$$

The parameter $\gamma^{*}$is determined from the corresponding geometric average value of maximum and minimum shear stress at 600 and 3 RPM reading, $\tau^{*}$, which is determined by equation 2.18 [39].

$$\tau^{*} = \sqrt{\tau_{\min}\tau_{\max}} \tag{2.18}$$

## 2.9 Viscoelasticity

Viscoelasticity is referred to the property of materials that display both viscous and elastic behavior simultaneously when undergoing deformation. The viscous part behaves according to Newton's law, and the elastic part behaves according to Hooke's law. Most of the materials are not completely solid nor completely liquid like synthetic polymers and metals at high temperature which exhibits significant viscoelastic effects. Drilling fluid is another example that exhibits viscoelastic behavior which is a very important property to evaluate gel structure, gel strength, and solid suspension [40, 41].

### 2.9.1 Oscillatory test

Oscillatory shear rheometry is the primary technique used to measure the viscoelastic behavior of drilling fluids on a rotational rheometer. Figure 2.16 shows the plate-plates model in which oscillatory shear test is applied on the fluid [42]

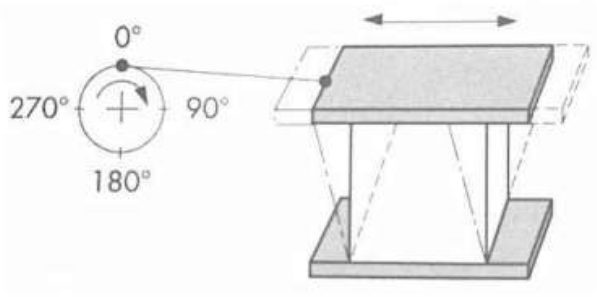


Figure 2.16: Plate-Plate models of an oscillatory test [42]

During an oscillatory test, the sinusoidal shear stress and strain applied on the viscoelastic material is illustrated in figure 2.17. The phase shift angle between the stress and strain is denoted by δ. The values are between 0º and 90º. [42]

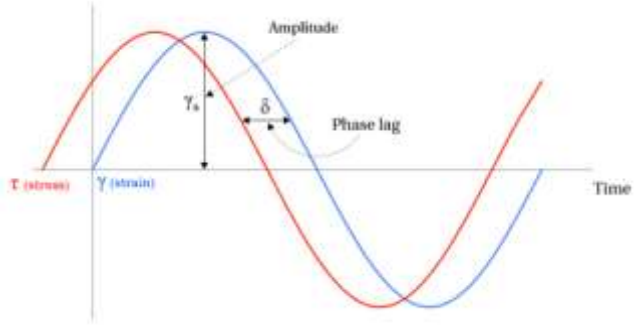


Figure 2.17: Transient shear stress and shear strain [42]

In an oscillatory test the rheometer subjects the drilling fluid to a sinusoidal shear deformation and then the resultant stress is measured. The applied shear strain, $\gamma(t)$, is defined by equation 2.19 [40].

$$\gamma(t) = \gamma_o \sin(\omega t) \tag{2.19}$$

the measured shear stress, $\tau(t)$ , is

$$\tau(t) = \tau_o \sin(\omega t + \delta) \tag{2.20}$$

Where:

- $\gamma_o$ = Shear strain amplitude [dimensionless]
- $\tau_o$ = Shear stress amplitude [Pa]
- $t$ = Time [s]
- $\omega$ = Angular frequency [rad/s]
- $\delta$ = Phase angle [degrees]

Using trigonometric and shear stress can be written in term of strain as:

$$\tau(t) = \tau_o \left[\sin(\omega t)\cos\delta + \cos(\omega t)\sin\delta\right] \tag{2.21}$$

This again can be rearranged as:

$$\tau(t) = \gamma_o \left[\left(\frac{\tau_o}{\gamma_o}\cos\delta\right)\sin\omega t + \left(\frac{\tau_o}{\gamma_o}\sin\delta\right)\cos\omega t\right] \tag{2.22}$$

Further, the shear stress can be written as:

$$\tau(t) = \gamma_o[G'\sin\omega t + G''\cos\omega t] \tag{2.23}$$

Where storage modulus (G') and loss modulus (G'') are given as:

$$G' = \frac{\tau_A}{\gamma_A}\cos\delta \tag{2.24}$$

$$G'' = \frac{\tau_A}{\gamma_A}\sin\delta \tag{2.25}$$

The shear storage modulus (G'), measures the energy stored per cycle; the loss modulus (G'') measures the energy lost per cycle of sinusoidal deformation [42].

The phase of stress and strain are compared to reveal if the fluid is elastic, viscous, or viscoelastic. For a perfectly elastic material the phase angle is equal to 0°. For a perfectly viscous material the phase angle is equal to 90°. For a viscoelastic material, the phase angle will fall somewhere between 0° and 90°. This is displayed in figure 2.18 [43].

There are four different oscillatory tests to measure viscoelastic behavior. These four oscillatory tests include amplitude sweep, frequency sweep, time sweep, and temperature sweep [43].

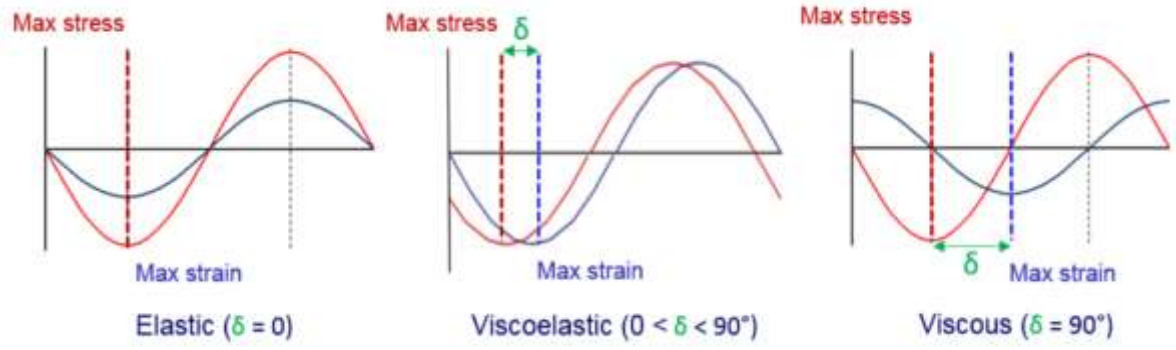


Figure 2.18: Stress and strain wave relationships for a perfectly elastic, perfectly viscous and a viscoelastic material

Table 2.1 shows further summary of the viscoelastic properties presented in figure 2.16. When the phase angle is 0º and 90º, the fluid systems possess ideally elastic and ideally viscous behaviors, respectively. For the case when the material behaves equal portions of viscous and elastic, the phase angle is 45º. This point is called a flow point, where the loss and storage moduli are equal. When the phase angle is between 90 º and 45 º, the fluid system is viscous dominated. On the other hand, when the phase angle is between 0 º and 45º, the fluid system is elastic dominated as compared with the viscous part. Here, the storage modulus is greater than the loss modulus. [44]

Table 2.1: Relationship between material behavior and phase shift angle, δ, [42]

| **Ideally viscous flow behavior** | **Viscoelastic liquid behavior** | **50/50 ratio between viscous and elastic portions** | **Viscoelastic gel or solid behavior** | **Ideally elastic behavior** |
|---|---|---|---|---|
| $\delta = 90^o$ | $90^o > \delta > 45^o$ | $\delta = 45^o$ | $45^o > \delta > 0^o$ | $\delta = 0^o$ |
| $tan\,\delta \rightarrow \infty$ | $tan\,\delta > 1$ | $tan\,\delta = 1$ | $tan\,\delta < 1$ | $tan\,\delta \rightarrow 0$ |
| $G' \rightarrow 0$ | $G'' > G'$ | $G' = G''$ | $G' > G''$ | $G'' \rightarrow 0$ |

## 2.9.2 Temperature sweep

In the oscillatory temperature sweep test, temperature is ramped while both the amplitude and the frequency are kept constant. The aim of a temperature sweep test is to investigate the stability of the drilling fluid with temperature with respect to the change in temperature. This test with increasing temperature will help to anticipate the change of structure of fluid along the borehole, since high temperature is often encountered along the wellbore.

# 3 Experimental work

This section presents the brief description of materials and characterization methods, drilling fluid synthesis, experimental design, experimental setup and procedures.

## 3.1 Materials and methods

### 3.1.1 Materials

#### 3.1.1.1 Sodium formate

Sodium format is a white crystalline powder. The Sodium salt of formic acid has the chemical formula HCOONa or $HCO_2Na$ and a molecular weight 68.007. Sodium is an alkali metal which has only an electron in its outer shell ($Na^+$) and therefore it is placed in group 1 in the periodic table. In general, alkali metals are highly reactive and easily react with other elements. The Sodium has a positive charge and can react with formic acid which has a negative charge ($HCOO^-$). The Sodium formate is produced by reaction between these two elements and the solubility in water at 0 °C is 43.82 g/100mL. The solubility of sodium formate increases as the temperature increases. The density of sodium formate is 1.92 $g/cm^3$ at 20 °C [45, 46, 47].

#### 3.1.1.2 Potassium formate

Potassium formate with the chemical formula $CHKO_2$ and a molecular weight 84.12 is a high purity crystalline powder. Potassium formate is the potassium salt of formic acid and is soluble in water and alcohol. Potassium formate is a useful chemical compound in the oil and gas industry particularly as completion fluids. It is also an eco- friendly brine that can be used as drill-in fluids. The potassium salt of formic acid is a result of the chemical reaction between the acidic component of ($HCOO^-$) and alkali metal ($K^+$). The solubility in water at 0 °C is 32.8 g/100mL and 25 °C is 331 g/100mL. The solubility of potassium formate also increases as the temperature increases. The density of potassium formate is 1.908 $g/cm^3$ [48].

#### 3.1.1.3 Starch

Starches are carbohydrates with a chemical formula of (C6H10O5)n. It is insoluble in cold water, alcohol, or other solvents. Starches are the product of all green plants such as potatoes, rice and wheats and seeds [49]. In the drilling fluid industry, starch is used as a filtrate controlling agent in the drilling fluid composition. In this thesis, Starch is purchased from food

store and the detail of the product is not provided by the manufacturer. The reason we used it is according to the drill-in fluid recipe [50].

#### 3.1.1.4 Xanthan gum

Xanthan gum is a natural polysaccharide and an important industrial biopolymer. In the drilling industry Xanthan gum is used to increase the drilling fluid's viscosity. When blended into water xanthan gum swells, and the mixture takes on a gel-like consistency that is an excellent carrier of drill cuttings [51,52].

#### 3.1.1.5 Calcium carbonate, $CaCO_3$

Calcium carbonate ($CaCO_3$) is a chemical compound formed by calcium, carbon, and oxygen. It is one of the most used LCM in the petroleum industry. Calcium carbonate density varies between 2.7-2.9 specific gravity. In drill-in fluids calcium carbonate acts as a weighting material preferable to barite due to its solubility to hydrochloric acids which is easily washed away and does not cause formation damage. In the form of limestone, calcium carbonate is a biogenic rock, and is more compacted than chalk and as a marble, calcium carbonate is a coarse-crystalline, metamorphic rock, which is formed when chalk or limestone is recrystallized under conditions of high temperature and pressure [53].

#### 3.1.1.6 Pistachio shell

The pistachios were purchased from the shop, which was originally imported from Iran, and then shells of pistachios were separated and milled. Afterwards, the milled shell was sieved to a predetermined particle size distribution. Davoodi et. al, (2018) investigated the characteristics of the solubility of the pistachio shell particles in three concentrations of hydrochloric acid including 15%, 28% and 37% respectively. The test results after 72 hrs. exposure with the acids showed that the solubility of the pistachio powder was by 22.5%, 53.6% and 82%, respectively. Based on the results, the authors concluded that the pistachio shell powder can be used in reservoir sections without causing skin since the pistachio shell powder is completely soluble in concentrated acid. Moreover, the authors have studied the effect of particle sizes of the pistachio shell powder on the filtrate and the viscosity properties on the drilling fluids. Results showed that comparing the particle size of less than 75 μm with the 120-150μm, the smaller particles reduced the filtrate loss of the base drilling fluid by %44 fluid loss and increased the plastic viscosity, yield point, and gel strength [13].

Because of these mentioned desired properties, in this thesis work, pistachios nutshell powder was used to investigate its bridging performance in the drill-in fluid with the objective of using the particles with $CaCO_3$, which is commonly in the reservoir section.

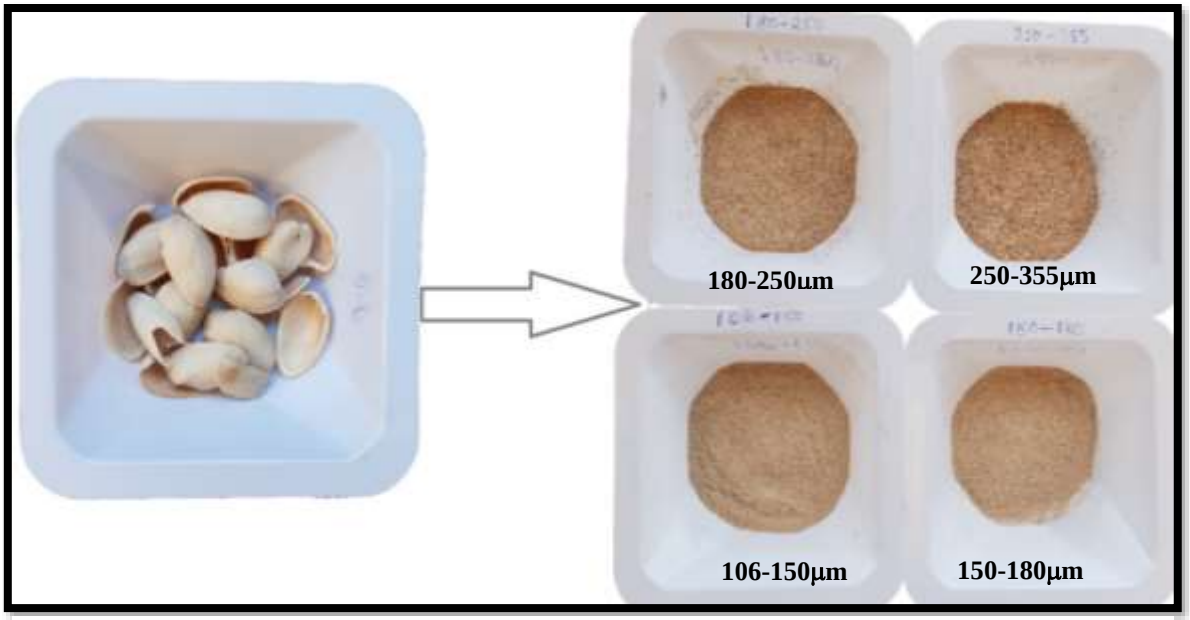


Figure 3.1: The profiles of pistachio shell: Un-milled shell (left) and milled shell (right)

### 3.1.1.7 Nutshell

The nutshells were purchased from the shop, and then shells of nutshell were separated and milled. Afterwards, the milled shells were sieved and categorizes into fine, medium, and coarse particle sizes. Nutshell is a widely used LCM in the petroleum industry to treat lost circulation during drilling of an oil and gas well. Nutshell particles apparently seemed to be

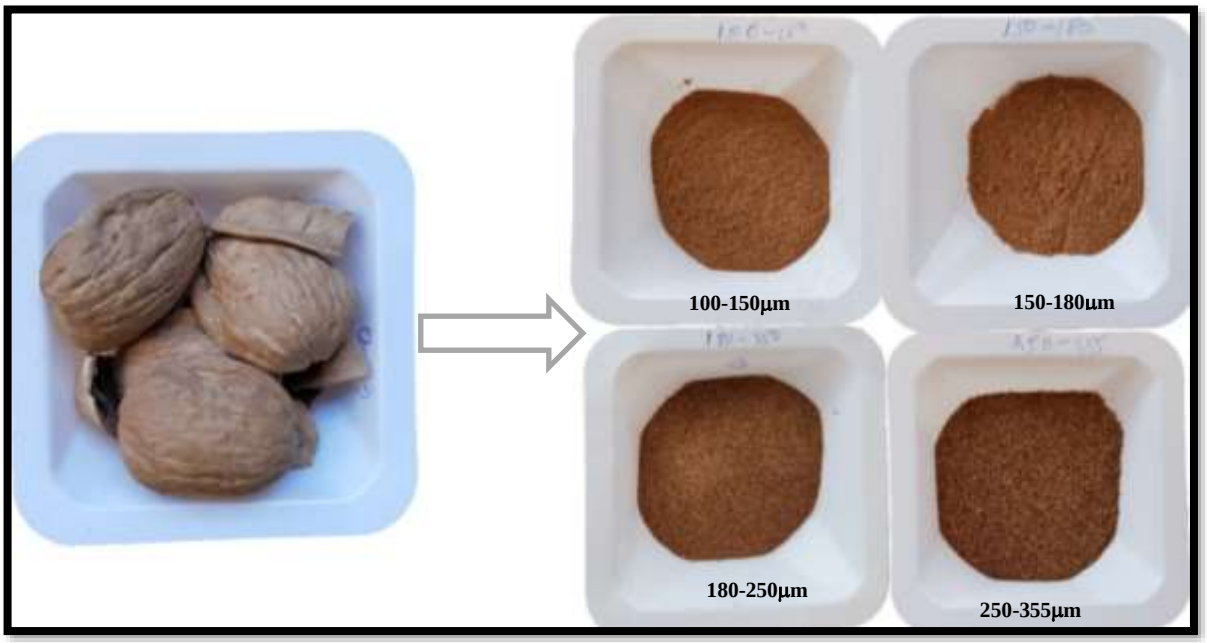


Figure 3.2: The profiles of nutshell shell: Un-milled shell (left) and milled shell (right)

lighter than pistachio when the same mass was measured and filled into a graduated cylinder (Figure 3.3).

Figure 3.3: The same amount of LCM in graduated cylinder left ($CaCO_3$), middle (pistachio), and right (nutshell)

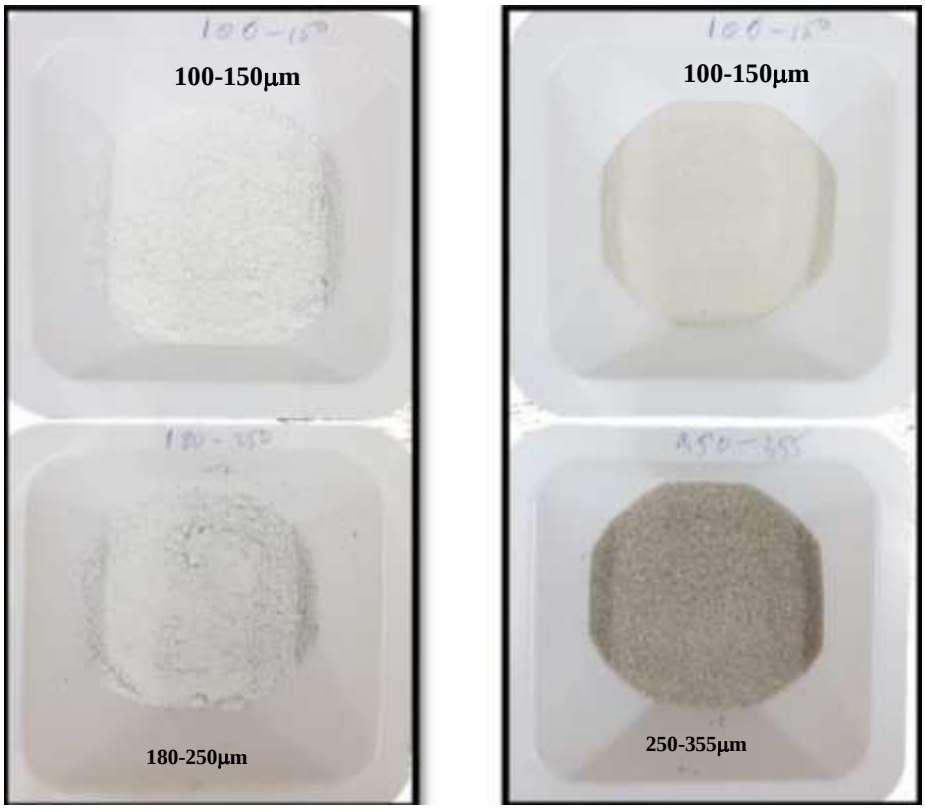


Figure 3.4: The profiles of $CaCO_3$ (left) and Quartz (right)

### 3.1.2 Drilling fluids and LCM's PSD synthesis

This section presents the brief description of the sodium and potassium formate based drilling fluid preparation used for loss circulation experimental study. Moreover, the LCM particles sieving, and design of particle size distribution (PSD) will also be presented.

#### 3.1.2.1 Sodium formate drilling fluid formulation

Sodium formate based drill-in fluids were prepared at the laboratory of the University of Stavanger. It is based on the article published by Gaurina-Medimurec, (2008), [50]. Table 3.1 and 3.2 present the sodium and potassium formate-based fluid system with composition, mixing steps, mixing method and time.

Table 3.1: Sodium formate fluid system composition with mixing method and time.

| Steps | Additive | Amount | Units | Mixing method | Mixing time |
|---|---|---|---|---|---|
| **1A.** | Water | 250 | ml | - | |
| **1B.** | 45 weight% Na-formate | 250 | ml | Manually stirred with a spoon until uniformly distributed | 1-2 min |
| **2.** | Starch | 15.8 | g/l | Both manually stirred with a spoon, and then mixed at medium speed mud mixer until uniformly distributed | 5 min |
| **3.** | Xanthan Gum (Mixing In-situ) | 1.58 | g/l | Mixed at medium speed | 5 min |
| | Add defoamer (as required) | | | | |
| **4.** | $CaCO_3$ (71-90µm) | 50 | g/l | Mixed at high speed | 5 min |
| | Add defoamer (as required) | | | | |
| **5.** | Xanthan Gum (Mixing Ex-situ) | 1.2 | g/l | Mixed at medium speed | 5 min |

The correct amount of Sodium Salt of Formic Acid was measured using a digital scale weight lab to prepare 45 weight % Na-formate (i.e., 45g salt per 100ml water). Then, the measured weight was added to water and stirred well with a spoon until the sodium salt was visually uniform.

The drill-in fluid was prepared by mixing 250 ml water and 250 ml 45 weight% Na-formate together. These were stirred manually with a spoon between 1-2 minutes to ensure an even distribution. Afterwards, starch was added and mixed for 5 minutes. Initially, stirred with a spoon and then mixed at medium speed with a Hamilton Beach mixer. Next, Xanthan gum was added very carefully in-situ to avoid flocculation and mixed at medium speed using Hamilton Beach mixer. The mixing performed at medium speed to ensure no fluid spill out of the cup, since the fluid was still too little viscous at this mixing step. The mixing time for these steps are not dependent on time to obtain a homogenous mixture. However, the blend time for these steps was approximately 11-12 minutes.

An anti-foaming agent was required since the fluid system created foam. Three droplets of defoamer were added using pipette during the mixing of Xanthan polymer to reduce the amount of the bubbles that developed in the fluid system. Subsequently, $CaCO_3$ was added and mixed at high speed for a period of 5 minutes to accomplish a uniform distribution. In this step, the fluid was viscous enough to deal with high-speed mixing without spilling out of the cup. The main purpose of blending calcium carbonate at high speed was to ensure that $CaCO_3$ was uniformly distributed in the fluid system. Also, three droplets of defoamer were added into the mud system to remove air/gas that was created during mixing. Finally, Xanthan Gum was added very carefully ex-situ and mixed at medium speed for 5 minutes. The medium speed was selected to avoid breaking the bonding in the polymer structure. The main purpose of the in-situ/ex-situ polymer treatment was to simply control the total polymer concentration added to the fluid system after the system was already in-situ blended and to reduce the filtrate loss to an acceptable value. Thus, the ex-situ procedure is more like a controllable parameter if the results indicate high filtrate loss.

Foam was developed in almost every step during fluid formulation but was particularly high when xanthan and calcium carbonate were added to the drilling fluid system. The reason for this may originate from hydrolysis, where $CaCO_3$ particles react with other chemicals that are present in the system and separate the calcium carbonate molecule into other molecules such as carbon dioxide. The foam may also develop due to the reactions between these different additives such as starch, xanthan gum and other chemicals that are found in the system.

To avoid issues such as clumps, (i.e., form polymer balls), only xanthan gum was selected as polymer additive for all the fluid system, since the polymers have a higher ability to establish clumps in the system. Consequently, not create a well distributed uniform fluid system.

The same procedure used to formulate the sodium formate drill-in fluid which is described in the previous section was used to prepare the potassium formate drill-in fluid system. Table 3.1 and 3.2 present the sodium and potassium formate-based fluid system with composition, mixing steps, mixing method and time.

Table 3.2: Potassium formate fluid system composition with mixing method and time.

| **Steps** | **Additive** | **Amount** | **Units** | **Mixing method** | **Mixing time** |
|---|---|---|---|---|---|
| **1A.** | Water | 250 | ml | - | |
| **1B.** | 45 weight% K-formate | 250 | ml | Manually stirred with a spoon until uniformly distributed | 1-2 min |
| **2.** | Starch | 15.8 | g/l | Both manually stirred with a spoon, and then mixed at medium speed mud mixer until uniformly distributed | 5 min |
| **3.** | Xanthan Gum (Mixed In-situ) | 1.58 | g/l | Mixed at medium speed | 5 min |
| | Add defoamer (as required) | | | | |
| **4.** | $CaCO_3$ (71-90µm) | 50 | g/l | Mixed at high speed | 5 min |
| | Add defoamer (as required) | | | | |
| **5.** | Xanthan Gum (Mixed Ex-situ) | 1.2 | g/l | Mixed at medium speed | 5 min |

### 3.1.2.2 LCM particles

Figure 3.5 shows the Haver EML 200 sieve and used to separate particles with the desired size spectrum. Based on the selected particles size, the same particle size distribution plot of nutshell and pistachio are shown in Figure 3.6. This PSD is used in test design #4 (i.e., section §3.2.4) to compare the bridging performance of the two types of shells. For the other test designs, certain size ranges of LCM particles were selected for the experiments due to limitation of materials in the laboratory.

Figure 3.5: Haver EML 200 Sieving equipment.

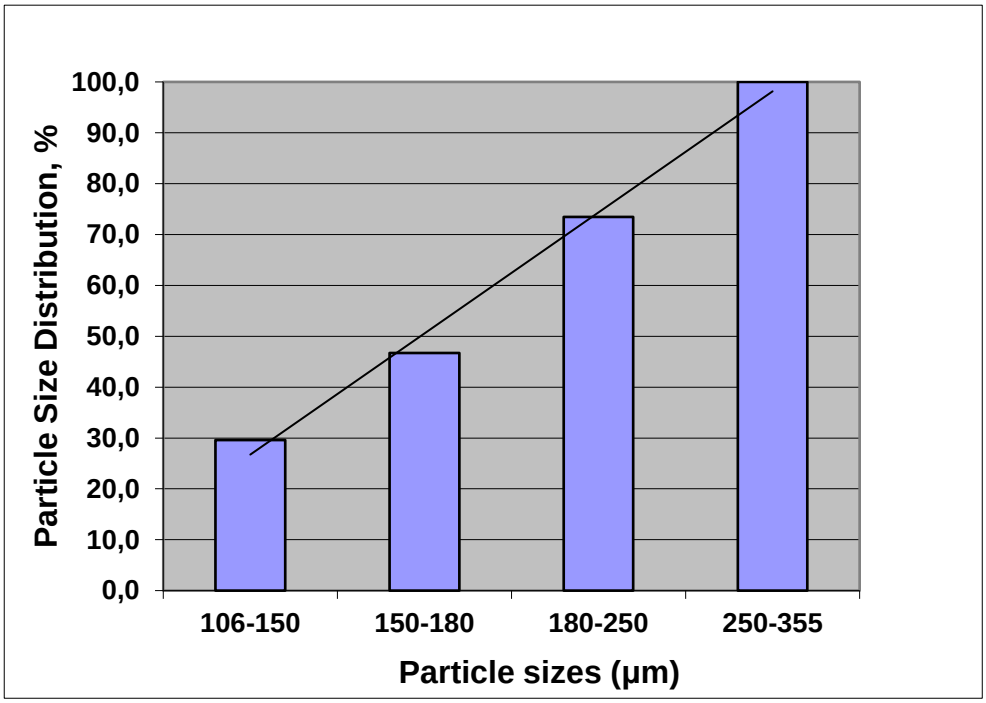


Figure 3.6: The particle size distribution plot of nutshell and pistachio

## 3.1.3 Characterization methods

### 3.1.3.1 Fann 35 viscometer model

To characterize the rheological properties of drilling fluid, a Fann 35 viscometer was used in the laboratory. This instrument is a rotational type viscometer in which the test fluid is contained in the small gap between coaxial cylinders. The outer cylinder rotates at known speed and the viscous drag exerted by the fluid creates a torque on the inner cylinder. The deflection angle of a precision spring caused by this torque is measured. The device allows six dial readings at rates of 3, 6, 100, 200, 300, and 600 revolutions per minute (rpm). The gel strength of drill-in fluid was measured in 10 seconds and 10 minutes

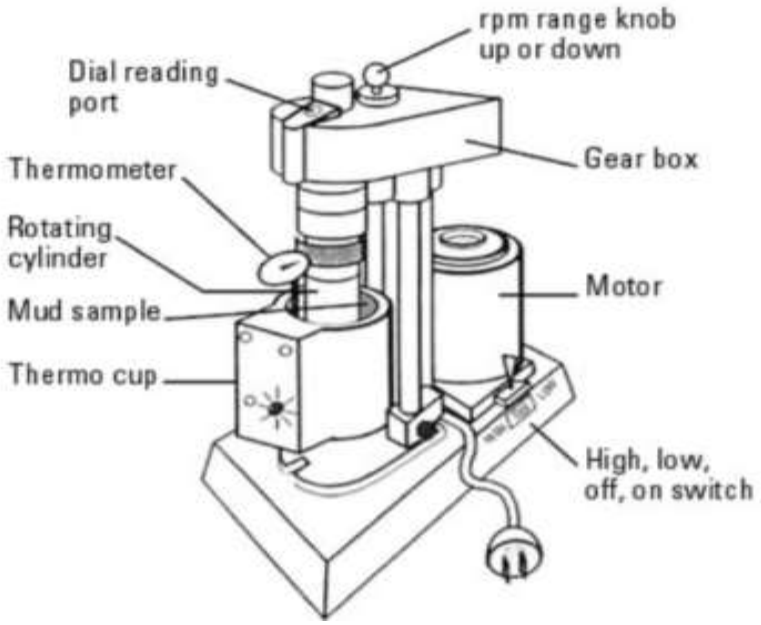


Figure 3.7: Fann 35 viscometer model [54]

### 3.1.3.2 Static bridge apparatus

The static bridge apparatus, constructed of steel vessel, was used to evaluate bridging pressure capacity of LCMs. The apparatus consists Lab-View (1), Gilson pump, Valve to control air/ fluid flow (3), Cake (4), Drilling fluid with suspension (5), Valve to control mudflow (6), Opening slots (7), Cylinder (8) and Fluid/air outflow (9). A schematic overview of the bridge apparatus is shown in figure 3.8. To simulate a fracture in the formation a single line-opening slot is placed at the bottom of the cylinder. The maximum capacity of the Gilson pump is 60MPa. The test was performed at room temperature, which of course does not simulate the reservoir temperature. In addition, the experiment is performed at static conditions, which also deviate from actual wellbore conditions.

Three different slot sizes of 100, 150, and 200 were used to conduct the experiment. The experiment was run by filling the drill-in fluid with LCM particles into the cylinder, and then the Gilson pump started at 6 ml/min to remove air from the system. When air was removed and the air control valve closed, the pump started reinjecting to build pressure in the system, but with a lower rate of 2 ml/min. The experiment time for each test was 20 minutes.

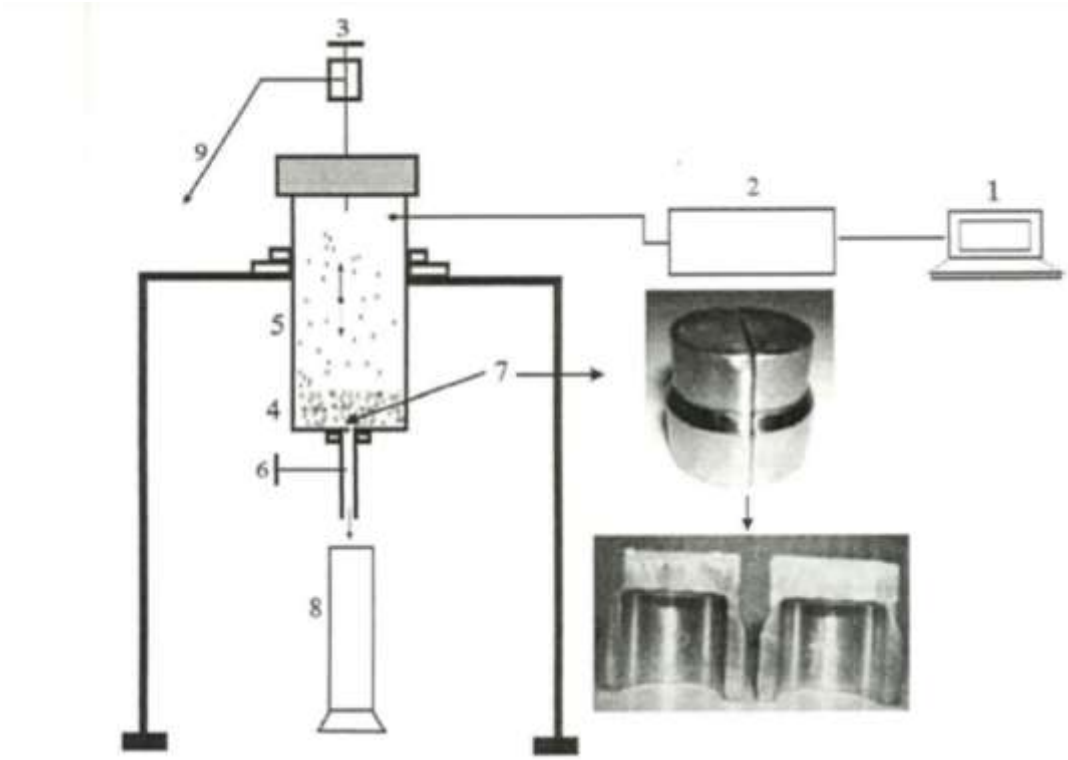


Figure 3.8: The static bridge apparatus [55].

### 3.1.3.3 Anton Paar Rheometer and testing procedure

The temperature sweep test was performed by the using of an Anton Paas MCR 302 rheometer, which is shown in figure 3.9. Anton Paas MCR 302 rheometer is highly technological, having several advanced functions. This instrument is highly accurate for the fluid systems viscoelastic measurements. The rheometer can perform tests in a wide range of temperatures in both rotational and oscillatory mode. In this thesis, the temperature sweep test was carried out using a rotational bob and cup setup. Once the bob was carefully attached into the open space under the black top cap, then the sample fluids were filled to the marked line in the cup and placed into the rheometer open hole. The temperature sweep investigation was set to perform linear temperature increase from 0°C to 80°C and measure the viscosity at a shear rate of 50 1/s. Moreover, the amplitude sweep

Figure 3.9: Anton Paar MCR 302 rheometer.

## 3.2 Experimental test design

LCM particles are blended in drilling fluids. Therefore, the concentration LCM is given in percentile. It means that the wt.% in this thesis is the weight percentile of LCM is by weight of the drilling fluid mixed with.

### 3.2.1 Test design #1

Test design #1 is aimed at investigating the effect of micro- and nanosized $CaCO_3$ LCM in potassium and sodium-fomate base fluids. The drilling fluid's formulations are presented in section §3.1.2. The bridging performance of the LCM was tested at 100, 150 and 200 micron slots.

***Test in Na-formate based drilling fluid***

1. 45% Na formate based fluid + 2wt.% 180-250micro $CaCO_3$.
2. 45% Na formate based fluid + 2wt.% 180-250micro $CaCO_3$ + 1wt% $CaCO_3$ nanoparticles

Test #2 is designed to investigate if the nanoparticle with the microparticle provide better bridging in Na-formate fluid.

***Test in K-formate based drilling fluid***

1. 45% K-formate based fluid + 2wt.% 180-250micro $CaCO_3$.
2. 45% K-formate based fluid + 2wt.% 180-250micro $CaCO_3$ + 1wt.% $CaCO_3$ nanoparticles

Here again, Test #2 above is designed to investigate if the nanoparticle with the microparticle provides better bridging in the k-formate fluid.

### 3.2.2 Test design #2

Based on the result of Test design 1, it was observed that the $CaCO_3$ particles and the considered sizes were not efficient after 150 microns in both fluid systems. Test design 2 is aimed at investigating the impact of small and large particles blending in K-formate fluid only. For this, the single effect of Quartz and $CaCO_3$ along with their mixtures was evaluated at 100, 200 and 300 microns.

Test in K-formate based drilling fluid

1. 45% K formate-based fluid + 2wt. % 100-150 + 250-350micron $CaCO_3$.
2. 45% K formate-based fluid + 2wt. % 100-150 + 250-355micron Quartz.
3. 45% K formate-based fluid + 1wt.% 100-150 + 250-350micron $CaCO_3$ + 1wt.% 100-150 + 250-355micron Quartz.

Test #3 above is designed to investigate if there is synergy between the particles.

### 3.2.3 Test design #3

To provide particle stability at the bridge, the single and $CaCO_3$ blended Pistachio nutshell was tested.

For this, K-formate based drilling fluid was synthesized and evaluated at 100, 200 and 300 microns.

1. 45%K-formate drilling fluid +2wt.% $CaCO_3$ (100-150 and 250-350 micron)
2. 45%K-formate drilling fluid +2wt.% Pistachio (100-150 and 250-350 micron)
3. 45%K-formate drilling fluid +1wt.% 100-150 + 250-350micron $CaCO_3$ +1wt.% 100-150 + 250-350micron Pistachio.

### 3.2.4 Test design #4

Test design #4 was designed to investigate and compare the bridging performance of nutshell and Pistachio nutshell. For this, the same particle sizes were sieved, and the same mass were measured in order to make the same particle size distribution. The particles were tested in K-fomate drilling fluids at 100, 150 and 175 micron slots. During the test, the bigger sizes, and the blending of the small and the bigger sizes were studied in order to investigate the effect of particles packing on the birding performances.

# 4 Results and discussion

This chapter presents the rheological and viscoelasticity property characterization of the Na- and K-formate drilling fluids. In addition, the brief discussions of the particle bridging experimental results.

## 4.1 Drilling fluids characterization

### 4.1.1 Viscometer responses and rheological parameters of the of the drilling fluids at room temperature

The rheological properties of both Na-formate -and K-formate drilling fluids were carried out at room temperature. Figure 4.1 shows the comparison of the viscometer responses of the 45 wt.% Na- and 45 wt.% K-fomate drilling fluids. As shown the viscometer responses of the K-formate based system is lower than the Na-formate based drilling fluid. Table 4.1 also provides the information about the gel strength, the filtrate loss, the density, and pH values of the two fluid systems. As shown in the table, except for the filtrate losses, the other mentioned parameters of the two fluids are quite comparable.

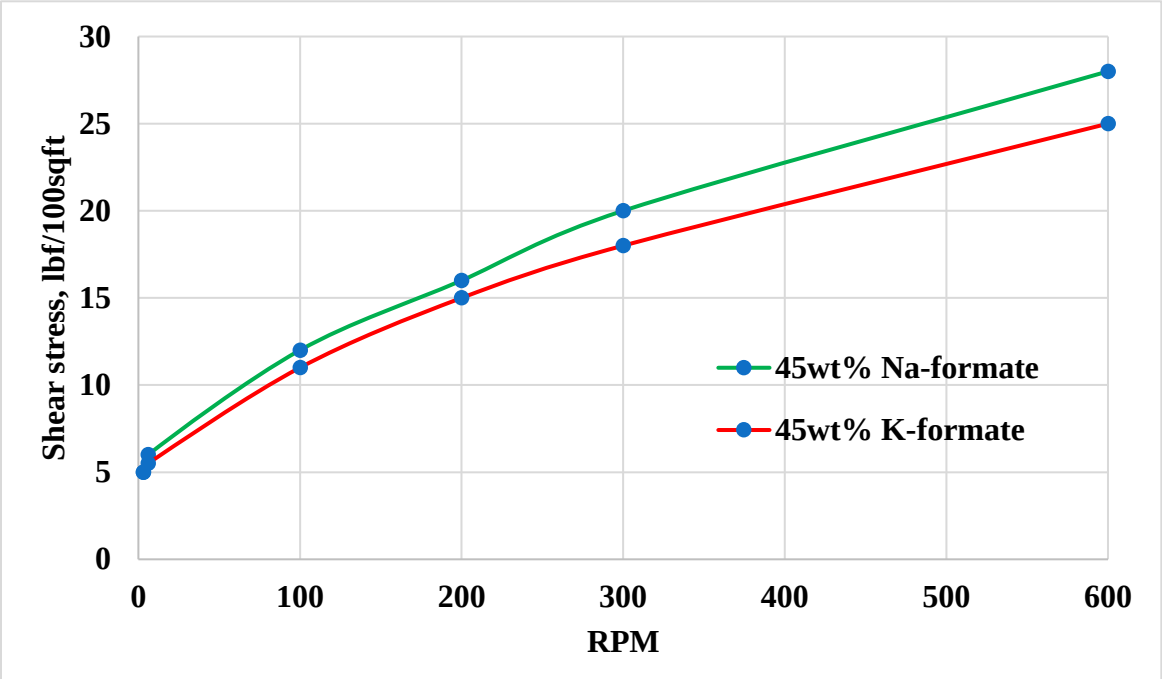


Figure 4.1: Viscometer responses of the K- and N-fomate based drilling fluids

Table 4.1: Comparisons of the gel strength, pH, filtrate loss and density of the Na- and K-formate base drilling fluid properties.

| **Parameters** | **Unit** | **45wt% Na-formate** | **45wt% K-formate** |
|---|---|---|---|
| **Gel strength (10 sec.)** | lbf/100sqft | 5 | 5.5 |
| **Gel strength (10 min.)** | lbf/100sqft | 6 | 6 |
| **pH Value** | - | 7.57 | 7.68 |
| **Mud Density** | S. G | 1.2 | 1.14 |
| **LTLP Filtrate Loss** | ml | 6.5 | 8 |

Based on the rheological models presented in section §2.8.2, the rheological parameters were calculated based on curve fitting, and the results are displayed in table 4.2. From the results, one can observe that the models estimate the rheology of the Na- and K-fomate drilling fluids with different values. The percentile error deviation is calculated as the average of the absolute sum difference between the model prediction and the measurement.

Table 4.2: Rheological parameters of Na- and K-formate drilling fluids.

| **Model** | **Parameters** | **45wt% Na-formate** | **45wt% K-formate** |
|---|---|---|---|
| **Herschel-Bulkley (Eq. 2.12)** | $\tau_o$ | 4.6135 | 4.8337 |
| | k | 0.3180 | 0.1801 |
| | n | 0.6337 | 0.7022 |
| | % Error deviation | 2.359 | 2.2403 |
| | | | |
| **Unified (Eq. 2.15)** | $\tau_{yl}$ | 4.2680 | 4.8015 |
| | k | 0.477 | 0.1924 |
| | n | 0.571 | 0.6918 |
| | % Error deviation | 2.9781 | 2.0117 |
| | | | |
| **Power law (Eq. 2.9)** | k | 3.0763 | 3.0396 |
| | n | 0.3074 | 0.2936 |
| | % Error deviation | 7.7807 | 7.8089 |
| | | | |
| **Bingham Plastic (Eq. 2.5)** | YS | 7.3215 | 6.987 |
| | PV | 0.0238 | 0.0208 |
| | % Error deviation | 15.5146 | 15.3614 |
| | | | |
| **Robertson -Stiff (Eq. 2.16)** | A | 0.9391 | 0.84 |
| | B | 0.4946 | 0.4961 |
| | C | 32.040 | 37.876 |
| | % Error deviation | 3.1005 | 0.9312 |

### 4.1.2 Effect of temperature on the drilling fluids

The effect of temperature on the viscosity of the Na- and K-formate based fluid as well as Na-formate drilling fluid blended with $CaCO_3$ were measured with "cup and bob" Anton Parr rheometer. The test is a sequence of temperature, where at first the temperature was raised up to 50$^o$C and waited for 10 min until cup wall temperature equilibrated with the drilling fluid's temperature. Once the test was done with 50$^o$C, again the system automatically increased the temperature to 80$^o$C and waited for 10 min before the test began. The shear rate was swept from 0.01 to 1000 1/s. However, at a higher shear rate, the rotational speed created turbulence in the narrow cup-bob annular spacing. Therefore, the reading above 400 1/s is not reliable and disregarded from the test results.

Figure 4.2 shows the measured shear stress vs shear rate. As shown in the figure, as temperature increases viscosity of the fluids decreases. One can also observe that like the room temperature results shown in figure 4.1, the viscometer responses of Na-formate fluid is higher than the K-formate fluid at 50$^o$C. But, at 80$^o$C, both fluids behave nearly the same. Another observation is that treating the Na-formate with 2wt.% micron and 1wt.% nanosized $CaCO_3$ didn't show any impact on the viscosity of the base fluid. The main reason is that the LCM $CaCO_3$ is not viscosifying agent and the concentration is low as well.

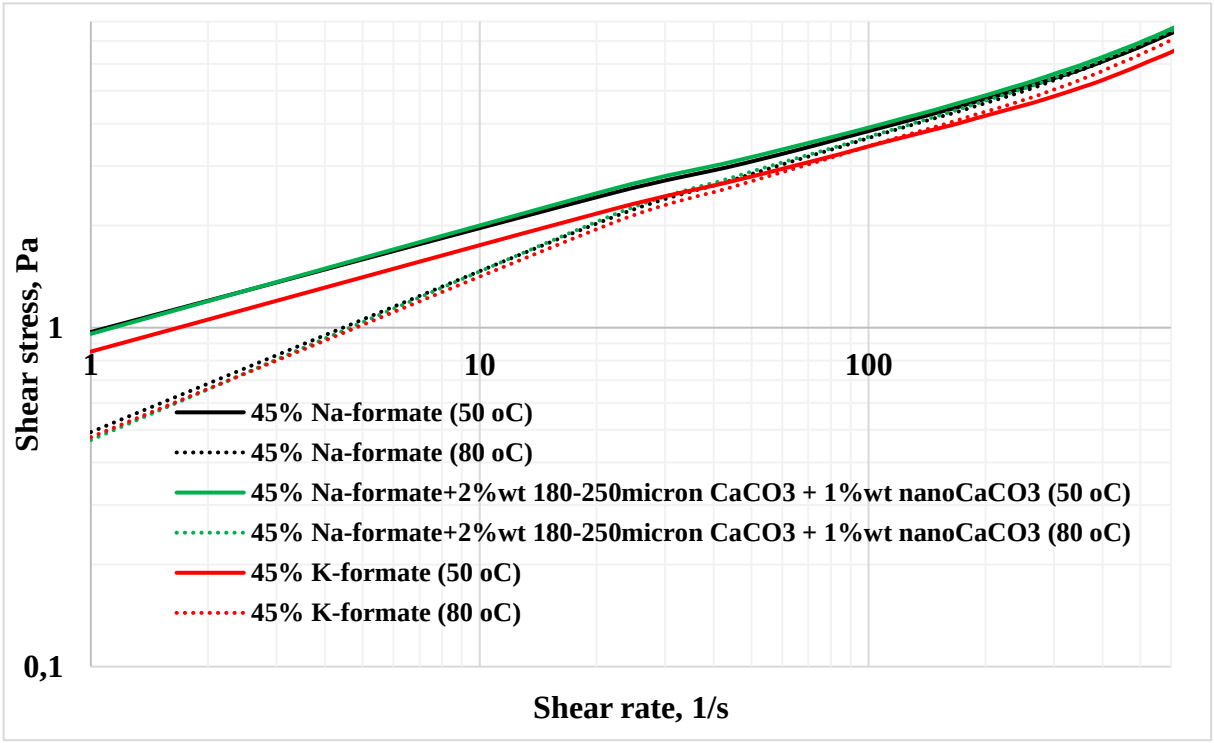


Figure 4.2: Effect of temperature and $CaCO_3$ on the Na- and K-formate base drilling fluids.

## 4.1.3 Viscoelasticity properties of the drilling fluids

### 4.1.3.1 Amplitude sweep

An oscillatory amplitude sweep test was conducted with plate-plate set up, where the fluid is filled between the plates and an amplitude sweep during testing. The shear rate varied 0.01% to 1000%. The angular rotational speed was 10rad/s. The tests were carried out at room temperature. Figure 4.3 shows the measured amplitude sweep test results comparison of the Na- and K-fomate based drilling fluids. As shown the viscoelasticity properties of the drilling fluids are nearly equal.

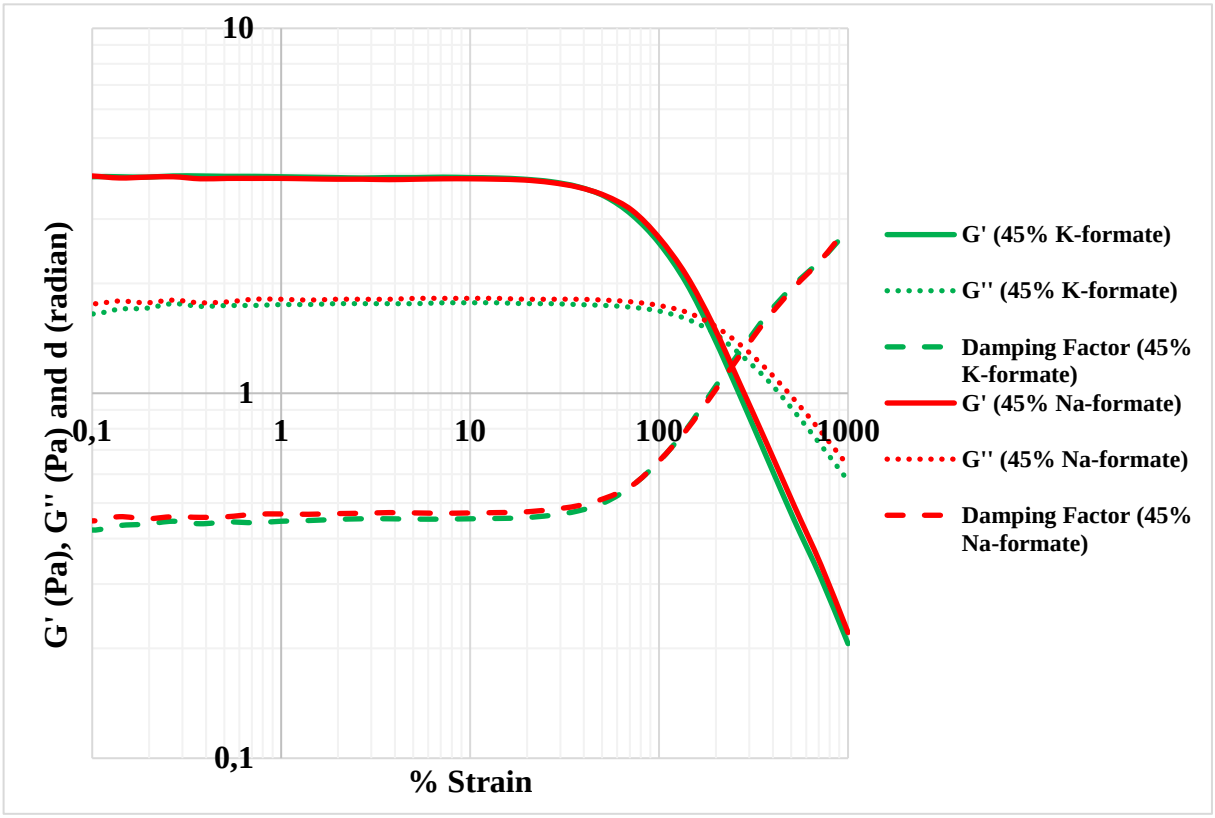


Figure 4.3: Amplitude sweep oscillatory test results of the Na- and K-fomate drilling fluids.

### 4.1.3.2 Temperature sweep of the drilling fluids characterization

Temperature sweeps for sodium formate base fluid and potassium formate base fluid as well as 2 wt.% of $CaCO_3$ and 1wt% nanoparticles in sodium formate base fluid are presented in Figure 4.4. From figure 4.4, we can see that the viscosity of fluids decreases as temperature increases as expected. We can also observe from the figure that the viscosity of fluid slightly increases when 2 wt.% of calcium carbonate and 1 wt.% nanoparticles were added to the fluid. Another observation is that the potassium formate base fluid reaches its lowest point approximately around 60 grads Celsius while sodium formate base fluid reaches its lowest point almost around 70 grads Celsius. The viscosity of both fluids increases again after they reach the lowest point which indicates that the gelation starts to form in the fluid system, hence the viscosity increases.

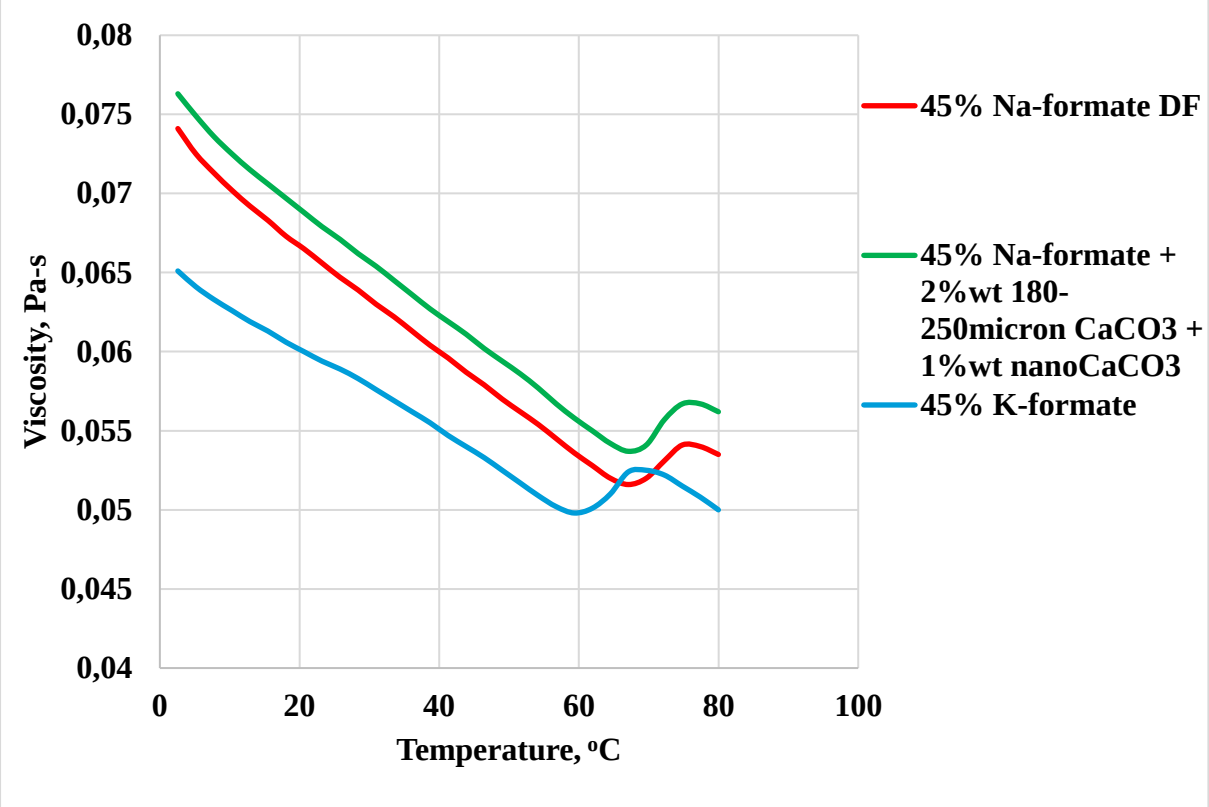


Figure 4.4: Temperature sweeps for Na-formate, K-formate base fluid, and Na-formate base containing 2wt% $CaCO_3$ and 1wt% nanoparticles.

## 4.2 LCM particles bridging performance evaluations

The experimental results for the bridging performance are presented and discussed in the following sections. The results are plotted to evaluate the bridging capacities of LCMs as the fracture widths vary in size. In most tests, fracture widths of three sizes were used to investigate the performances of different LCMs in two types of reservoir friendly fluids.

The base fluid basically contains 70-90 micron $CaCO_3$ as bridging material, which is 4.7wt % of the drilling fluid. Since the minimum slot size we had was 100microns, both the fluid systems were tested with and without nanoparticles blending. The results during the 20 min test showed that all the fluids were flowing through the slot, without building a bridge. The results indicate that the need to include large sizes more LCM particles. Please note that for all bridging tests, the LCM particle additives is by weight percent of the base fluid.

### 4.2.1 Effect of nanoparticle and micro $CaCO_3$ particles in Na-formate fluids

In this test, the drilling fluids were ex-situ blended with 180-250microns LCM particles and tested using three sizes of 100 µm, 150 µm, and 200 µm slots. Then, the effect of nanoparticles was studied by repeating the same experiment with the addition of 1wt% $CaCO_3$ nanoparticles in the micro seized LCM blended drilling fluid system.

The experimental outcomes of LCMs with and without nanoparticles blending in sodium formate base fluid are displayed in figure 4.5 and figure 4.6, respectively. During testing, as the bridge collapses, the drilling fluid is lost through the fracture. As the suspended LCM particles accumulate at the gate of the fracture, it forms a bridge, and the pressure builds up until it reaches the bridge collapse pressure. The figures below show the pressure build up and collapse phenomenon as a zig-zag profile.

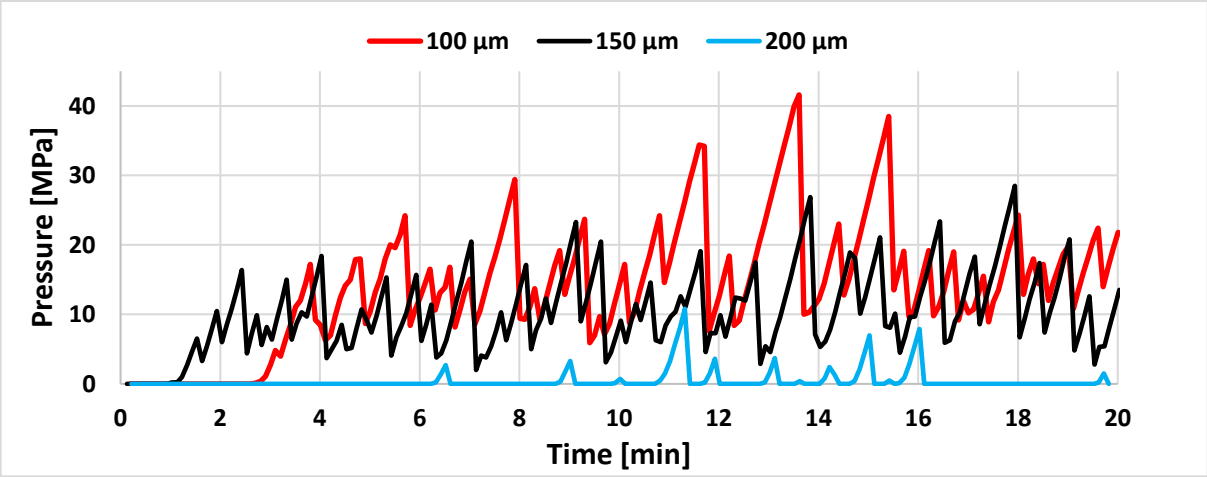


Figure 4.5: Pressure recording during the bridging test using $CaCO_3$ (180-250 µm) in Na-formate base fluid at 100 µm, 150 µm, and 200 µm slots

Observation of the pressure measurements during the experiments indicate the higher capability of the drilling fluid to bridge the smaller fractures. As the fracture width size increases, a significant reduction in bridging pressure is observed. The main reason is that the particle sizes become lower than the fracture width.

Based on figure 4.6, the addition of 1wt% nanoparticles had very little effect on the bridging performance. The bridging performances are good, with relatively high resisting pressure. The bridging performance is nearly identical to the results obtained without applied nanoparticles. This is mainly because the nanoparticles which were added to the LCM system have nearly identical chemistry to the particles in the fluids. The experimental results may be different if different types of nanoparticles were added to the LCM system.

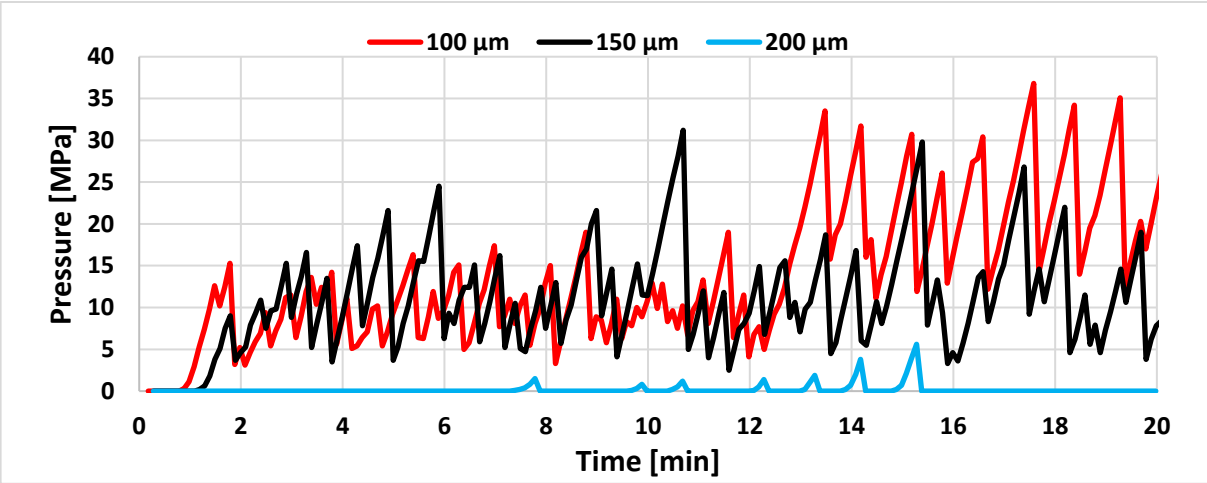


Figure 4.6: Pressure recording during the bridging test using $CaCO_3$(180-250 µm) + nanoparticles in Na-formate base fluid at 100 µm, 150 µm, and 200 µm slots

### 4.2.2 Effect of nanoparticle and micro $CaCO_3$ particles in K-formate fluids

The experimental results of potassium formate base fluid with the same concentration of LCM with and without nanoparticles on 100 µm, 200 µm and 300 µm wide slots are shown in figure 4.7 and figure 4.8. Clearly, when K-formate base fluid containing identical type of particles and concentration of LCM as previous test can create solid bridges over fractures less than 200 µm wide. As the slot size increases, the bridging becomes more unstable, and values of pressure level significantly decrease like the results obtained from Na-formate base fluid. As the experiment outcomes indicate, there are no significant differences between Na-formate fluid and K-formate fluid in terms of controlling lost circulation.

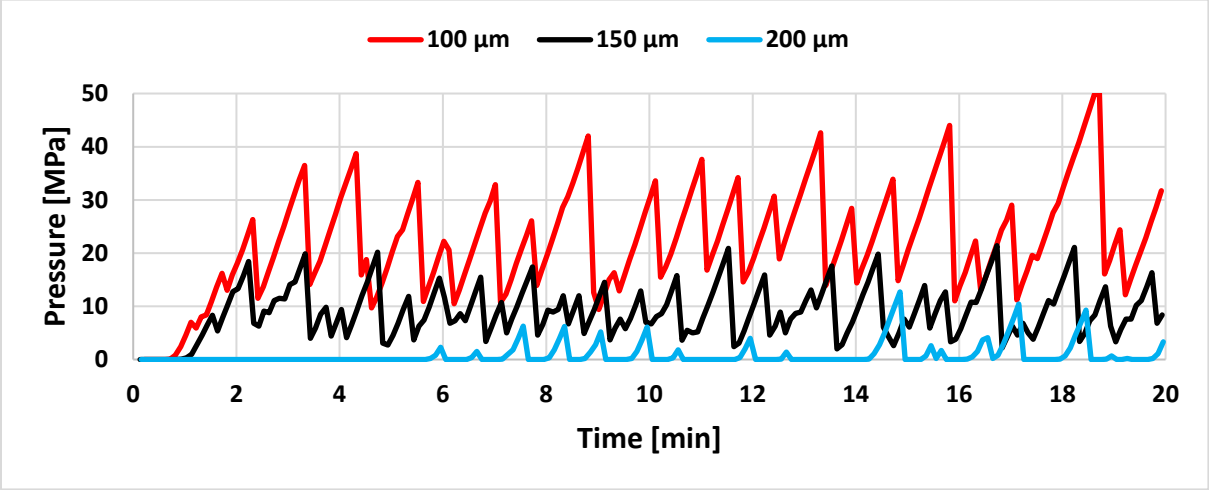


Figure 4.7: Pressure recording during the bridging test using $CaCO_3$(180-250 µm) in K-formate base fluid at 100 µm, 150 µm, and 200 µm slots

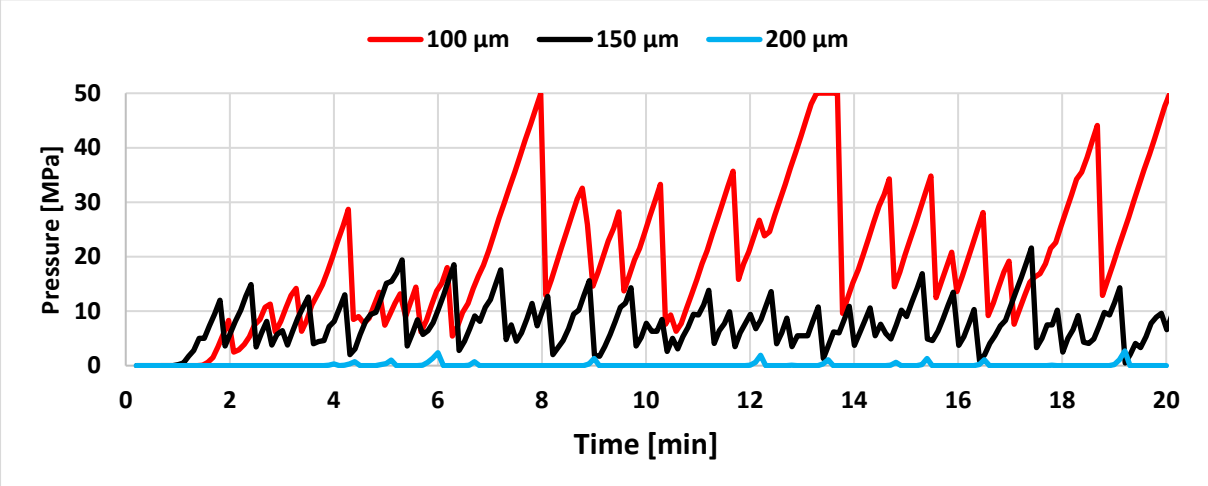


Figure 4.8: Pressure recording during the bridging test using $CaCO_3$ (180-250 µm) + nanoparticles in K-formate base fluid at 100 µm, 150 µm, and 200 µm slots

### 4.2.3 Effect of fine and coarse Quartz and $CaCO_3$, as well as the combination of both materials in K-formate base fluid

The capability of fine (100-150 µm) and coarse (250-350 µm) calcium carbonate and fine (100-150 µm) and coarse (250-355 µm) Quartz, as well as the combination of both materials to bridge various fractures has been shown on figure 4.9-4.11. As shown in the figures, $CaCO_3$, Quartz, and the combination of both materials forms a good bridge at the 100 µm fracture width. Quartz and the blending of both LCMs makes a solid bridge over the 100 µm slot that can hold the maximum pressure. The calcium carbonate's bridging performance over the same fracture wide is good but not as strong as Quartz or the combination of both materials since the bridging pressure fluctuated significantly during the experiment. This is mainly because calcium carbonate is a mechanically weak LCM compared to quartz which is much stronger mechanically. On Mohs scale, the hardness of Calcite and Quartz are 3 and 7, respectively. In addition, the opening size of the fracture has also an adverse effect on the strength of the bridge for both LCMs as it is seen in figure 4.9 and 4.10. However, the combination of both materials exhibits a significant enhancement effect on the strength of the bridge. This may be due to a higher friction value between the LCM particles. Based on this result, the combination of Quartz and $CaCO_3$ may be an alternative to combat lost circulation since the bridging pressure resistance is high over all fractures.

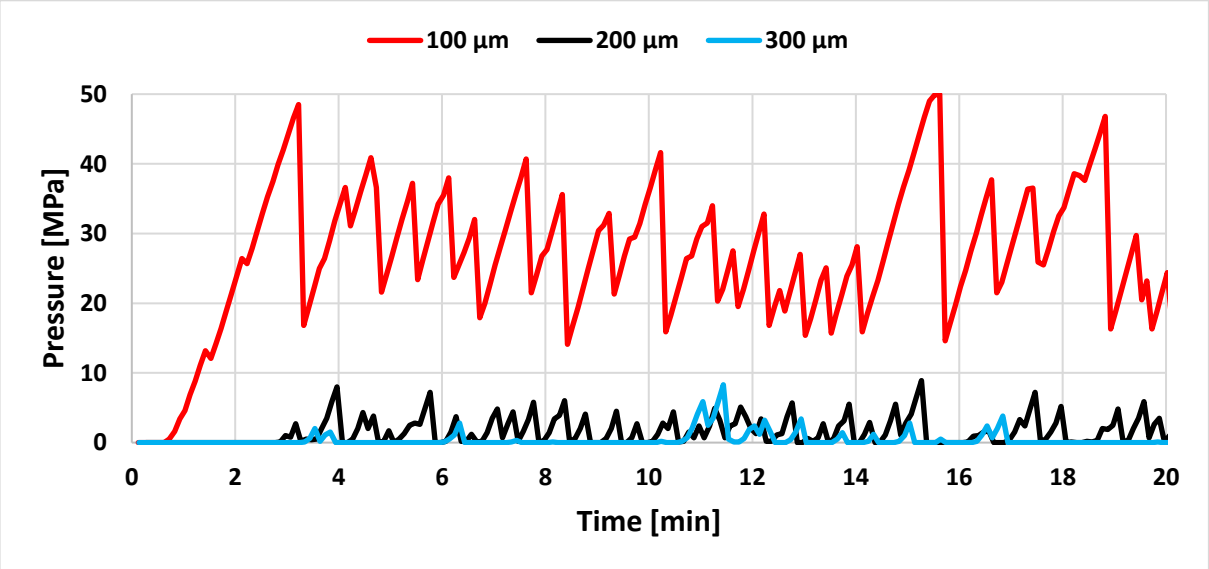


Figure 4.9: Pressure recording during the bridging test using fine (100-150 µm) and coarse $CaCO_3$(250-350 µm) in K-formate base fluid at 100 µm, 200 µm, and 300 µm slots

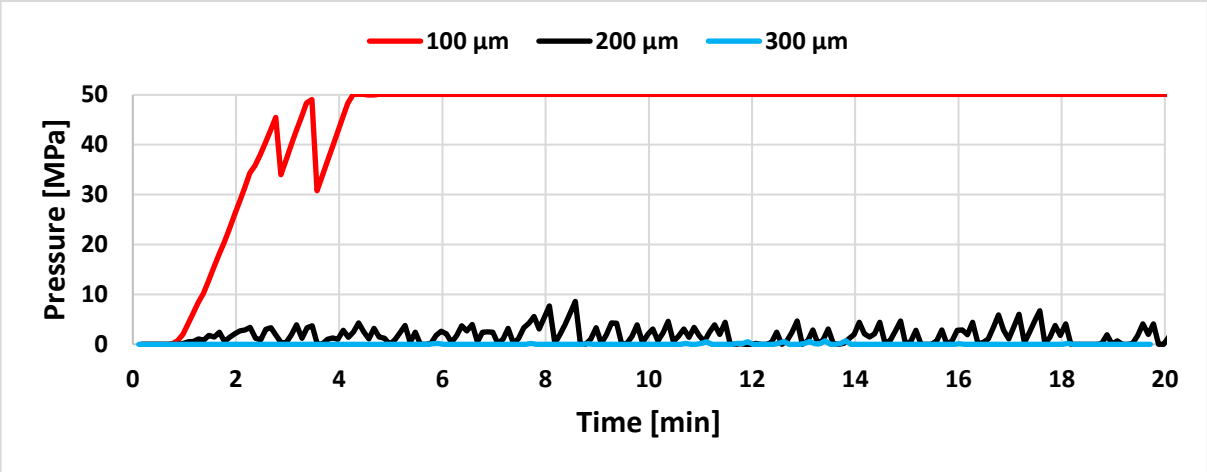


Figure 4.10 Pressure recording during the bridging test using fine (100-150 µm) and coarse (250-355 µm) Quartz in K-formate base fluid at 100 µm, 200 µm, and 300 µm slots

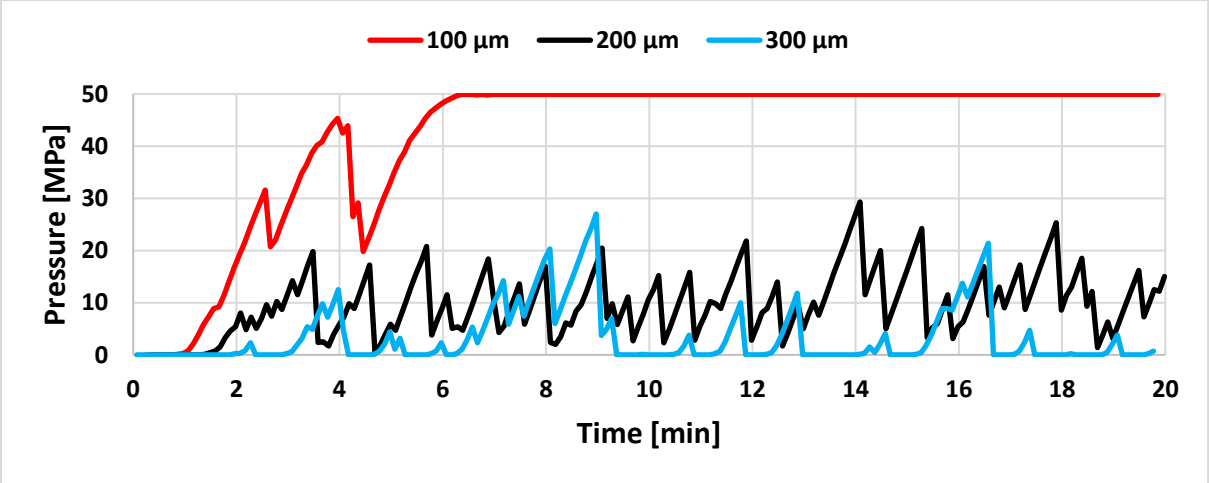


Figure 4.11: Pressure recording during the bridging test using fine and coarse Quartz (100-150 and 250-355µm) and $CaCO_3$ (100-150 and 250-350µm) in K-formate base fluid at 100 µm, 200 µm, and 300 µm slots

### 4.2.4 Effect of Pistachio on the bridging

In this test, Quartz was replaced with Pistachio LCM that is completely acid-soluble in concentrated hydrochloric acid. Fine (100-150µm) and coarse (250-350µm) particles with equal concentration were used to investigate the synergistic effect of both materials in potassium formate-based drilling fluid. The examination was performed using 100 µm, 200 µm and 300 µm slots. The test results obtained from the experiment are shown in figure 4.12 – 4.14. As observed from the results, none of the LCM systems were successful in controlling the drilling fluid flow through the largest fracture since no sealing barrier was formed in the test

using the 300 µm slot even though the drilling fluid contained LCM particles larger than this fracture. The main reason for this might be inappropriate particle size distribution. However, the pressure recording over the smallest fracture indicates that the pistachio LCM can resist twice as high pressure as calcium carbonate, or the combination of both materials can resist. As the fracture width increases, the observation of the pressure recording during the test indicates that the combination of both materials slightly improves the bridging performance as it is shown in figure 4.14.

Since no sealing barrier was formed in the test using the 300 µm fracture, another test was designed using the nutshells and pistachios instead of $CaCO_3$ due to the lack of $CaCO_3$ in the laboratory. The experimental results obtained from this test are illustrated in figure 4.15. Initially, ultra-coarse particles of both materials in the range of 500 µm to 1000 µm were tested in different concentrations. The experiment was conducted using a single fracture with fracture size of 650 µm slot opening. Since this spectrum created a pack with high permeability, no sealing barrier was formed in any of the tests. Based on the results, both fine and medium particle sizes were added which significantly improved the bridging performance even with low concentration specially using pistachio as LCM. This experimental observation also supports the theory of ideal particle packing [23].

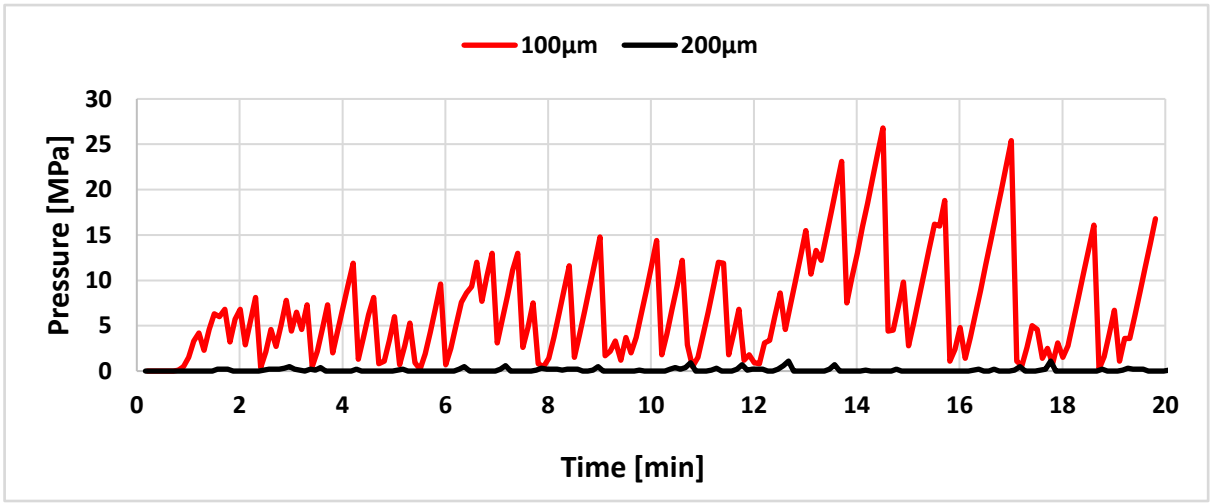


Figure 4.12: Pressure recording during the bridging test using fine (100-150µm) and coarse (250-350µm) Pistachio in K-formate base fluid at 100 µm, and 200 µm slots

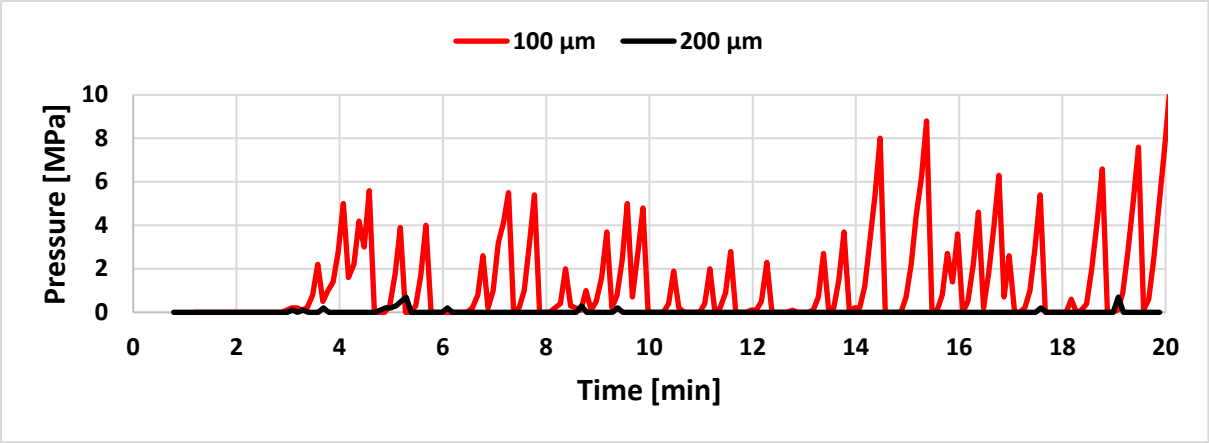


Figure 4.13: Pressure recording during the bridging test using fine (100-150 µm) and coarse $CaCO_3$(250-350 µm) in K-formate base fluid at 100 µm, and 200 µm slots

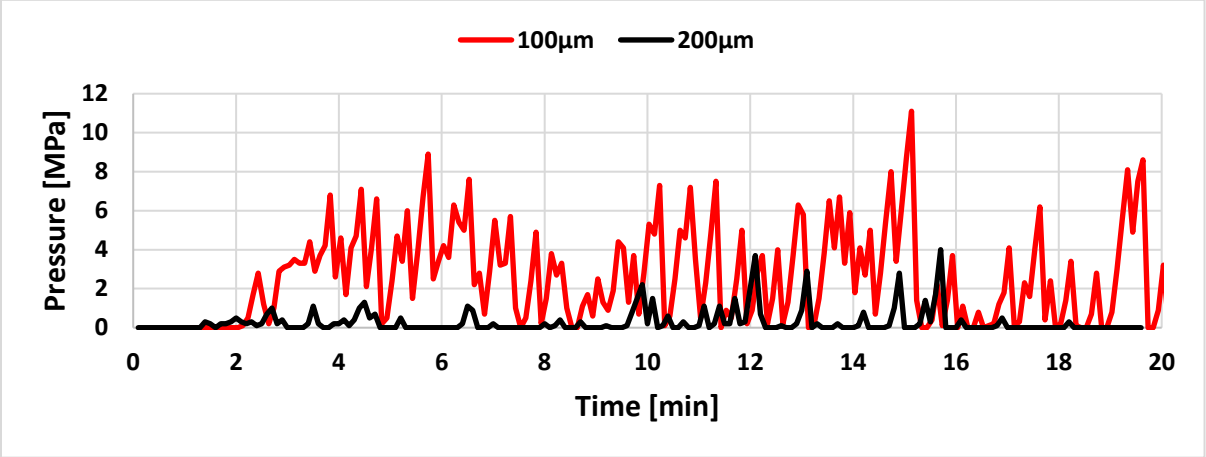


Figure 4.14: Pressure recording during the bridging test using fine (100-150 µm) and coarse (250-350 µm) $CaCO_3$ and Pistachio in K-formate base fluid at 100 µm, and 200 µm slots

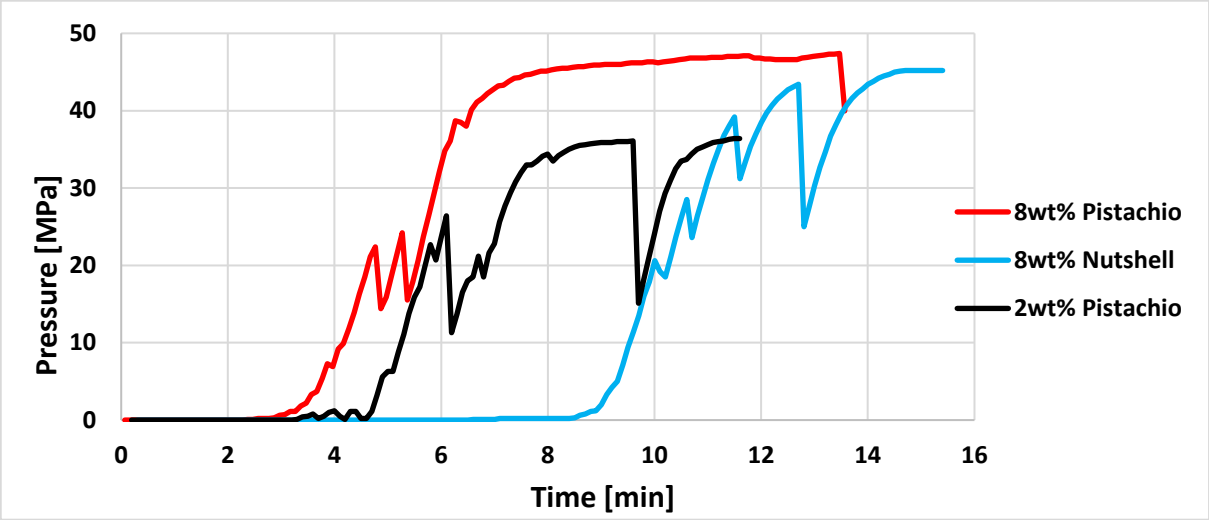


Figure 4.15: Pressure profiles of Nutshell (106-150, 180-250 and 500-1000 µm) and Pistachio (106-150, 180-250 and 500-1000 µm) with various concentrations in K-formate drilling fluid at 650 µm fracture opening

### 4.2.5 Bridging performance of Pistachio and Nutshell LCMs

In this experiment, Pistachio was compared to Nutshell to get insights into the plugging behaviors of Pistachio and Nutshell in potassium formate-based drill-in fluid. Bothe materials were prepared with equal particle size distribution (PSD) which is illustrated in figure 3.6, and $D_{50}$ was estimated to be around 175 µm. The experimental results of the bridging test using 100 µm, 175 µm and 225 µm slot openings are displayed in figure 4.16 and Figure 4.17. Results show that the bridging performance of both materials are quite similar over the smallest fracture, Nevertheless, as fracture sizes increase, the bridging performance of Pistachio is better than the Nutshell. The main reason is that the Pistachio particles are more compact compared to the Nutshell. The comparisons were made by taking equal masses amounts of the particles and filling in measuring cylinders. The results as shown in figure 3.3 indicate that the Pistachio particles have taken up less volume compared to Nutshell.

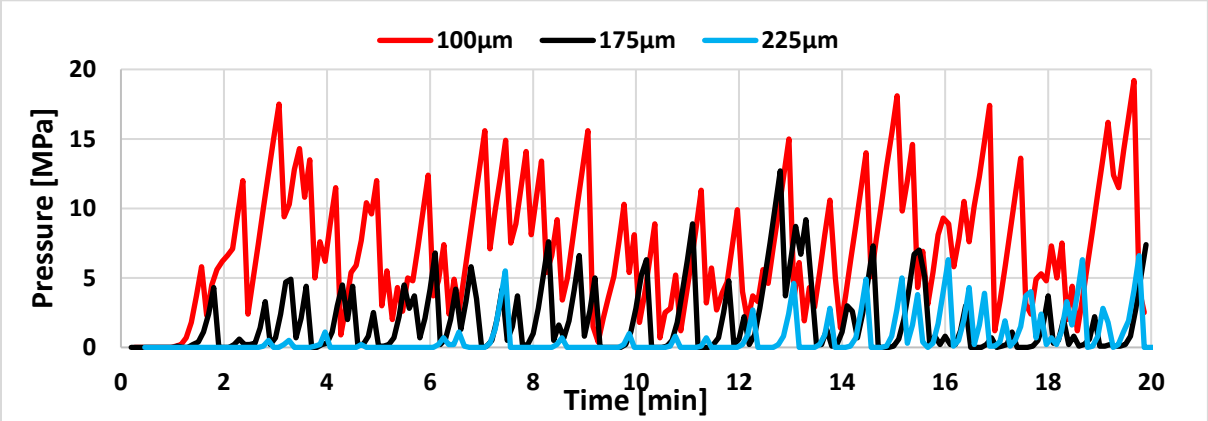


Figure 4.16: Pressure recording during the bridging test using Pistachio in K-formate base fluid at 100 µm, 175 µm and 225 µm slots

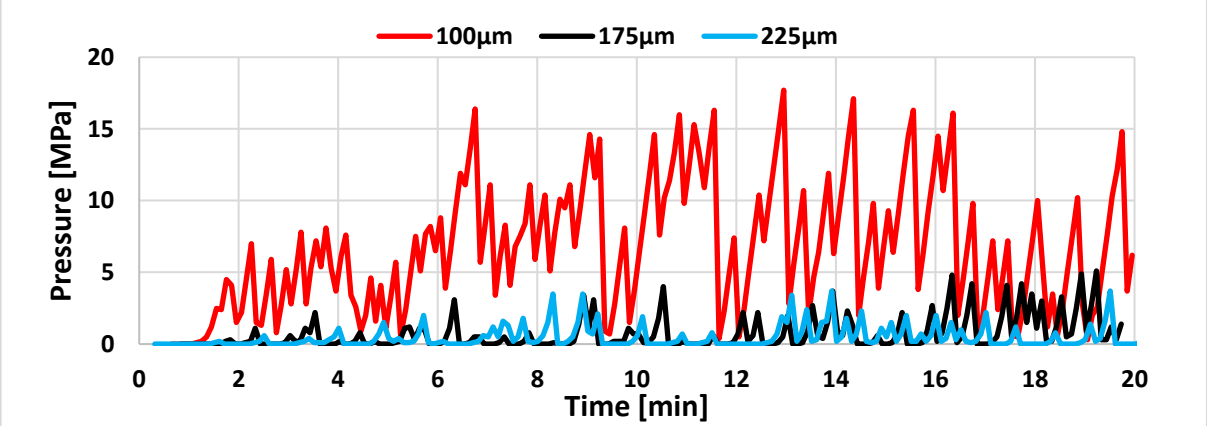


Figure 4.17: Pressure recording during the bridging test using Nutshell in K-formate base fluid at 100 µm, 175 µm and 225 µm slots

#### 4.2.5.1 Comparison of 100 µm, 175 µm, and 225 µm slots

Figure 4.18 – 4.20 display the bridging pressures of both LCMs side-by-side to give a better insight of plugging behaviors in terms of plugging pressure resistance. As it can be seen from the figures below the pressure resistances of both materials are quite similar over the smallest fracture except some minor variation at the beginning where pistachio has higher bridging pressure compared to nutshell. However, as fracture increases to 175 µm and 225 µm slots the pressure profile of Pistachio LCM becomes considerably higher than pressure recording of Nutshell.

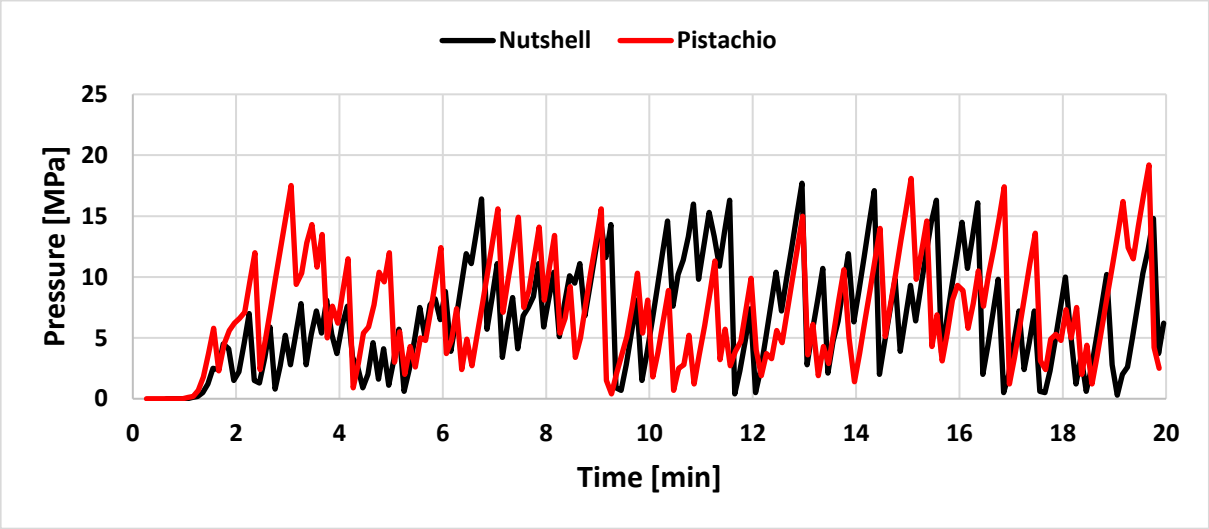


Figure 4.18: Comparison of Nutshell and Pistachio with 100 µm fracture

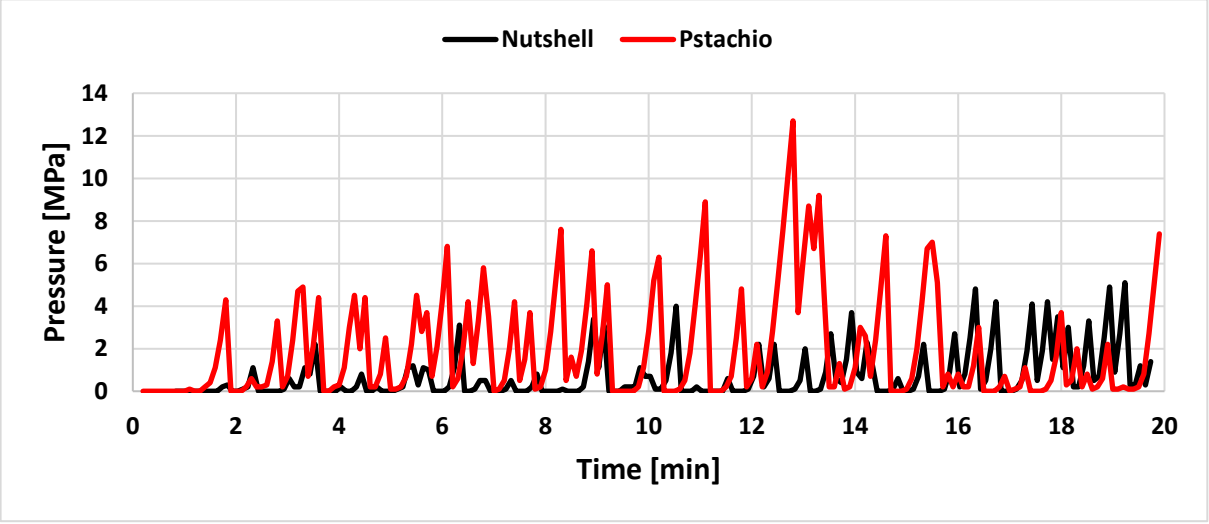


Figure 4.19: Comparison of Nutshell and Pistachio with 175 µm fracture

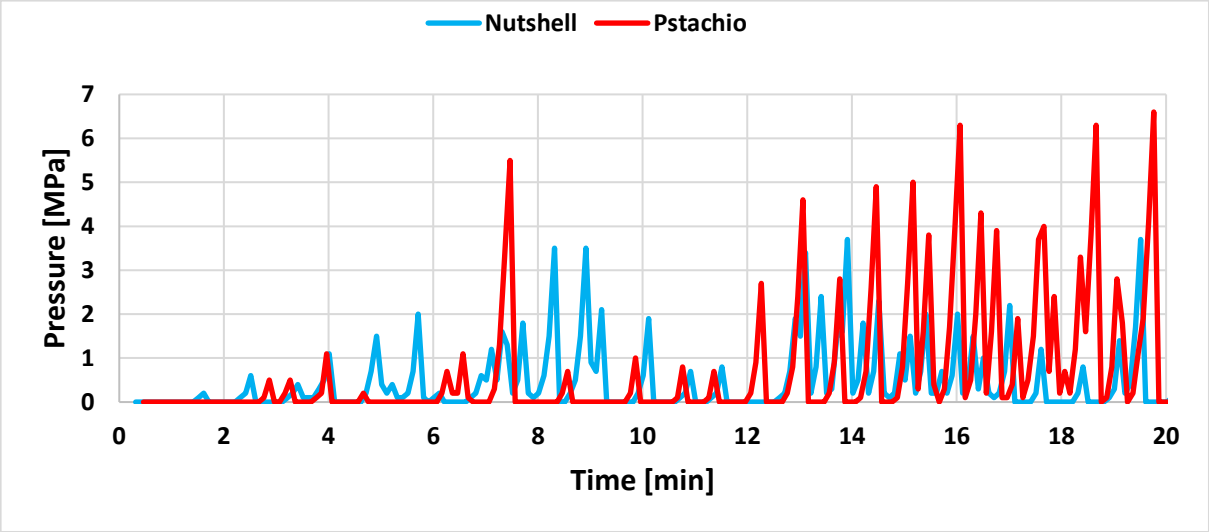


Figure 4.20: Comparison of Nutshell and Pistachio with 225 µm fracture

# 5 Analysis of bridging test results

A new set of parameters were defined by Torogi (2012) which aimed to assist in revealing more information about the bridging performance of LCM. [56]. Some of these parameters will be used in this thesis to further evaluate and get a deeper insight about the capabilities of particles in plugging fractures. These parameters include maximum pressure, average pressure, average peak pressure, and total number of bridges. All these parameters are influenced by the particle distribution, and drilling fluids lubricity, the properties of fluid to suspend the particles as well as fluid-particle interaction at the gate of the fracture. A brief definition of these parameters is as follow: [56]

- ***Maximum pressure:***

  The maximum pressure recorded during the 20 min test that the LCM can hold the external pressure at the get of the fracture.

- ***Average pressure:***

  The average pressure obtained during the investigation reveals information about the average strength of the bridge, which comprises the peak buildup -and collapse pressures during the 20min test period. This parameter will quantify qualitatively the overall performance of the particle in the considered drilling fluids. Moreover, the parameter may also be used for comparison of strengthening capabilities of drilling fluids.

- ***Total number of peaks:***

  The total number of peaks counted during the bridging in a 20 min duration. Each peak in the pressure plot illustrates the performance of the LCM particles in terms of creating new barriers once the barriers collapses.

- ***Average peak pressure:***

  The average peak pressure is the average of all the peak pressures during pressure build up in a 20 min testing period. This parameter provides information on the strengthening capability of the LCM system and indicates the pressure differential through the opening.

## 5.1 Analysis of maximum pressure, average pressure, total number of peaks and average peak pressure for the test design 1

In Figures 5.1 - 5.7, the maximum pressure, the average pressure, the total number of peaks, and the average peaks pressure of calcium carbonate with and without nanoparticles are illustrated in both Na-formate and K-formate base fluid respectively. As it is seen in figure 5.2, the potassium fluid containing calcium carbonate particles as LCM both with and without nanoparticles can reach a maximum pressure of 50 MPa for 100 µm slot, while the maximum pressure for the same LCM is a little lower in Sodium formate fluid. However, the pressure drop is considerably higher with K-formate fluid compared to Na-formate fluid as fracture enlarges to 150 µm. In Na-formate fluid the maximum bridging pressure drops from approximately 42 and 36 MPa to around 29 and 31 MPa without and with the presence of nanoparticles respectively. Furthermore, the pressure drop is slightly higher for the fluid containing nanoparticles compared to none containing nanoparticles fluid over the largest fracture opening.

As it is shown in figure 5.3, the average pressure of $CaCO_3$ with and without nanoparticles in Na-formate fluid is identical but in K-formate fluid the average pressure of fluid without nanoparticles is slightly higher (Figure 5.4). The total number of peaks appears the same over the smallest fracture both with and without nanoparticles in K-formate fluid while they slightly vary over the other fracture openings (Figure 5.5).

The average peak pressure indicates that the fluid containing calcium carbonate without nanoparticles can withstand slightly higher pressure across all fractures except over the 150 µm slot opening in sodium formate fluid where the average peak pressure is equal both with and without the presence of nanoparticles in the sampling fluid. This result indicates that the addition of nanoparticles may have a minor adverse effect than improved performance in terms of controlling lost circulation.

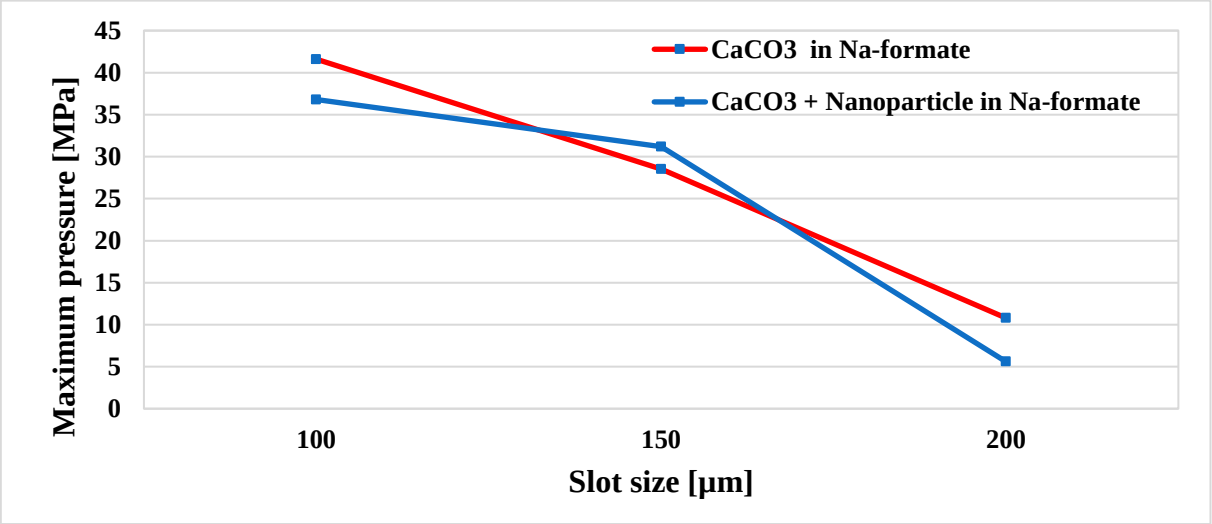


Figure 5.1: Maximum pressure of $CaCO_3$ with and without nanoparticle in Na- formate fluid

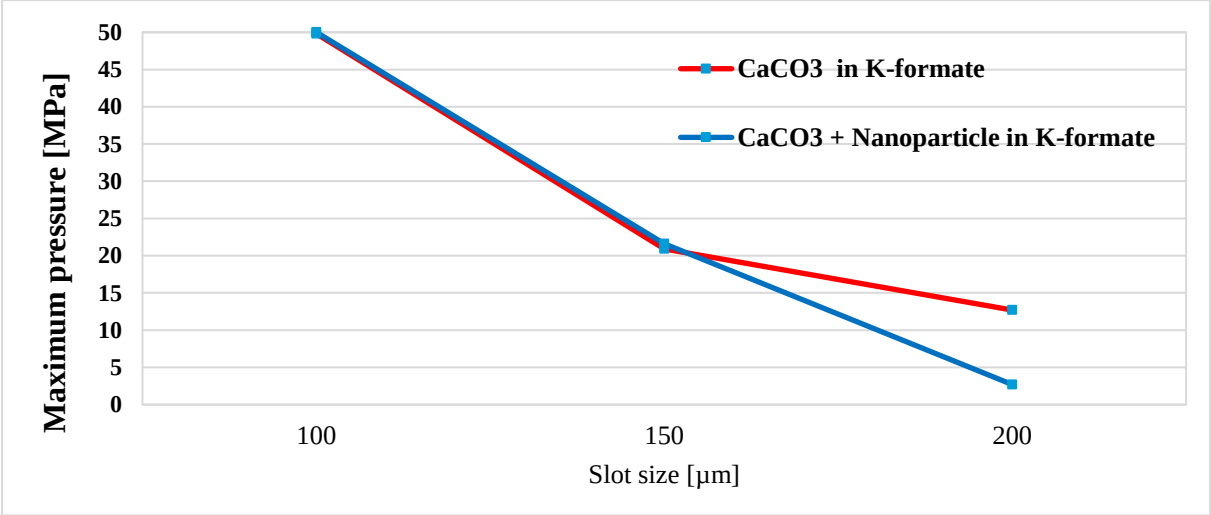


Figure 5.2: Maximum pressure of $CaCO_3$ with and without nanoparticle in K- formate fluid

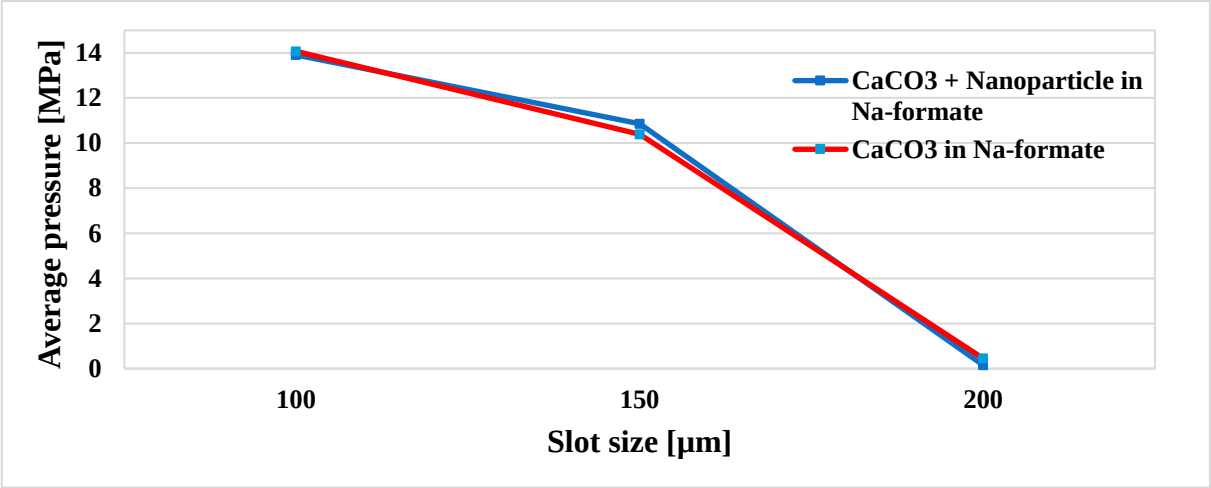


Figure 5.3: Average pressure of $CaCO_3$ with and without the nanoparticle in Na-formate fluid

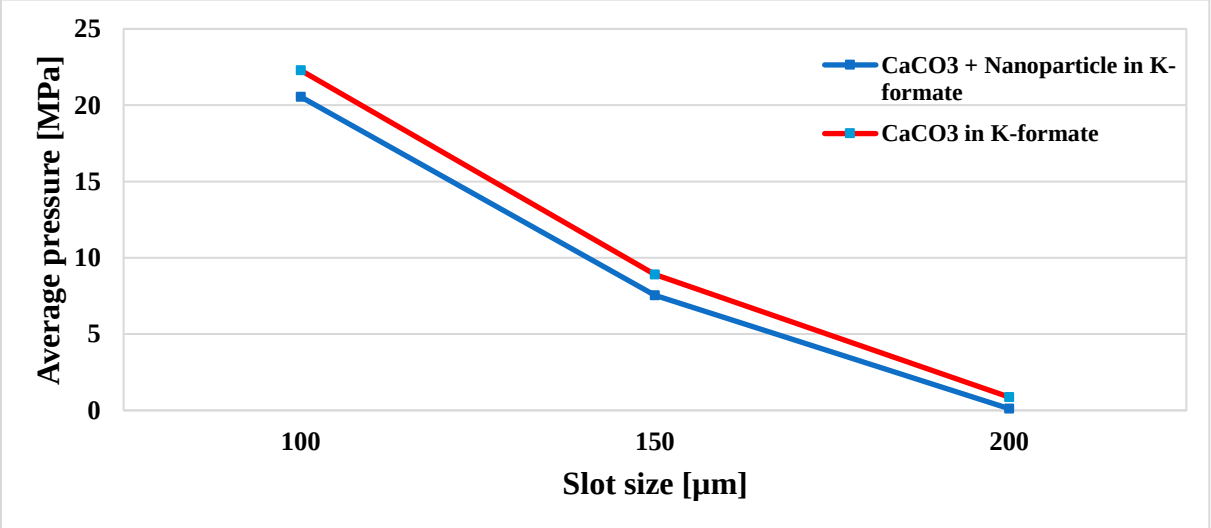


Figure 5.4: Average pressure of $CaCO_3$ with and without the nanoparticle in K-formate fluid

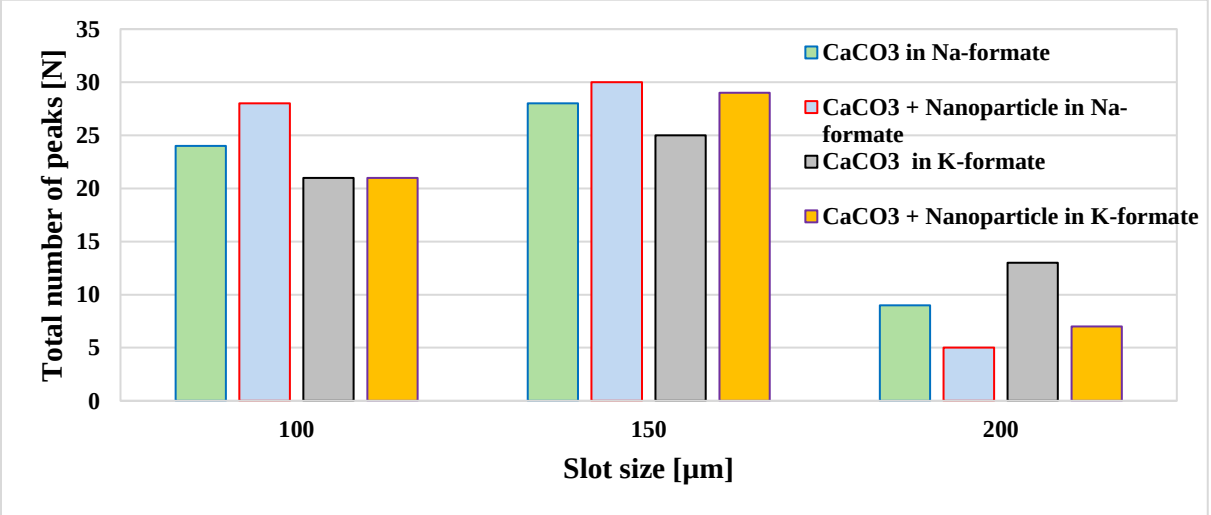


Figure 5.5: Total number of peaks for the test design 1

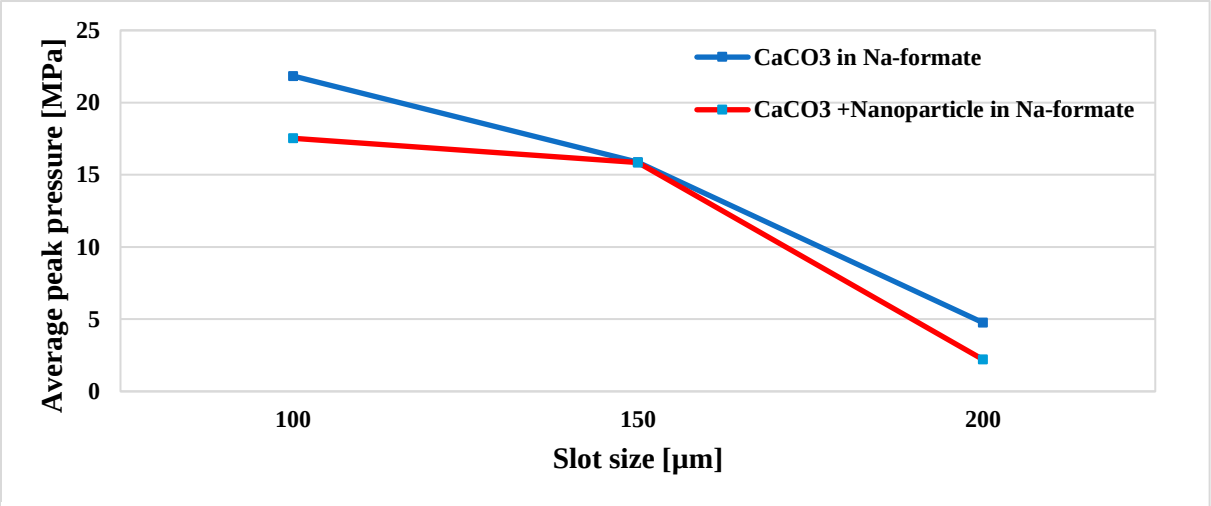


Figure 5.6 : Average peak pressure for the test design 1 in Na-formate fluid

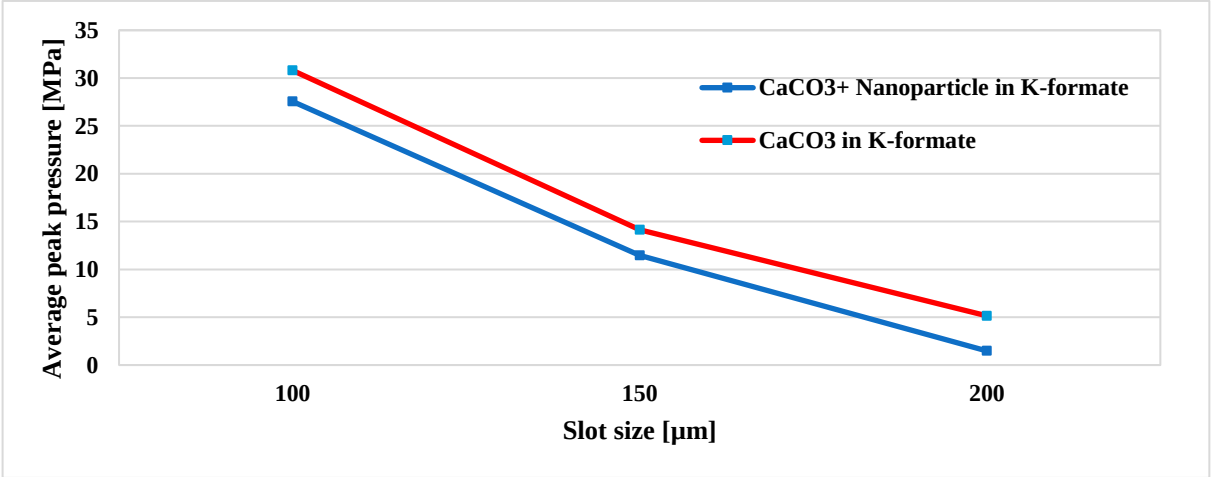


Figure 5.7: Average peak pressure for the test design 1 in K-formate fluid

## 5.2 Analysis of maximum pressure, average pressure, total number of peaks and average peak pressure for the test design 2

The results of the maximum pressure, the average pressure, the total number of peaks, and the average peaks pressure of quartz, $CaCO_3$ and combination of both materials are presented in Figures 5.8 – 5.11. As it is seen in Figure 5.8, none of the LCM systems can reach the maximum pressure over the fracture greater than 200 µm, but the mixture of both martials can hold substantially higher pressure throughout the experiments over all slot openings. In addition, the average pressure of the combination of both materials is significantly higher compared to calcium carbonate and quartz. This means that the loss of circulation may be easier to control by combining calcium carbonate with a mechanically strong LCM such as quartz.

This result is also confirmed by the average peak pressure except the value of peak pressure over the smallest slot opening where Quartz experiences a better bridging performance. However, Quartz experiences a dramatical pressure drop as fractures increase.

In the bar graph shown below, the LCM systems capability to form a bridge over the fracture is shown. The total number of peaks alone does not give any reliable information about the strength of the bridge. Observations obtained from the bar diagram below is that the number of peaks considerably decreases over the 200 µm slot opening compared to 100 µm and 150 µm slot openings, while there is a slight increase in total number of peaks from the 100 mm slot to the 150 slots. Another observation is that the combination of the $CaCO_3$ and Quartz has higher amounts of peaks over the largest fracture, while this pattern is the opposite over the 100 µm and 150 µm slots.

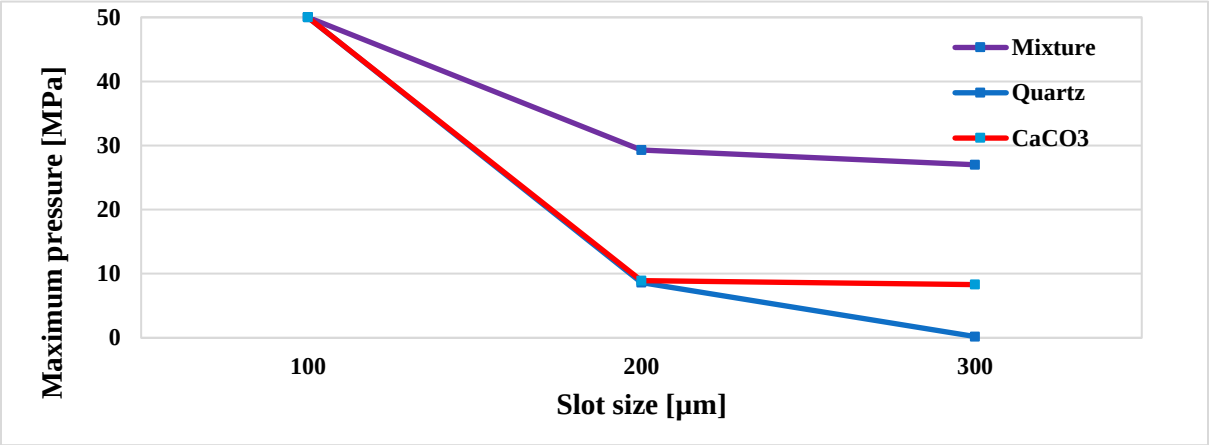


Figure 5.8: Maximum pressure of Quartz, $CaCO_3$ and their mixture in K-formate fluid

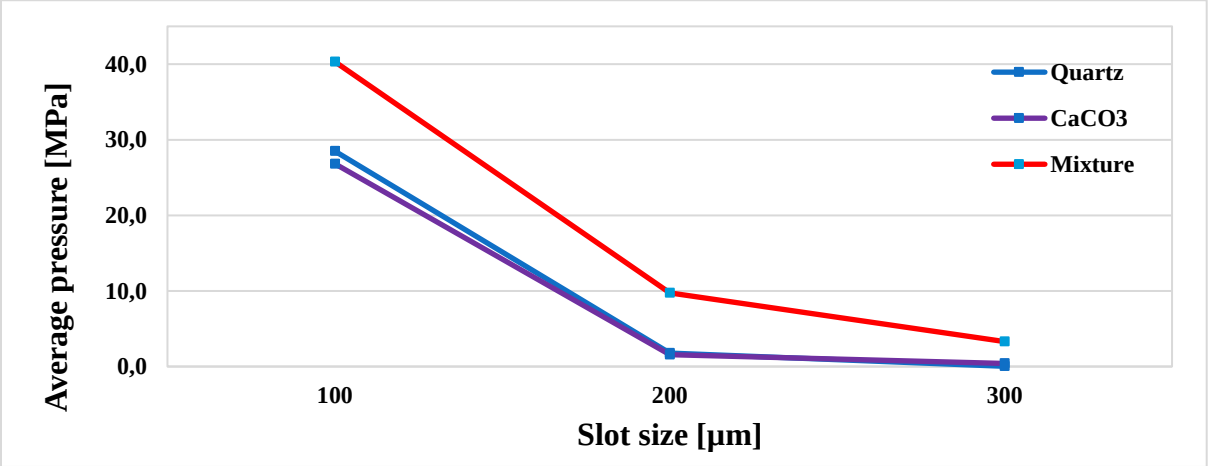


Figure 5.9: Average pressure of Quartz, $CaCO_3$ and their mixture in K-formate fluid

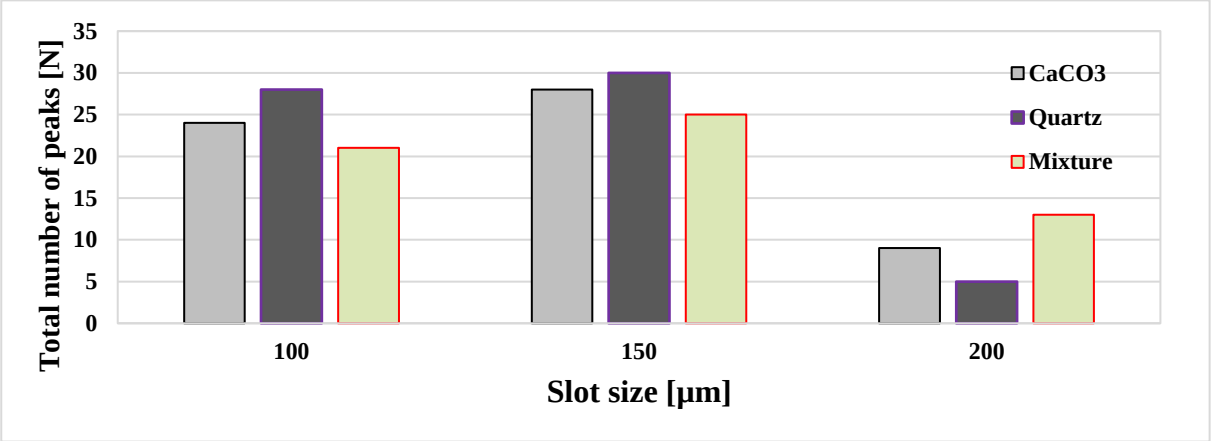


Figure 5.10 : Total number of peaks of Quartz, $CaCO_3$ and their mixture in K-formate fluid

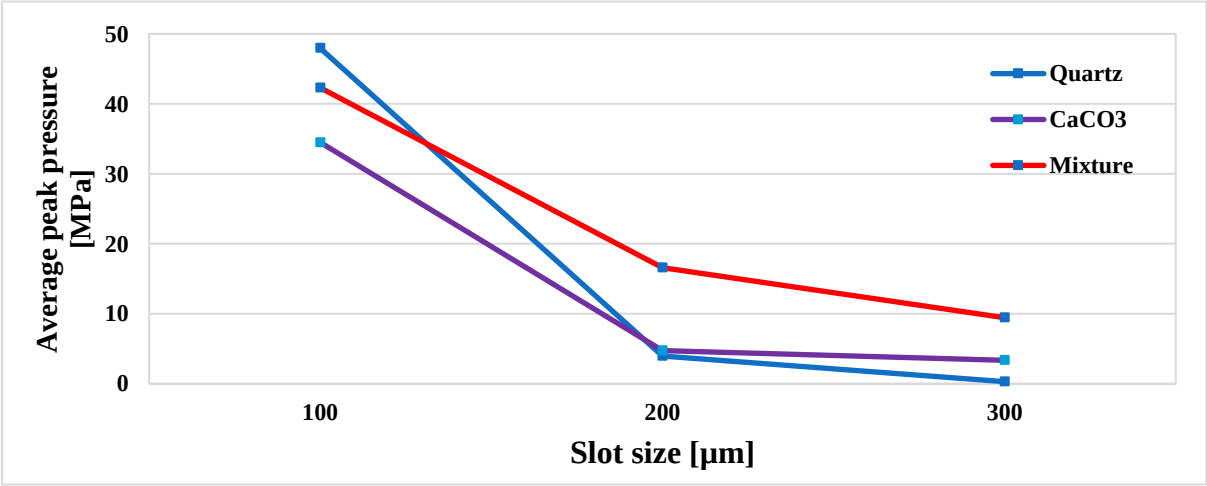


Figure 5.11 : Average peak pressure of Quartz, $CaCO_3$ and their mixture in K-formate fluid

## 5.3 Analysis of maximum pressure, average pressure, total number of peaks and average peak pressure for the test design 3

Figures 5.12 – 5.15 show the maximum pressure, the average pressure, the total number of peaks, and the average peak pressures of $CaCO_3$, Pistachio, and the blending of both materials respectively. As it has seen from the plot, the drilling fluid containing pistachio resists much higher pressure over the 100 µm slot but the maximum pressure dramatically drops as fracture doubles to 200 µm slots. However, the combination of both materials has higher maximum pressure over 200 µm slots, and no bridges were formed when the tests were repeated using 300 µm slot.

As can be seen in figure 5.13, the calcium carbonate and pistachio can withstand a relatively high average pressure compared to the combination of both materials. However, as fracture increases from 100 µm to 200 µm, the combination of both materials can withstand a slightly higher average pressure, and based on figure 5.14, the combination of pistachio and calcium carbonate have a higher number of peaks both over 100 µm slots and 200 µm slots. The average peak pressure of the pistachio shows much superior average peak pressure over the smallest fracture but as fracture increases the mixture of both materials exhibits a higher average peak pressure.

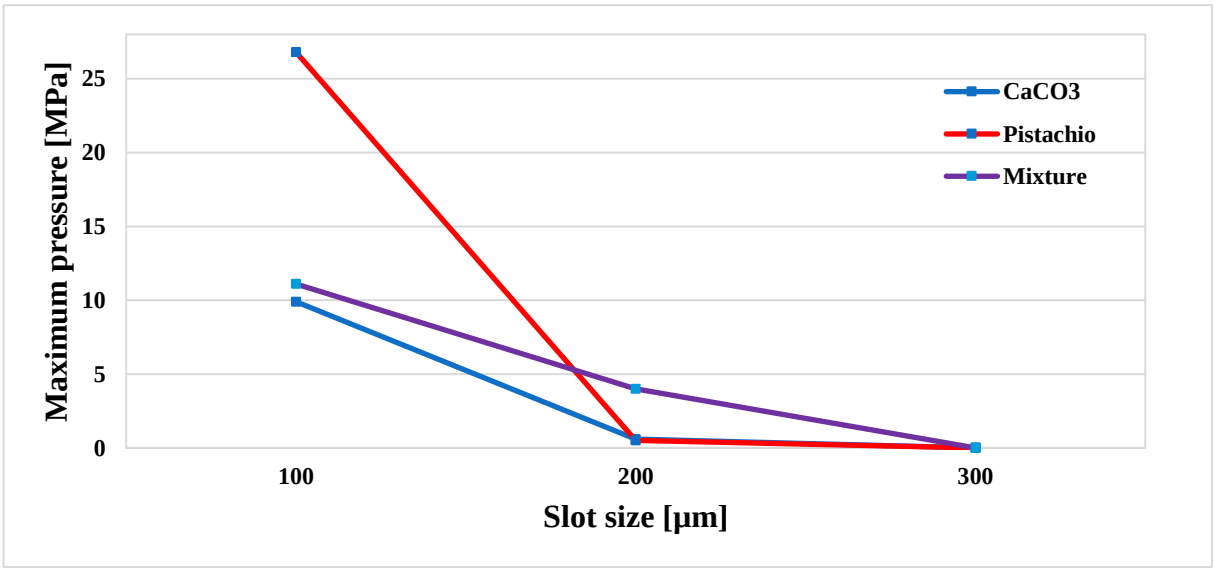


Figure 5.12: Maximum pressure of Pistachio, $CaCO_3$ and their mixture in K-formate fluid

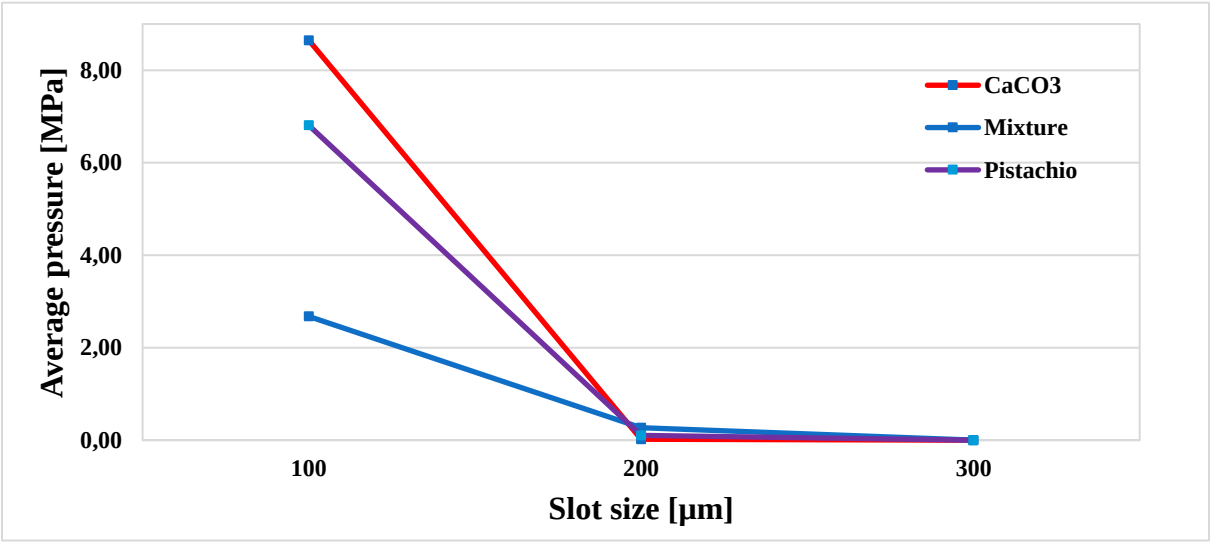


Figure 5.13: Average pressure of Pistachio, $CaCO_3$ and their mixture in K-formate fluid

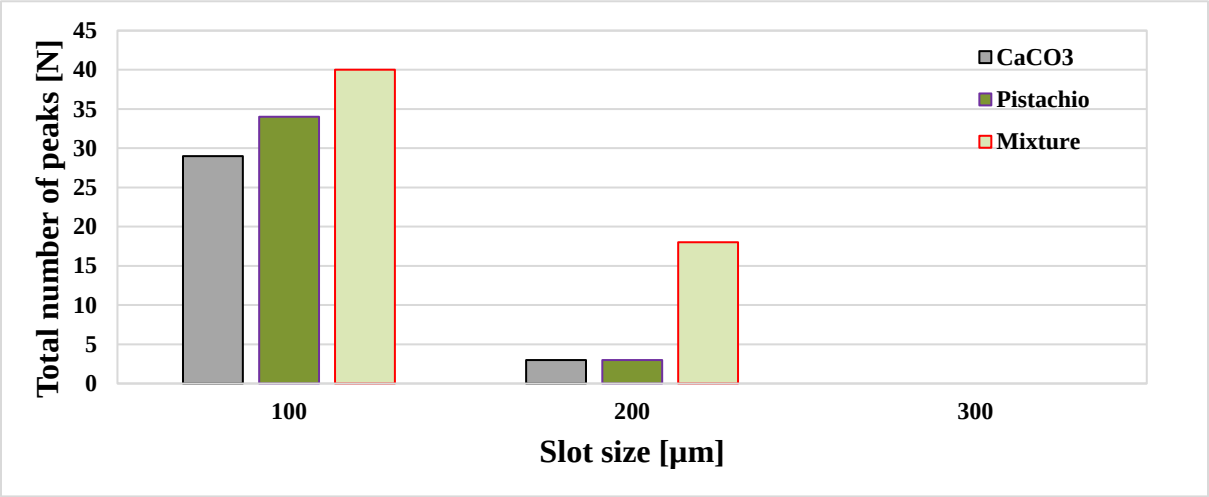


Figure 5.14: Total number of peaks of Pistachio, $CaCO_3$ and their mixture in K-formate fluid

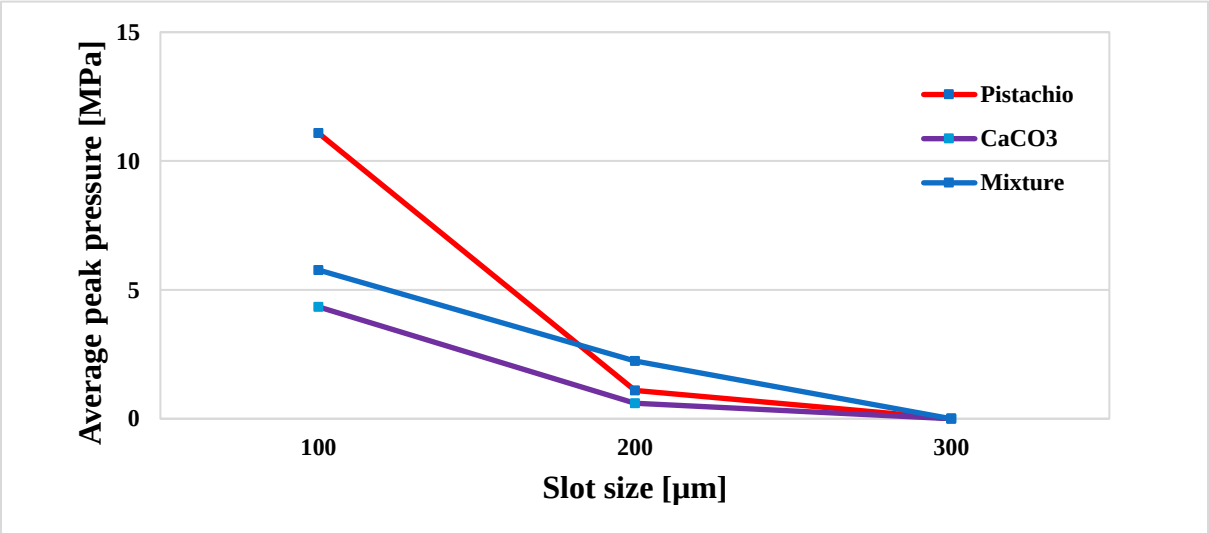


Figure 5.15: Average peak pressure of Pistachio, $CaCO_3$ and their mixture in K-formate fluid

## 5.4 Analysis of maximum pressure, average pressure, total number of peaks and average peak pressure for the test design 4

In Figures 5.16 – 5.19, the maximum pressure, the average pressure, the total number of peaks, and the average peak pressures of nutshell and pistachio are compared side-by-side respectively. The maximum pressure of the drilling fluid containing pistachio is higher throughout the test compared to nutshell. There is a linear decline in maximum pressure when fracture opening increases. The drilling fluid containing nutshell experienced a steeper drop in maximum pressure from the 100 µm slot to the 175 µm slot, and from 175 µm slot to 225 µm slot the maximum pressure dropped further by approximately 1 MPa.

Based on figure 5.17, Pistachio has slightly higher average pressure over all three fractures that were used during the experiment. The decrease in average pressure due to increased fracture sizes nearly experienced the same trend. Observation obtained from the bar diagram is that the number of peaks decreases as slot opening increases. Another observation is that pistachio has slightly lower number of peaks except over the fracture of 175 µm where the total number of peaks is higher than nutshell. The average peak pressure of Pistachio is considerably higher compared to Nutshell and the average peak pressure of both materials decreases from the 100 µm fracture to the 175 µm fracture. Afterward, the average peak pressure of both materials approximately remains flat from the 175 µm slot to 225 µm fracture opening.

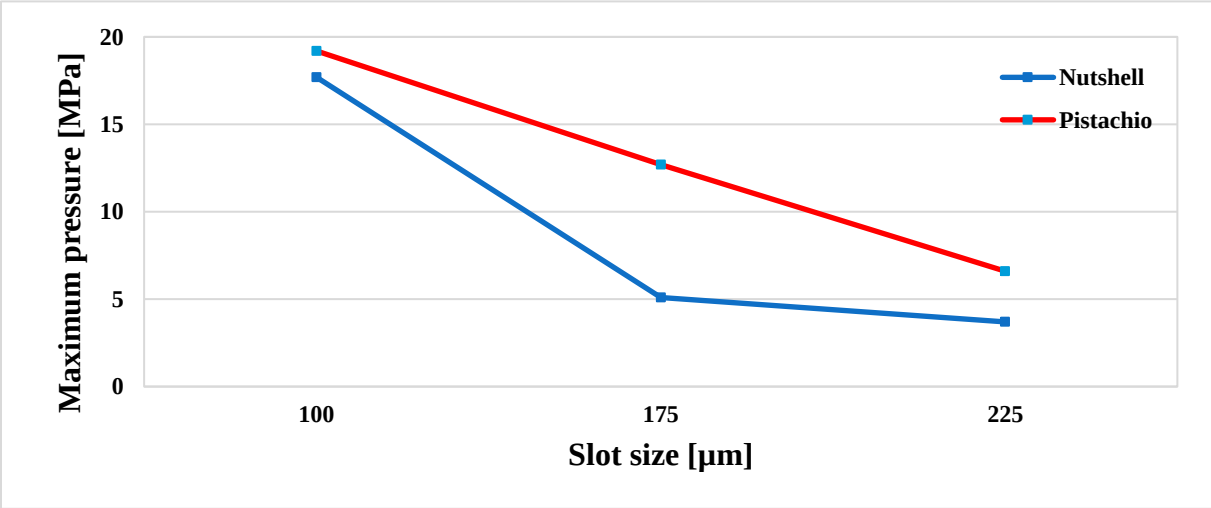


Figure 5.16: Maximum pressure of Pistachio and Nutshell in K-formate fluid

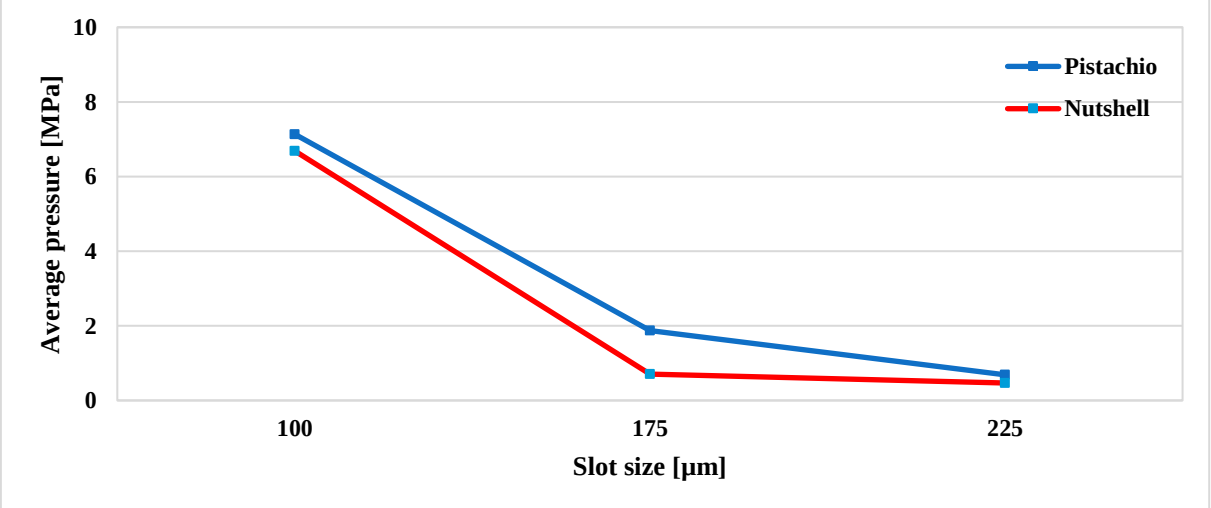


Figure 5.17: Average pressure of Pistachio and Nutshell in K-formate fluid

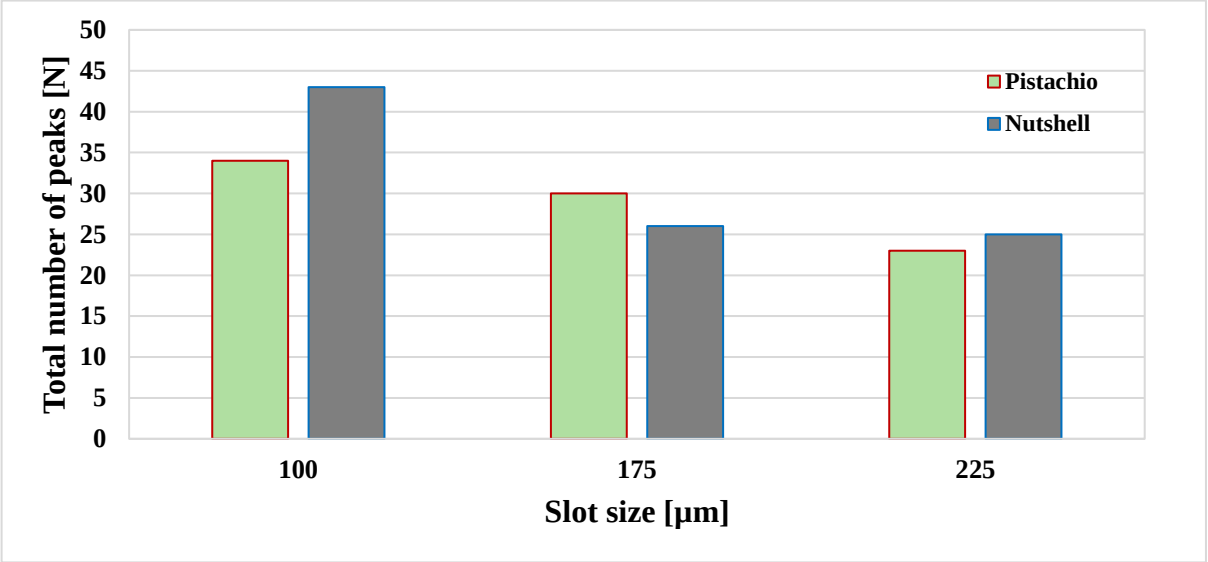


Figure 5.18 : Total number of peaks of Pistachio and Nutshell in K-formate fluid

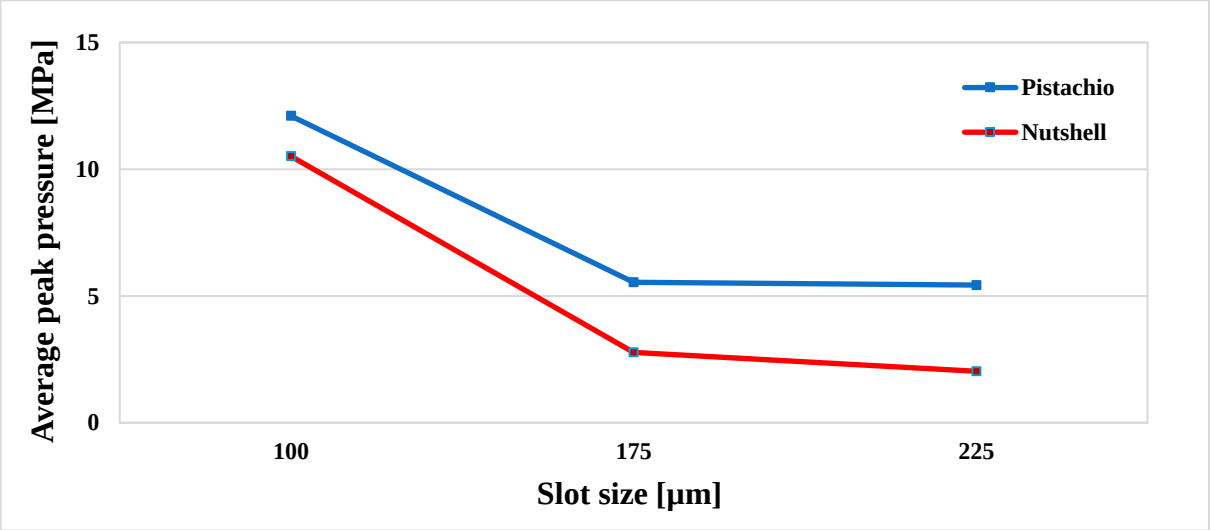


Figure 5.19 : Average peak pressure of Pistachio and Nutshell in K-formate fluid

# 6 Conclusion

Field case studies showed that loss circulation often occurs during drilling and cementing operations. The NPT associated with loss circulation issues cost the oil industry a lot. To combat loss circulation, the preventive and corrective methods are the main techniques to manage the loss circulation in a wellbore. During drilling or prior to drilling, the common practice is to use appropriately designed loss circulation corrective measures to hinder fluid loss in the formation as well as preventive action by increasing the wellbore strength. For these, loss circulation materials play the key role. The application of loss circulation material treatment depends on the degree of the severity of the losses. The sealing performance of loss circulation materials depends on the mechanical strength, the particle size distribution, the particle packing, the concentration and the shape of the loss circulation materials can be mentioned.

In this thesis, a total of four experimental tests have been designed to systematically investigate the bridging performance of LCM in the laboratory synthesized K- and Na-formate drilling fluids.

The main observations from the work are summarized as:

- The bridging performance of LCM materials in the considered K-formate and Na-fomate are almost similar. The experimental results showed that the K-and Na atomic weight differences did not make any significant impact on the bridging strength.
- The blended 1 wt.% of nanosized $CaCO_3$ with micro sized $CaCO_3$ had almost adverse effect on the bridging strength in K- formate and Na-formate fluids. However, more research is required to investigate the effect of nanosized particles in drill-in fluids.
- Strong fracture bridge is obtained by blending very small with medium and coarse particles that improves the packing efficiency of the bridge. The experimental test result supported the Ideal Packing Theory proposed by reference [23]
- The common LCM used in drill-in drilling fluid, $CaCO_3$, is mechanically weak. The blending of $CaCO_3$ with Quartz increased the bridge strength and showed positive synergy as compared with their separate performances.
- The fracture sealing performance of Pistachio is better than the Nutshell in terms of strength as well as the early sealing performances. However, more research is required to compare these two in different drilling fluids.

# 7 References

[1]. Bourgoyne, A. T., Millheim, K. K., Chenevert, M.E. et. al., 1991. Applied Drilling Engineering. Second printing. Texas, USA: Richardson.

[2]. Rodrigue. B Ramire , .C Vela'que , . Conejo . Martine Annular flow analysis by tracers in drilling operations // Journal of Petroleum Science and Engineering, Volume 41, Issue 4, February 2004, Pages 287–296

[3]. Robert F. Mitchell and Stefan Z. Miska 2011 //Fundamentals of Drilling Engineering //SPE Textbook Series No. 12 IS BN: 978-1-55563-207-6

[4]. Feng, Y., and Gray, K. E., 2018, Lost Circulation and Wellbore Strengthening, Springer, New York.

[5]. S. Salehi, "Numerical simulations of fracture propagation and sealing: Implications for wellbore strengthening," 2012.

[6]. Messenger, J.U., Lost Circulation, PennWell Books, 1981.

[7]. Y. Feng and K. Gray, "Review of fundamental studies on lost circulation and wellbore strengthening," Journal of Petroleum Science and Engineering, vol. 152, 2017.

[8]. Sigve Hovda; Henrik Wolter; Glenn-Ole Kaasa; Tor Stein Olberg. Potential of Ultra-High-Speed Drill String Telemetry in Future Improvements of the Drilling Process Control, SPE-115196-MS. In Proceedings of the IADC/SPE Asia Pacific Drilling Technology Conference and Exhibition, Jakarta, Indonesia, 25–27 August 2008.

[9]. Cook, J., Growcock, F., Guo, Q., Hodder, M. and VAN OORT, E. (2011). Stabilizing the wellbore to prevent lost circulation. Oilfield Review, 2012, 4.

[10]. Pilisi, N.; Wei, Y.; U.; Holditch, S.A. Selecting Drilling Technologies and Methods for Tight Gas Sand Reservoirs, IADC/SPE 128191. In Proceedings of the 2010 IADC/SPE Drilling Conference held in New Orleans, LA, USA, 2–4 February 2010

[11]. Redden J: "Advanced Fluid Systems Aim to Stabilize Well Bores, Minimize Nonproductive Time," The American Oil & Gas Reporter 52, no. 8 (August 2009): 58–65.

[12]. Harald, H., 2020. "Drill-in fluids and hydraulic fracturing characterization of lost circulation material". MSc.Thesis, Universitet i Stavanger

[13]. Davoodi, S.; SA, A. R.; Jamshidi, S.; Jahromi, A. F. A novel field applicable mud formula with enhanced fluid loss properties in high pressure-high temperature well condition containing pistachio shell powder. J. Pet. Sci. Eng. 2018, 162, 378−385.

[14]. Gaurina-Meñimurec, B. Pašić, K. Simon, D. Matanović, M. Malnar: F 2008// FORMATE-BASED FLUIDS: FORMULATION AND APPLICATION // Rud.-geol.-naft. zb., Vol. 20, 2008.

[15]. E. Jøntvedt, M. Fjeldheim, J. Løchen, S. Howard, S. Leon, C. Busengdal and K. R. Gyland, "Deployment of Cesium Formate Drill-in and Openhole Completion Fluid in the Martin Linge High Pressure, High Permeability Gas Reservoir Enhances Total's Operation Efficiency and Radically Improves Well Performance," SPE-189550-MS, p. 28, 7-9 February 2018.

[16]. Caenn, R.; Darley, H. C.; Gray, G. R. Composition and Properties of Drilling and Completion Fluids; Gulf Professional Publishing, 2011

[17]. Alcheikh, I. M.; Bisweswar G. "A Comprehensive Review on the Advancement of Non-damaging Drilling Fluids." (2017).

[18]. Pablo, S., Almagro, B., Frates, C., Garand, J., Meyer, A.: Sealing Fractures: Advances in Lost Circulation Control Treatments. Oilfield Review (Autumn 2014:26, no.3).

[19]. M. Alsaba et al., "Review of lost circulation materials and treatments with an updated classification," in AADE National Technical Conference and Exhibition, Houston, TX, Apr, 2014, pp. 15–16.

[20]. https://glossary.oilfield.slb.com/en/terms/f/fiber_lcm (Last accessed 09 October 2021).

[21]. B. S. Aadnoy, Modern well design. CRC Press, 2010.

[22]. A. Abrams et al., "Mud design to minimize rock impairment due to particle invasion," Journal of petroleum technology, vol. 29, no. 05, pp. 586–592, 1977.

[23]. M. Dick et al., "Optimizing the selection of bridging particles for reservoir drilling fluids," in SPE international symposium on formation damage control. Society of Petroleum Engineers, 2000.

[24]. S. Vickers et al., "A new methodology that surpasses current bridging theories to efficiently seal a varied pore throat distribution as found in natural reservoir formations," Wiertnictwo, Nafta, Gaz, vol. 23, no. 1, pp. 501–515, 2006.

[25]. D. Whitfill et al., "Lost circulation material selection, particle size distribution and fracture modeling with fracture simulation software," in IADC/SPE Asia Pacific drilling technology conference and exhibition. Society of Petroleum Engineers, 2008.

[26]. M. W. Alberty et al., "A physical model for stress cages," in SPE annual technical conference and exhibition. Society of Petroleum Engineers, 2004.

[27]. https://www.drillingmanual.com/2021/01/stress-cage-pill-theory-wellbore-strengthen.html (Last accessed 09 November 2021).

[28]. M.S. Aston, M.W. Alberty, M.R. McLean, H.J. de Jong and K. Armagost //Drilling Fluids for Wellbore Strengthening //IADC/SPE 87130, p. 8, 2-4 March 2004

[29]. Fred E. Dupriest, "Fracture Closure Stress (FCS) and Lost Returns Practices". SPE, ExxonMobil. SPE/IADC 92192

[30]. Arunesh Kumar, Sharath Savari, Donald L. Whitfill, and Dale E. Jamison, 2010, // Wellbore Strengthening: The Less-Studied Properties of Lost-Circulation Materials// SPE 133484 paper was prepared for presentation at the SPE Annual Technical Conference and Exhibition held in Florence, Italy, 19–22 September 2010.

[31]. Musaab I.Magzoub, Saeed Salehi, Ibnelwaleed A.Hussein,Mustafa S.Nasser 2020// Loss circulation in drilling and well construction: The significance of applications of crosslinked polymers in wellbore strengthening: A review// Journal of Petroleum Science and Engineering Volume 185, February 2020, 106653

[32]. F. Irgens, Rheology and Non-Newtonian Fluids, 1st edition ed., Cham: Springer, 2014.

[33]. Kolle, G.& Mesel, R. (1998). *Brønnvæsker*: Vett & viten

[34]. A. P. L. A. P. O. E. F. B. Folayan J. Adewale, "Selecting the Most Appropriate Model for Rheological Characterization of Synthetic Based Drilling Mud," International Journal of Applied Engineering Research, p. 16, 2017.

[35]. Baker Hughes drilling fluids reference manual revision 2006

[36]. https://www.drillingformulas.com/types-of-flow-and-rheology-models-of-drilling-mud/ (Last accessed 18 November 2021)

[37]. PC Barman, RR Kairi, A Das, R Islam. *An overview of non-Newtonian fluid:* International Journal of Applied Science and Engineering (2016)

[38]. Viloria Ochoa, M., Analysis of drilling fluid rheology and tool joint effect to reduce errors in hydraulics calculations. 2006, Texas A&M University.

[39]. Robertson, R. and H. Stiff Jr, An improved mathematical model for relating shear stress to shear rate in drilling fluids and cement slurries. Society of Petroleum Engineers Journal, 1976. 16(01): p. 31-36

[40]. Bui, B.; Saasen, A.; Maxey, J.; Ozbayoglu, M.E.; Miska, S.Z.; Yu, M.; Takach. N.E. Viscoelastic Properties of Oil-Based Drilling Fluids. Annu. Trans. Nord. Rheol. Soc. 2012, 20.

[41]. Saasen, A.; Dawei, L.; Marken, C. Prediction of Barite Sag Potential of Drilling Fluids from Rheologicial Measurements, SPE 29410. In Proceedings of the SPE/IADC Drilling Conference, Amsterdam, 28 February–2 March 1995.

[42]. Mezger, T.G., The rheology handbook: for users of rotational and oscillatory rheometers. 3rd rev. ed. ed. European coatings tech files. 2011, Hannover: Vincentz.

[43]. Malvern Instruments (2016). *A Basic Introduction to Rheology*

[44]. Sharman, T., Characterization and performance study of OBM at various oil-water ratios. 2015, University of Stavanger, Norway

[45]. hhttp://www.sciencemadness.org/smwiki/index.php/Sodium_formate (Last accessed 06 December 2021).

[46]. https://ptable.com/#Egenskaper/Atomvekt (Last accessed 06 December 2021).

[47]. https://pubchem.ncbi.nlm.nih.gov/compound/Sodium-formate (Last accessed 06 December 2021).

[48]. https://www.americanelements.com/potassium-formate-590-29-4 (Last accessed 06 December 2021)

[49]. https://www.britannica.com/science/starch (Last accessed 06 December 2021)

[50]. Medimurec, G.; Pašić, B.; Kayarina, S. "Formate-based fluids: Formulation and application" (2008).

[51]. Akpan, E.U.; Enyi, G.C.; Nasr, G.G. Enhancing the performance of xanthan gum in water-based mud systems using an environmentally friendly biopolymer. J. Petrol. Explor. Prod. Technol. 2020, 10, 1933–1948.

[52]. Desai, A. K; Desai, A. B, Bisen, M; Gupta, "Non-damaging eco-friemdly drilling fluid system". S.I. Program 2021.

[53]. https://pubchem.ncbi.nlm.nih.gov/compound/Calcium-carbonate (Last accessed 06 December 2021)

[54]. https://glossary.oilfield.slb.com/en/terms/d/direct-indicating_viscometer.aspx

[55]. M. Belayneh, "Experimental and analytical borehole stability study." University in Stavanger, 2004.

[56]. S. Mostafavi Toroqi, "Experimental analysis and mechanistic modeling of wellbore strengthening," Ph.D. dissertation, University of Calgary, 2012.